NORTHWESTERN UNIVERSITY

Proprioceptive Coding in the Cuneate Nucleus of Awake Monkeys

A DISSERTATION

SUBMITTED TO THE GRADUATE SCHOOL

IN PARTIAL FULFILLMENT OF THE REQUIREMENTS

for the degree

DOCTOR OF PHILOSOPHY

Field of Biomedical Engineering

By

Christopher Versteeg

EVANSTON, ILLINOIS

December 2021

Abstract

Proprioception, or the sense of one's body in space, provides critical feedback that the brain uses to generate controlled movements. When proprioceptive feedback is lost, people find it difficult to perform even basic motor tasks. Despite its importance, proprioceptive coding of single neurons in the cuneate nucleus (CN), the most peripheral somatosensory nucleus of the brain, had never been studied in awake animals.

During my doctoral work, I developed methods to record single neurons in CN of awake animals for the first time ever. I examined two fundamental properties of CN neurons, 1) how their sensitivity to proprioceptive information changes across contexts and 2) how many muscles typically compose their receptive fields (RFs).

I recorded from CN of monkeys trained to perform reaching tasks and to tolerate bumps applied to their hand. I found that in contrast to the typical "sensory gating" of tactile signals, the responses of proprioceptive CN neurons to movement are, on average, modestly potentiated during reach compared to rest. I propose that CN modulates sensitivity to enhance relevant information and attenuate irrelevant information.

I also found that CN neurons with muscle-like RFs have properties that resemble those of muscle spindle afferents and don't typically include signals from more than a single muscle, evidence for limited spatial convergence in CN. Looking for signs of processing along the

neuraxis, I compared proprioceptive responses in CN to previous recordings from somatosensory cortex and found that many features of cortical proprioceptive neurons are already evident in CN, perhaps inherited from muscle receptors themselves.

These results suggest that although CN relays proprioceptive signals that resemble muscle receptors, it does so in a context-dependent manner that allows for flexible representation of the sensory input, potentially to build "smart" brainstem and transcortical reflexes or to improve proprioceptive acuity when required by the task.

My experiments, conducted as part of a research group focused primarily on motor control, sought to understand how proprioceptive coding in the medulla contributes to the generation of motor behaviors; however, a prevailing theory of motor cortical activity, neural dynamical systems (NDS), doesn't typically take proprioceptive inputs into consideration. To address this shortcoming, I developed a model of motor cortex that combines the field of Optimal Feedback Control with NDS, in which feedback controllers in motor cortex are built using the intrinsic dynamics of sensory and motor cortices. In this dissertation, I lay out the features of this model and propose experiments that could validate or falsify its key predictions.

Acknowledgements

Research, as all scientists know, can be a frustrating and demoralizing affair. While the basic procedure of playing basketball or selling cars doesn't change much over time, pushing the frontier of knowledge requires that we *only* do things that no one has ever done before. There can be no routine in scientific discovery, which means that we encounter a lot of dead-ends, failed experiments, and bad ideas. To overcome these setbacks, we need support from our colleagues, friends, and family, who I thank profusely here.

Dr. Lee Miller, my PhD advisor, has been a supportive and kind mentor, allowing me freedom to pursue my often half-baked ideas and support when they failed (often) or succeeded (occasionally!). He was always willing to listen and provide valuable feedback and help keep me grounded in the day-to-day. I would especially like to highlight how his editing of my writing has taught me to restrain my more florid instincts (though I am indulging them here). Thanks Lee for your great mentorship; it will serve me well for the rest of my career.

To the members of the Miller lab, past and present; you've been great friends and colleagues. You've listened to me vent about my failures and helped me rise and try again. I can only hope that I have done the same for you.

To my committee, Drs. Sliman Bensmaia, Matthew Tresch, and Hermann Riecke, thank you for all the valuable input on my project over the years. The final product is greatly improved by

your wise criticism and advice.

To the broader neuroscience community, especially Drs. Richard Nichols, Alex and Mackenzie Mathis, Leah Krubitzer, Chethan Pandarinath, Sara Solla, Lena Ting, and Jessica Allen. You started me on the path and kept me motivated with your amazing discoveries.

To my family for their constant encouragement. For hearing my arcane thoughts at Thanksgiving and having the decency to not tell me to shut up. That's what family is for.

Finally, to my wife, Andrea, who has borne my load for me when I could not. May we continue to bloom like children and play together like dogs.

Table of Contents

List of Tables and Figures

Chapter 1 - Introduction

"Hofstadter's Law: It always takes longer than you expect, even when you take into account Hofstadter's law."

While moving and interacting with objects in the world, a person needs to sense both their external environment and themselves. For instance, as I write this introduction, I see a cup of coffee on my desk and decide to reach out, grasp it, and take a sip. Even this simple motor task requires extensive information about the external world and the internal configuration of my body. Consequently, the process of collecting this information takes two distinct forms, sensing my surroundings and sensing myself. I sense my surroundings (the location and orientation of the cup relative to my eyes) through receptors in my retina, but I sense myself (where my hand is) primarily through receptors in my muscles. This "sense of oneself" is known as proprioception.

Humans only have weak conscious awareness of the conformation of their bodies; proprioception wasn't even recognized as a sense until the 19th century. Despite low conscious availability, the motor system depends heavily on proprioceptive feedback (Sainburg, Ghilardi, Poizner, & Ghez, 1995). In a rare autoimmune disorder, immune responses can attack the nerve fibers that have their origin in the muscles and skin. As these nerve fibers die, the affected person loses their ability to sense the intrinsic conformation of their body and, consequently, finds it difficult to perform basic motor tasks and often is unable even to stand (Cole, 1996).

Proprioceptive inputs are essential for the brain to produce controlled movement.

Uncovering how the brain processes proprioceptive information relies on recording neural activity from proprioceptive areas during behavior. The best-studied region of the brain that processes proprioceptive information is somatosensory cortical area 2. Neurons in this region fire action potentials at rates related to the velocity, position, and forces of the hand and arm (Chowdhury, Tresch, & Miller, 2017; Prud'homme, Cohen, & Kalaska, 1994; Prud'homme & Kalaska, 1994). These neurons also receive inputs from motor cortex. This motor cortical input may influence how the somatosensory cortex processes sensory inputs (Brian M London & Miller, 2013; Umeda, Isa, & Nishimura, 2019). Disruption (or ablation) of somatosensory cortex hampers the learning of new tasks, but not execution of previously learned tasks (M. W. Mathis, Mathis, & Uchida, 2017; Pavlides, Miyashita, & Asanuma, 1993). Unfortunately, beyond these general descriptions, we still don't understand *how* ensembles of neurons in somatosensory areas use proprioception to accomplish perceptual or motor goals.

Researchers have recorded single neurons from both the proprioceptive periphery and cortex during behavior. In contrast, firing rates of single neurons in an intermediate somatosensory area, the Cuneate Nucleus (CN), had never been recorded from awake animals prior to our work. In my doctoral study, I sought to improve our understanding of how the proprioceptive sense of the upper limb is encoded at the CN, the first stage of somatosensory processing in the brain. By contrasting the proprioceptive representations that I found in CN with those found in the periphery and somatosensory cortex, I attempted to infer the processing goals of the

proprioceptive pathway.

Prior to our collaborative efforts with Drs. Joshua Rosenow (NU neurosurgeon) and Sliman Bensmaia at the University of Chicago (UC), all recordings from single CN neurons had been collected from anesthetized animals. In Chapter 2, I describe experiments conducted in conjunction with the lab at UC in which we developed techniques to implant recording electrodes chronically into CN in monkeys (Suresh et al., 2017). Leveraging these techniques, I investigated how CN neurons encode proprioceptive signals associated with reaching, described in Chapter 3 (Versteeg, Rosenow, Bensmaia, & Miller, 2021). I then compared CN proprioceptive coding with that of somatosensory cortical area 2, detailed in Chapter 4 (Versteeg, Chowdhury, & Miller, 2021). In Chapter 5, I present a model that incorporates proprioceptive feedback into dynamical models of motor cortex, an attempt to build a bridge between the fields of optimal feedback control and neural dynamical systems. I present a broad overview of my findings, as well as their implications and suggestions for future work in Chapter 6.

Proprioceptive signals end up in many regions throughout the brain, but nearly all pass through the dorsal column nuclear complex (DCN) which serves as an important early routing station. Because processing in CN depends on both the character of the somatosensory inputs and the eventual processing goals, I begin this review in the periphery and move centrally to the cortical proprioceptive areas. At each area, I will review our understanding of proprioceptive coding and

relevant anatomy (Figure 5.1A).

After these background sections, I will take up a specific description of the open questions in

CN, and close with an overview of the functional roles of proprioception. In this last section, I

will detail how proprioceptive processing pathways contribute to the motor control and

perception of the limbs, with particular emphasis on how CN may contribute to this processing.

Figure 1.1: Anatomy of the cortical proprioceptive pathway. A: Diagram of selected regions of the ascending dorsal-column medial lemniscal pathway. B: Diagram of anatomy of muscle spindle afferents. C: Cross-section of spinal cord. Portion highlighted in red indicates Cuneate Fasciculus. D: Diagram of dorsal column nuclei. Region highlighted in red indicates CN. E: Somatosensory (areas 3a, 3b, 1,2,5) and motor (area 4) cortical areas. Area 2 is highlighted in red. CS and IPS indicate central sulcus and intraparietal sulcus, respectively.

Dorsal Column Medial-Lemniscal Proprioceptive Pathway:

Sensory origin of proprioception:

Proprioception is a vaguely defined term that doesn't refer to any individual class or even location of receptor, rather the collective sensation of body position and movement (Proske & Gandevia, 2012). Interestingly, both visual information and efferent motor commands can influence the perceived state of the body, demonstrating that non-somatosensory and motor information contributes to the conscious proprioceptive sense (Gandevia, Smith, Crawford, Proske, & Taylor, 2006; Holmes & Spence, 2005; Izumizaki, Tsuge, Akai, Proske, & Homma, 2010; Walsh, Gandevia, & Taylor, 2010a). However, given that my recording sites were in CN (a somatosensory nucleus), in this dissertation I only consider somatosensory contributions to proprioception.

Somatosensory receptors are best categorized by their location in the muscles, skin, or joints (Proske & Gandevia, 2012; Tsay, Giummarra, Allen, & Proske, 2016). Cutaneous and muscle-based somatosensory signals are separate from one another until they converge onto single neurons in the somatosensory cortex, evidence that tactile and proprioceptive sensory signals are processed by different circuits in the ascending pathway (Friedman & Jones, 1981; E. G. Jones & Porter, 1980; Lucier, Rüegg, & Wiesendanger, 1975). For this reason, I devote more time to introducing the muscle-based receptors than receptors in the skin.

Evidence from joint replacement (Karanjia & Ferguson, 1983), thoracic-level dorsal column lesions that spare muscle spindle inputs (Wall & Noordenbos, 1977), and vibration-induced

proprioceptive illusions (Eklund, 1972; Goodwin, McCloskey, & Matthews, 1972a) point to muscle spindles being the most important receptor for the conscious proprioceptive sense (Proske & Gandevia, 2012). I review here the principal somatosensory contributions to proprioception, with special emphasis on muscle spindle afferents. For a detailed overview of cutaneous afferents see one of the many reviews on the subject (McGlone & Reilly, 2010; Hannes P. Saal & Bensmaia, 2014).

Muscle Spindle Anatomy:

Muscle spindles are sensory organs composed of "intrafusal" fibers wrapped in a sheath that isolates them from the force producing fibers of the muscle ("extrafusal" fibers) (Boyd, 1962; Hasan, 1983). Three intrafusal fiber types exist within a muscle spindle, named bag1, bag 2, and chain fibers, which have different mechanical properties. These intrafusal fibers are selectively innervated by different types of sensory and motor axons. I show a basic diagram of muscle spindle anatomy in Figure 1.1B.

Sensory endings of axons innervate regions of the intrafusal muscle fibers. Stretching the intrafusal fibers depolarizes the sensory endings and causes the afferent axon to fire action potentials. Two types of sensory axons emanate from the muscle spindle, primary (or Ia) and secondary (or type 2) axons. The pattern and extent of intrafusal fiber innervation depends on the afferent axon type in question. Primary muscle spindle afferents innervate all three types of intrafusal fiber, while secondary afferents only innervate bag2 and chain fibers (Blum, Lamotte

D'Incamps, Zytnicki, & Ting, 2017; Boyd, 1962).

In addition to these sensory axons emanating from the muscle spindle, efferent signals to the muscle spindle control the activation of the intrafusal muscle fibers. The control of the intrafusal fiber activation is known as gamma drive (in contrast with alpha drive, or the drive to the extrafusal fibers by alpha motoneurons) (Bennett, De Serres, & Stein, 1996; A. Prochazka, Hulliger, Zangger, & Appenteng, 1985a).

Gamma drive has two sub-types, static and dynamic gamma drive, which target different intrafusal fiber types. Bag fibers receive dynamic gamma innervation, while chain fibers receive static gamma innervation (M. Dimitriou, 2014; Ribot-Ciscar, Hospod, Roll, & Aimonetti, 2009; A. Taylor, Ellaway, Durbaba, & Rawlinson, 2000). The combination of gamma drive and intrafusal fiber type determines how different kinematic features of the muscle are transduced into action potentials in the afferent axons (Hasan, 1983; J. C. Houk, Rymer, & Crago, 1981; Mileusnic & Loeb, 2006). These variations in innervation and gamma properties lead to qualitative differences in the kinematic variables encoded by primary and secondary spindle afferents.

In brief summary, different afferent axon types are excited by deformation of different combinations of intrafusal fibers, which in turn are activated by different classes of gamma motor neurons. More briefly, muscle spindles are complicated.

Muscle spindle proprioceptive coding

It is quite difficult to record signals from muscle spindle afferents, especially during unconstrained movements such as reaching. Most of our knowledge of muscle spindle firing properties, therefore, comes from microneurography studies of humans or cats during very simple tasks, e.g., movements about single joints. Seminal experiments found that primary afferent firing rates are correlated with both length and velocity of the muscle, while secondary muscle spindle afferent firing rates are correlated principally with the length of the muscle (J. C. Houk et al., 1981; Proske & Gandevia, 2012).

Muscle spindles don't only respond to muscle kinematics. For example, lengthening of an active muscle causes much larger firing rates than does passive lengthening due to concomitant increases in alpha and gamma drive (M. Dimitriou, 2014; Michael Dimitriou & Edin, 2008). Muscle spindles also respond robustly during isometric contraction (Vallbo, 1971).

Many features of muscle spindle responses can be explained by idiosyncrasies in the transformation of mechanical deformation into firing rates, which depend on muscle fiber properties such as cross-bridge cycling. Models of muscle spindles that account for these features find that tension in the intrafusal fibers can explain the dynamics of primary afferent firing, even in response to purely passive stretches (Blum et al., 2017).

Some non-natural stimuli can also change muscle spindle firing rates. Muscle spindles respond to vibration applied to the muscle belly or tendon, often phase-locking to the frequency of the applied vibration. This effect can produce proprioceptive illusions (Goodwin, McCloskey, &

Matthews, 1972b; Izumizaki et al., 2010) and has been used to isolate muscle spindle afferents during peripheral nerve recordings (Eklund, 1972; Goodwin et al., 1972a; Izumizaki et al., 2010).

Gamma drive affects muscle spindle firing rates substantially. Increases in static gamma drive increase the length sensitivity of muscle spindle primary and secondary afferents, while increases in dynamic gamma drive increase the velocity sensitivity of primary afferents only. We still don't know why the brain modulates gamma drive during movement, though a few hypotheses have been posed.

First, the "alpha-gamma coactivation" hypothesis predicts that gamma activation matches the alpha drive to the extrafusal fibers. If intrafusal fibers go slack, the muscle spindle afferent's firing rate drops to zero, rendering it unresponsive to subsequent changes in length. Given matched alpha and gamma activation, the intrafusal fibers should not go slack during concentric muscle contraction (Macefield & Knellwolf, 2018). By preventing this slackening, gamma drive can allow muscle spindles to remain useful length sensors across many muscle lengths.

In contrast to alpha-gamma coactivation, the "fusimotor set" hypothesis predicts that the brain controls gamma drive independently from alpha drive. This hypothesis suggests that by modulating the sensitivity to stretch across motor actions, the nervous system can produce sensory afferent signals that allow reflex circuits in the spinal cord to more easily produce desired movements (A. Prochazka, Hulliger, Zangger, & Appenteng, 1985b). This hypothesis

implies that independent control of gamma is integral to movement execution, and that learning a movement involves not just learning alpha activations but gamma activations as well. The fusimotor set hypothesis has support from investigations of the cat locomotor system, where alpha-independent changes in gamma drive across the gait cycle seem to contribute to changes in phase of gait, such as the transition between stance and swing (Bennett et al., 1996; Ellaway, Taylor, & Durbaba, 2015a).

Yet another hypothesis suggests that gamma drive provides inputs to the muscle spindle that allow it to act as a forward model. A forward model, generally, generates a sensory prediction given the current state and the motor command. A muscle spindle forward model could use gamma inputs to "predict" the future muscle kinematics (Michael Dimitriou & Edin, 2010). These predictions would be useful to circumvent the conduction delay of afferent proprioceptive information, leading to smoother feedback control of the movement (Kawato, 1999). The role of gamma drive during movement remains a major open question in our understanding of the motor system; my recordings from spindle-receiving CN neurons can give some insight into gamma drive during reaching tasks.

Golgi Tendon Organs

Animals also possess a sense of muscular tension that informs the brain about the forces exerted by the body (Proske & Gandevia, 2012). Golgi tendon organs (GTOs) underlie this sense (J. Houk & Simon, 1967; Mileusnic & Loeb, 2006; Proske & Gandevia, 2012). Sensory endings of GTOs innervate the region of the muscle where extrafusal fibers connect to the tendon. When a

muscle activates, deformation of mechanoreceptors in the sensory endings excite the endings of 1b afferents. This generates action potentials related to the tension caused by the muscle activation.

Each GTO has endings that sense the tension from more than 10 extrafusal fibers. Many of the extrafusal fibers that compose the receptive field (RF) of a single GTO are activated by different motor units; i.e., GTOs "pool" inputs across fibers from many motor units (Jami, 1992; Arthur Prochazka & Ellaway, 2012). Consequently, GTOs tend to encode the average tension across the whole muscle rather than the tension of individual motor units. Classically, GTOs were thought to respond primarily to actively-generated muscle tension (Jami, 1992; Jansen & Rudjord, 1964). Some recent studies have shown that passive muscle stretch can also activate GTOs (Gregory, Brockett, Morgan, Whitehead, & Proske, 2002; Vincent et al., 2017). GTOs are also sensitive to vibration (Fallon & Macefield, 2007) and electrical stimulation of the parent muscle (Pratt, 1995).

Cutaneous Receptors:

Cutaneous receptors also play a role in the sensation of body conformation, especially in the sensation of finger position where muscle lengths are a function of potentially many joints (Proske & Gandevia, 2012). Evidence suggests that signals from cutaneous receptors can be used to accomplish proprioceptive goals. First, firing rate changes of cutaneous receptors during joint flexion can resemble those of muscle spindle afferents when the RF of the cutaneous field spans the joint (Edin, 1992; Edin & Johansson, 1995). Artificially stretching the skin *as if* the

joint were flexing evokes an illusory perception of an altered joint angle, even when the joint itself is stationary (Collins, Refshauge, Todd, & Gandevia, 2005). Cortical neurons with cutaneous receptive fields (RFs) can be used to decode limb position with accuracy similar to that obtained using neurons with muscle-like RFs (Weber et al., 2011). These data support a secondary role for cutaneous afferents in the proprioceptive sense, supplementing the signals from muscle receptor afferents.

Joint Receptors:

Less is known about joint receptors than either cutaneous or muscle receptors. Early studies considered them to be an important source of information about the kinematics of the limb; since then, recordings from these receptors have demonstrated that they do not typically respond across the full range of joint movement. Instead, they only modulate their firing rates when near extremes of joint position (Burgess & Clark, 1969; Burke, Gandevia, & Macefield, 1988), making them a poor sensor for joint kinematics. Joint replacement surgery has little effect on kinematic proprioceptive acuity, even when the entire joint capsule is removed along with all joint receptors (Karanjia & Ferguson, 1983).

Though joint receptors don't seem to encode joint kinematics, that doesn't mean they are not an important proprioceptive receptor. Joint receptors are probably important in tasks where the internal stresses of the joint itself need to be controlled, such as during weightlifting or to compensate for an injury (Alessandro, Rellinger, Barroso, & Tresch, 2018; Proske & Gandevia, 2012). There is no standard test to identify these receptors from passive mapping of RFs, so I

was unable to identify the responses of this afferent class in my CN recordings.

Dorsal Column Nuclei

Proprioceptive signals travel centrally via at least two major sensory pathways, which share the dorsal column until the brainstem. Pseudo-unipolar axons transmit action potentials from somatosensory receptors into the spinal cord via the dorsal roots. The axons of these neurons join the dorsal columns, the predominant ascending tracts of the spinal cord (Fig 1.1C) (Kandel, Schwartz, & Jessell, 1991). The dorsal columns are divided into two major compartments, the gracile and cuneate fasciculi, which carry somatosensory signals from the lower and upper limbs, respectively. The axons in the dorsal column tracts are not exclusively first order sensory neurons (i.e., not all are direct axons from sensory receptors); many are spinal interneurons that send collateral axons into the dorsal columns. Estimates put the percent of first-order axons in the dorsal columns at around 60% (Giesler, Nahin, & Madsen, 1984).

Dorsal Column Anatomy

Proprioceptive signals travel widely across the brain and subserve processes that underlie the perception of the body and the generation of movement. The cuneate and external cuneate nuclei lie at the base of this extensive processing pathway. Most of the upper limb proprioceptive information is transmitted through these nuclei, while lower limb somatosensory information travels through the gracile nucleus (Figure 1.1D). Given the location and size of these areas, they have received little attention relative to the more accessible cortical

somatosensory areas.

Anatomically, CN is divided into a few distinct subnuclei (Biedenbach, 1972; Loutit, Vickery, & Potas, 2021). The rostral CN (rCN) lies rostral to the obex and is composed of neurons with large cell bodies that receive "deep" inputs primarily from the forelimb and torso (Bermejo, Jiménez, Torres, & Avendaño, 2003; Cheema, Whitsel, & Rustioni, 1983; Fyffe, Cheema, & Rustioni, 1986). rCN and the external cuneate nucleus (ECN) lie close to each other and neurons in these areas have similar receptive field properties, making the boundary between the regions difficult to distinguish.

A second subnucleus, called the middle cuneate nucleus (CuM), lies caudal to rCN (Loutit et al., 2021). CuM is further subdivided into the shell, clusters, and ventral regions, each of which contains neurons with distinctive RF profiles. The clusters have the smallest RFs of any region of the CN, typically located on the hands, suggesting that this region may specifically transmit tactile information that has fine spatial requirements (C. X. Li, Yang, & Waters, 2012). The shell receives inputs from proximal arm muscles and skin receptors. Ventral CN ("pars triangularis" in primates) also receives primarily muscle-related signals from the proximal arm (Hummelsheim & Wiesendanger, 1985; Hummelsheim, Wiesendanger, Wiesendanger, & Bianchetti, 1985).

The caudal CN (CuC) has properties similar to CuM, but with a higher percentage of Pacinian-like responses (responsive to high frequency cutaneous vibration) (Cheema et al., 1983; Dykes,

Rasmusson, Sretavan, & Rehman, 1982). Overall, CN has a complex somatotopic arrangement of modality and receptive field location across its various subnuclei.

CN projects to various brainstem and midbrain nuclei in addition to the canonical connection to thalamus via ML. The clusters (responsible for discriminative touch), send projections to pontine nuclei, as well as back down into the spinal cord. The shell regions of CN send projections to inferior olive, zona incerta, peri-aqueductal grey, tectum, and pretectal regions. Rostral CN sends projections to and receives inputs from the reticular formation. ECN and ventral CN send inputs back down the spinal cord, as well as reciprocal connections with the magnocellular region of the red nucleus (Loutit et al., 2021).

These connections, too numerous to describe in significant detail here, demonstrate that the DCN is the base of a distribution hub for proprioceptive information throughout the subcortical brain in addition to the somatosensory cortex. Further research into each of these connections will help determine how CN contributes to the processing of somatosensory information for sensation and motor control.

Proprioceptive Thalamus:

Thalamic Anatomy:

Axons from cuneate and gracile nuclei join into a white-matter tract known as the medial lemniscus (ML). The ML decussates in the medulla and projects to the contralateral thalamus. Neurons with cutaneous RFs project to ventroposterolateral nucleus (VPL) while those with

proprioceptive RFs project primarily to regions known as ventroposterior oralis (VPo) or ventroposterior superior (VPS) (Hummelsheim & Wiesendanger, 1985; J. H. Kaas, Nelson, Sur, Dykes, & Merzenich, 1984; Mackel & Miyashita, 1993; Rosén, 1969). Anatomically, proprioceptive thalamus has various designations that vary across species, making it difficult to draw a simple picture of proprioceptive anatomy in the thalamus.

Thalamic Proprioceptive Coding:

We understand even less about proprioceptive coding in thalamus than CN. To my knowledge, there are no published recordings of single neurons in proprioceptive thalamus during arm movements of an awake animal. Recordings from VPL of anesthetized monkeys reveal a moderate convergence of cutaneous and muscle primary afferents, with around 40% of neurons responding to stimulation of both cutaneous and proprioceptive peripheral nerves (Home & Tracey, 1979). Recordings from VPL during head and neck rotations show that VPL neurons preferentially encode externally applied rather than self-generated movements (though this study notes that these properties are inherited from the cerebellum rather than the medial lemniscus) (Dale & Cullen, 2019). We need to characterize thalamic responses during awake behavior before we can understand how the thalamus contributes to the processing of proprioceptive stimuli.

Somatosensory Cortex:

Somatosensory Cortical Anatomy:

From the thalamus, somatosensory signals project to four distinct cortical areas. Moving caudally from the central sulcus, Brodmann's areas 3a, 3b, 1, and 2 comprise the primary somatosensory cortex (S1), though this designation is facing increasing skepticism due to the multimodal nature of area 2 (Figure 1.1E) (Delhaye, Long, & Bensmaia, 2018). These areas have distinct cytoarchitectural and receptive field properties, suggesting that they serve different roles in the processing of somatosensation.

Each of these regions receives specialized thalamic and cortical inputs that hint at their function (Huffman & Krubitzer, 2001a; Padberg et al., 2009; Padberg, Cooke, Cerkevich, Kaas, & Krubitzer, 2019). Area 3a, deep in the central sulcus and closely connected to the adjacent primary motor cortex (area 4), receives a plurality of its thalamic input not from somatosensory thalamus, but from ventrolateral posterior thalamus (VLp), which is typically considered a "motor" thalamic nucleus (Krubitzer, Huffman, Disbrow, & Recanzone, 2004). Neural responses in VL often occur coincidentally with movement, rather than with the lag caused by conduction delays. This suggests that VL receives output from a forward model (Dooley, Sokoloff, Blumberg, & Dooley, 2021). Area 2 receives convergent inputs from cutaneous and proprioceptive regions of thalamus (VPS and VPL) (Padberg et al., 2009).

Interestingly, there seem to be relatively weak connections between area 3a and area 2, contrary to the commonly assumed areas 3a-to-2 route for proprioception. This split suggests that there

are parallel streams of proprioceptive information at the cortical level, with a rostral branch

travelling to area 3a and a second caudal branch travelling to area 2 (Padberg et al., 2019).

Caudal to area 2 lies the most rostral of the posterior parietal cortices, area 5, which has strong

connections from area 2 (Gardner, Babu, Ghosh, Sherwood, & Chen, 2007; Padberg et al.,

2019). Area 5 is tightly coupled with the multimodal association area 7, which is part of the

dorsal visual stream. Area 5 and area 7 project strongly to premotor cortical areas, suggesting a

role for the caudal pathway comprising areas 2, 5 and 7 in the planning and correction of

visually guided movements (Inoue & Kitazawa, 2018).

Proprioceptive coding in somatosensory cortex

Area 3a, due to its inaccessibility deep in the central sulcus, has received relatively little

attention. Neurons in area 3a typically receive only muscle receptor inputs, which makes it an

attractive region for the study of proprioception. Experiments in area 3a indicate a relatively low

degree of convergence at the level of single neurons, with only ~10% of neurons responding to

more than one of two proprioceptive peripheral nerves in the forearm (Phillips, Powell, &

Wiesendanger, 1971). Neurons in 3a respond to vibratory stimuli with low latency and high

fidelity, suggesting they largely resemble the signals from primary muscle spindle afferents (E.

G. Jones & Porter, 1980; Phillips et al., 1971). One experiment found, as expected, that firing

rates of area 3a wrist flexor-receiving neurons increased during passive wrist extension.

Strangely, only half of those neurons' firing rates increased during active wrist extension

(Yumiya, Kubota, & Asanuma, 1974). The other half increased their firing rates during active

wrist flexion. The researchers suggested that gamma drive may invert the preferred direction in some cases.

Recordings from area 2 during reaching tasks have laid the groundwork for understanding how the brain encodes proprioceptive information. Prud'homme and Kalaska found tuning properties reminiscent of those reported in primary motor cortex, namely sinusoidal tuning to endpoint velocities across directions (A P Georgopoulos, Kalaska, Caminiti, & Massey, 1982; Prud'homme & Kalaska, 1994). Based on these results, and the then-prevalent hypothesis that motor cortex controls the endpoint rather than muscles, many hypothesized that somatosensory cortex might also transform intrinsic (i.e., muscle-based) coordinates to an extrinsic (i.e., hand centered) coordinate frame. This transformation would allow somatosensory cortex to supply motor cortex with feedback in the coordinate frame of its presumed control (Apostolos P. Georgopoulos, Schwartz, & Kettner, 1986). Recent results, however, indicate that somatosensory encoding in area 2 retains information about the conformation of the entire arm. This finding does not support the endpoint-coordinate hypothesis, which predicts that proprioceptive representations should be invariant to changes in the posture of the arm that do not change the endpoint kinematics (Chowdhury, Glaser, & Miller, 2020).

Responses of neurons in area 5 have sinusoidal tuning with respect to the hand endpoint velocity, much like responses of area 2 neurons. However, while area 2 firing rates encode endpoint force, area 5 neurons do not (Prud'homme et al., 1994). Area 5 has strong reciprocal connections with area 7, a multi-modal visual area and part of the dorsal visual stream (the

"vision-for-action" pathway (Hebart & Hesselmann, 2012)) (Padberg et al., 2019). Since forces are not visible, area 5 may remove force-like signals so that proprioceptive and visual models of the arm can be combined. This tight coupling of area 5 to area 7 as well as the connections of area 5 to premotor areas, suggest that the posterior parietal cortex is involved in visual guided reaching behaviors (Inoue & Kitazawa, 2018; Schaffelhofer & Scherberger, 2016).

Cerebellar Proprioceptive Pathway:

A second major pathway for proprioceptive information is through the cerebellum. The upper and lower limb proprioceptive spinocerebellar pathways have modest differences in their anatomy. For the lower limb, a large fraction of proprioceptive afferents terminate in a spinal nucleus known as Clarke's column (Bloedel & Courville, 1981). Axons from Clarke's column travel up the dorsal spinocerebellar tract and through the inferior cerebellar peduncle, where they branch and synapse in both the cerebellar cortex and nuclei (interpositus, dentate, and fastigial) (Thanawalla, Chen, & Azim, 2020).

For the upper limb, ECN (near to rCN in the medulla) serves as the forelimb analog to Clarke's column (Loutit et al., 2021; Rosén & Sjölund, 1973). ECN projects primarily (though not exclusively) to the cerebellum via the inferior cerebellar peduncle and forms a portion of the mossy fiber inputs (Hummelsheim & Wiesendanger, 1985). The cerebellum also receives substantial descending motor inputs, possibly efference copy signals (Kawato, Ohmae, Hoang, & Sanger, 2020; R. C. Miall & Wolpert, 1996; Shadmehr & Krakauer, 2008).

The cerebellum has only a single class of output neuron, the deep cerebellar nucleus neuron (Kandel et al., 1991). These neurons project to a variety of locations in the brain, including thalamus, red nucleus, inferior olive, and back down the spinal cord (Thanawalla et al., 2020). The function of these cerebellar projections is still an ongoing topic of research, but some of these pathways may help to generate movements and learn new environments. Disruption of cerebellar thalamus or cerebellum itself disrupts learning, for example (Chen, Hua, Smith, Lenz, & Shadmehr, 2006). Additionally, signals sent to the inferior olive are thought to help update the cerebellar forward model in light of prediction errors (Herzfeld, Kojima, Soetedjo, & Shadmehr, 2018; Shadmehr, 2020).

Cerebellum also projects to the ventrolateral thalamus (VL) (Dooley et al., 2021). VL has strong projections to premotor and motor cortices, as well as to area 3a (Huffman & Krubitzer, 2001b; Padberg et al., 2009). I discuss the hypothesis that the cerebellum provides predicted proprioceptive signals to cortex via this cerebellar circuit in the sections below, and in detail in Chapter 5.

Open questions of proprioceptive coding in CN

Studies of the dorsal column pathways began in earnest in the 1950s and quickly pinned down anatomical and morphological features of the dorsal column nuclei (CHANG & RUCH, 1947). These studies discovered a diverse set of projection targets from different sub-regions of the DCN, discussed above (Berkley, Budell, Blomqvist, & Bull, 1986). During this period, researchers characterized the effects of descending drive and temporal patterning of inputs on

the transmission through CN (Andersen, Eccles, Oshima, & SCH, 1964; Andersen, Eccles, Schmidt, & Yokota, 1964a, 1964b).

With notable exceptions, these experiments were conducted on anesthetized animals (Ghez & Pisa, 1972). Interest in CN waned in the late 20th century, but in the past few years optogenetic and electrophysiological techniques have revitalized interest in this first stage of somatosensory processing in the brain. In this section, I review the major open questions regarding proprioceptive encoding in CN.

Sensory gating in CN

Many early experiments studying CN of anesthetized animals demonstrated that descending signals have a strong effect on how CN encodes sensory inputs. Andersen et al., 1964 probed the effects of descending drive by pairing cortical and peripheral nerve stimulation in the cat. In this experiment, they electrically stimulated a tactile peripheral nerve while recording from the medial lemniscus (ML) (Andersen, Eccles, Oshima, et al., 1964). The magnitude of the ML evoked potential is related to the strength of the signal that passes through CN and into the thalamus. When they paired stimulation of the nerve with stimulation of motor cortex, they found that the response evoked from the nerve was smaller than without the cortical stimulation. This attenuation lasted for around 100 ms and, in subsequent experiments, was shown to be related to presynaptic inhibition in CN.

From these experiments, we know that motor cortex exerts significant presynaptic inhibition onto the first and second order afferent terminals in CN. These findings suggested that descending drive might "gate" irrelevant somatosensory information during movement in a process similar to saccadic suppression (Azim & Seki, 2019; Crevecoeur & Kording, 2017). This sensory gating hypothesis has been an influential theory for how processing in CN affects somatosensory coding.

To test this sensory gating hypothesis, Ghez and Pisa recorded from the medial lemniscus of a cat performing a lever-pressing behavior. By stimulating tactile peripheral nerves at different phases of stance and lever pressing, they quantified evoked activity in ML as a function of descending motor output. As predicted by the sensory gating hypothesis, tactile sensory gain was negatively correlated with the speed of the cat's paw. The level of presynaptic inhibition also increased as a function of paw speed (Ghez & Pisa, 1972). These results strongly support the sensory gating hypothesis for the tactile system.

While it is possible that most tactile signals are irrelevant during a reaching task, proprioceptive signals are particularly important during active movements. An external force that moves the arm may not be relevant when your arm is hanging at your side, but it is extremely important when you are climbing a rock wall. Blanket reduction in proprioceptive gain during movement doesn't seem to make much sense. In my research, I tested whether there was sensory gating of proprioceptive signals during active monkey reaching tasks.

Receptor convergence in CN

How receptors converge along the sensory pathway underlies the most basic goals of a sensory system, combining signals to generate useful representations of the world. In the tactile sense, receptor convergence produces neurons in CN with receptive fields that can perform simple edge detection, and these combinations go a long way towards explaining the variety of tactile responses in somatosensory cortex (Suresh et al., 2021). In a similar vein, proprioceptive convergence in CN could create useful combinations of receptors that simplify control of the limb.

The extent of proprioceptive convergence onto single CN neurons is still unclear. One study showed that most CN neurons respond to stimulation of more than a single peripheral nerve, even nerves of different sensory modalities (C. L. Witham & Baker, 2011). A second study, in which muscles of the forearm were disarticulated and pulled independently, showed that most CN neurons respond to signals from only a single muscle (Hummelsheim & Wiesendanger, 1985). This discrepancy was difficult to reconcile, until a recent study using patch clamp recordings of CN neurons demonstrated that while there are potentially many hundreds of synaptic inputs to single CN neurons, typically only 4-8 have substantial weights and dominate the rest (Bengtsson, Brasselet, Johansson, Arleo, & Jörntell, 2013a). This organization may serve an important function in allowing CN to flexibly reroute inputs.

Functional Roles of Proprioception:

The brain does not exist to represent movements, but to generate them (Shenoy, Sahani, & Churchland, 2013). Therefore, the proprioceptive processing in CN described above must serve a functional goal. In this section, I will review some functional goals of proprioception, emphasizing how modulation and convergence at the level of CN may contribute to these goals. I also emphasize the control systems approach to understanding the motor system, providing important background for the dynamical feedback control model presented in Chapter 5.

Hierarchical Reflex Loops:

An important role for proprioception is to generate automatic, subconscious responses to perturbations. A well-known example is the spinal stretch reflex, in which a muscle contracts involuntarily to counteract an externally applied stretch. This reflex acts through synapses that connect muscle spindle primary afferents directly to alpha-motoneurons of the stretched muscle. This direct connection provides low latency feedback that can rapidly correct for unexpected perturbations. While the stretch reflex is very simple, reflexes in the spinal cord can also produce more complex motor patterns, including those that take into account the posture of the whole arm (Weiler, Gribble, & Pruszynski, 2019).

Without the ability to modulate spinal reflexes, we would struggle to move. If the stretch reflex were always active, intentional elbow flexion would evoke the stretch reflex in triceps, halting the desired movement. To prevent this from happening, descending signals inhibit the presynaptic terminal of the connection from triceps muscle spindle primary afferents to triceps

alpha-motoneurons. This presynaptic inhibition turns down the gain on the stretch reflex, allowing voluntary movements to proceed unimpeded by reflexive activity (Meunier & Pierrot-Deseilligny, 1989).

While spinal reflexes are relatively simple, reflexes that rely on circuits in the brainstem and cortex can evoke even more complex, context-dependent responses to perturbation; these responses can switch targets and avoid obstacles within 100 ms of a perturbation (Nashed, Crevecoeur, & Scott, 2014). Studies of human motor control have revealed a hierarchy of reflexes that convert proprioceptive signals into muscle activity with impressive flexibility and speed (Kurtzer, Pruszynski, & Scott, 2008; Maeda, Cluff, Gribble, & Pruszynski, 2018; Pruszynski et al., 2011a; Scott, 2016). It is still unclear how these long-latency reflexes gain the ability to respond with such a high degree of flexibility.

Modulation of sensory gain at the level of CN may play an important role in fine-tuning sensory-motor reflex loops, but prior to my work the sign and magnitude of proprioceptive gain modulation was unknown. By testing the strength of the encoding of proprioceptive information at the level of CN across conditions, we can begin to unravel the mechanisms behind context-dependent reflexes.

Error Correction and Model Update

When we act in the real world, things do not always go according to plan. For example, say you are out playing tennis on a windy day. You go to return a serve and the wind picks up as you hit

the ball, causing your shot to veer wide. This change in environment and resulting motor error has the potential to be catastrophic (especially if it's your job to hit tennis balls). It is critical that the motor system recognize motor errors when they occur, correct them quickly, and update the control system in light of the error. A recent paper suggests that CN may compute these prediction errors by combining information from descending signals and ascending sensory information (Conner et al., 2021), but this prediction-error hypothesis has never been tested during awake behavior.

In order to have a prediction error, one first needs to have a prediction (R. C. Miall & Wolpert, 1996). In control theory, a block that takes in motor commands ("efference copy") and outputs a sensory prediction is known as a "forward model". A comparator, compensating for timing mismatches, can subtract this prediction from the actual incoming sensory information to compute an error signal, or the deviation of the actual sensory information from predicted sensory information. Putting it another way, the forward model computes the expected sensory consequences of an action ("prediction") and the comparator subtracts that from the actual signals ("afference") to compute the deviation from the prediction ("error"). If the afference is composed entirely of signals that are generated by the movement ("reafference") and the model is correct, there will be zero error. Non-zero error signals could arise from a combination of existing inaccuracies in the forward model ("I need to practice my return!") or unexpected changes in the environment (exafference, i.e., "I need to compensate for the wind").

Work done primarily in the oculomotor system has found components that resemble parts of a

forward model and a comparator in the Purkinje cells, deep cerebellar nuclei, and inferior olive.

This interpretation has been extended recently to the vestibular and proprioceptive senses

(Brooks, Carriot, & Cullen, 2015). The authors of one study found that cerebellar output

neurons selectively cancel reafference and encode only exafference. This exafferent signal is

present in somatosensory thalamus (VPL) (Dale & Cullen, 2019), suggesting that the

somatosensory cortex may receive information about motor errors from the cerebellum. Motor

cortex may use this error signal to perform online correction of motor errors and to update

future motor plans.

Damage to the cerebellum compromises the ability to adapt to both novel dynamical

environments and to visual perturbations, such as visuomotor rotations (Earhart & Bastian,

2001; Izawa, Criscimagna-Hemminger, & Shadmehr, 2012; M. A. Smith, Ghazizadeh, &

Shadmehr, 2006). Patients with cerebellar damage are typically unable to adapt their motor

plans, even in the face of consistent errors in performance. Disruption of cerebellar thalamus

similarly disrupts adaptation (Chen et al., 2006), suggesting that the cerebello-thalamo-cortical

pathway transmits these error signals for use by motor planning modules in cortex.

Interestingly, intact cerebellar circuits are not the only proprioceptive areas required to adapt to

a new environment. In a study by Mathis et al., inhibition of somatosensory cortex abolished the

ability of mice to adapt to a force field. Inhibiting S1 after partial adaptation prevented further

learning but did not cause the mice to revert to the pre-adaptation state (M. W. Mathis et al.,

2017). The mice instead "cached" their learning but could not continue to learn without S1. This suggests that both the cerebellum and the somatosensory cortex are necessary to consolidate motor learning. If the cerebellum provides the error signal, how are signals from somatosensory cortex used to help adapt the motor plan? This question is the topic of ongoing research.

While the prevailing hypothesis is that the cerebellum builds forward models (Shadmehr & Krakauer, 2008), other groups have suggested that CN may also perform this function (Conner et al., 2021). In this hypothesis, the combination of descending inputs from motor areas and ascending sensory information computes a prediction error. No one has explicitly tested whether CN computes prediction errors for proprioceptive or tactile signals. As part of my research, I addressed this question using recordings in CN of a monkey performing a well-learned motor task, in which the sensory inputs should be predictable across trials. I found no evidence that neurons in CN preferentially encode prediction error signals; predictable actively generated movements are slightly *more* strongly encoded in CN than unpredictable passive movements.

Conscious Perception of Limb State

Nothing in the above functional roles of proprioception requires that information about the state of the limb be consciously available. Indeed, both reflexes and model updates can occur without conscious awareness that they are occurring (Albert et al., 2020; J. A. Taylor, Krakauer, & Ivry, 2014; Whelan, 1996). Therefore, it is necessary to call out conscious sensation of limb state separately from the functions described above.

Perhaps the most striking examples of conscious proprioception are "phantom limbs" that remain after amputation. For example, many transradial amputees feel as though their hand is still there and can even "open" and "close" their phantom hands (Proske & Gandevia, 2012; Walsh, Gandevia, & Taylor, 2010b). Interestingly, congenital amputees almost never feel these phantoms, while they are relatively common for acquired amputees (Hahamy et al., 2017; Wesselink et al., 2019). This suggests a developmental process by which the limb is incorporated into the conscious body image. Synaptic inputs to CN neurons are pruned heavily during development, which coincides with invasion of CN from corticobulbar fibers (Fisher & Clowry, 2009). CN may be important for generating this conscious model of the limb, but how exactly this process of developmental pruning occurs is still unclear. I investigated the convergence properties of individual neurons in CN, which might give insight into how this conscious model of the arm is generated.

Studies of area 5 and area 7 suggest that they may cooperate to generate a model of the arm using proprioceptive and visual information, respectively. A woman with a lesion in superior parietal lobe "lost" her contralateral arm when she was deprived of vision of it for more than a few seconds (Wolpert, Goodbody, & Husain, 1998). Similarly, researchers ablated either area 5 or area 7 in monkeys and tested their ability to reach in either light or darkness. Monkeys with area 5 lesions could not make reaches in darkness but could do so when the lights were on. Monkeys with area 7 lesions could make reaches in darkness, but not in light (Rushworth, Nixon, & Passingham, 1997). Without visual input (in darkness), you need area 5 to reach. With visual input, you need area 7 to reach. How exactly the motor system might use this combined

visual and proprioceptive model of the arm is unclear; I lay out a model in Chapter 5 that considers this question through the lens of optimal feedback control.

Summary

In this introduction, I described the receptors that comprise the sense of proprioception, various pathways by which proprioceptive information branches throughout the brain, an overview of research into CN and its specific functional role at the base of this proprioceptive tree, and how proprioception contributes to motor control and perception of limb state. The following chapters will detail my doctoral work examining neural representations in CN and comparing them with recordings from area 2 of the somatosensory cortex. In a final review and perspective, I present a novel framework that seeks to explain how proprioceptive feedback is transformed into motor output via dynamics in motor cortex.

Chapter 2 focuses on the methodological and surgical advances developed to record chronically from the CN of awake monkeys. In this paper, I detail the first ever recordings of single neurons in CN of an awake behaving animal. I quantify the longevity and stability of these arrays, and briefly describe the tuning properties of the recorded proprioceptive neurons.

In Chapter 3, I further investigate the extent of sensory gain modulation and convergence properties in CN. A hypothesized role of CN is to gate sensory signals during movement as to stop them from interfering with motor execution. I was able to test this hypothesis in the awake monkey, and found that the proprioceptive signals are mildly potentiated, on average, rather

than broadly attenuated as the sensory gating hypothesis predicts.

Chapter 4 broadly compares the proprioceptive encoding properties of CN and area 2, finding that many response properties of proprioceptive cortical neurons exist already at the level of CN, and likely at the receptor level itself. This raises a pressing question; to what end are signals processed along the somatosensory neuraxis? I discuss this problem at a high level and present a review of our understanding of proprioception along the neuraxis.

Finally, in Chapter 5 I present a model that links proprioceptive feedback to motor control circuitry. This model attempts to build a bridge between two major paradigms in the study of motor control in the brain, optimal feedback control and neural dynamical systems. The final chapter will discuss the implications of these results, and detail methodological improvements needed to advance our understanding of the role of CN at the base of the proprioceptive sense in the brain.

Chapter 2 – Methodological considerations for a chronic neural interface with the cuneate nucleus of macaques

Aneesha K. Suresh, Jeremy Winberry, Christopher Versteeg, Raeed Chowdhury, Tucker Tomlinson, Joshua M. Rosenow, Lee E. Miller, & Sliman J. Bensmaia

Foreword

The following was adapted from a manuscript published in the Journal of Neurophysiology in December 2017. I contributed data for Figures 2.2, 2.5, 2.6, 2.8, and Table 2.1. My contribution to this manuscript details the procedure and history of awake recordings from CN, focusing on the proprioceptive sense.

Abstract

While the response properties of neurons in the somatosensory nerves and anterior parietal cortex have been extensively studied, little is known about the encoding of tactile and proprioceptive information in the cuneate nucleus (CN) or external cuneate nucleus (ECN), the first recipients of upper limb somatosensory afferent signals. The major challenge in characterizing neural coding in CN/ECN has been to record from these tiny, difficult to access brainstem structures. Most previous investigations of CN response properties have been carried out in decerebrate or anesthetized animals, thereby eliminating the well-documented top-down signals from cortex, which likely exert a strong influence on CN responses. Seeking to fill this gap in our understanding of somatosensory processing, we describe an approach to chronically implant arrays of electrodes in the upper limb representation in the brain stem in primates. First,

we describe the topography of CN/ECN in Rhesus macaques, including its somatotopic

organization and the layout of its submodalities (touch and proprioception). Second, we describe

the design of electrode arrays and the implantation strategy to obtain stable recordings. Third,

we show sample responses of CN/ECN neurons in brainstem obtained from awake, behaving

monkeys. With this method, we are in a position to characterize, for the first time,

somatosensory representations in CN and ECN of primates.

Introduction

A central question in neuroscience is how sensory representations are transformed as they

ascend the neuraxis. In primates, the coding of tactile and proprioceptive information has been

extensively studied in the nerve and in anterior parietal cortex (APC), which encompasses

Brodmann's areas 3a, 3b, 1 and 2. Sensory representations in APC differ from those at the

periphery in several important ways. First, while cutaneous and proprioceptive nerve fibers can

be classified into a small number of submodalities, each responding to a different aspect of skin

or muscle/tendon stimulation, individual APC neurons integrate sensory signals from multiple

submodalities (Prud'homme & Kalaska, 1994; Hannes P. Saal & Bensmaia, 2014). Second,

APC neurons tend to respond selectively to behaviorally relevant stimulus features, while

afferents are less selective (Bensmaia, Denchev, Dammann, Craig, & Hsiao, 2008; Michael A.

Harvey, Saal, Dammann, & Bensmaia, 2013). In the context of proprioceptive responses,

cortical neurons convey complex information about limb state compared to peripheral afferents

(Costanzo & Gardner, 1981; Gardner & Costanzo, 1981; B. M. London & Miller, 2013; Brian

M London, Torres, Slutzky, & Miller, 2011). Little is known about the coding of upper limb

tactile and proprioceptive information in brainstem nuclei and the ventroposterior nucleus of the

thalamus. Here, we discuss methodological issues associated with recording from the cuneate

nucleus (CN) and external cuneate nucleus (ECN) of awake primates using chronically

implanted electrode arrays (see also Richardson et al. 2015, 2016) and discuss preliminary

results on the response properties of CN/ECN neurons in awake primates.

Recording from the CN/ECN of awake primates may offer key insights into sensorimotor

representations of the upper limb. First, while CN responses are modulated by descending

cortical input (Andersen, Eccles, Oshima, et al., 1964; Andersen, Eccles, & Schmidt, 1962), the

properties of CN neurons have been almost exclusively studied in anesthetized or decerebrate

cats (Andersen et al. 1964b; Andersen et al. 1964; Jabbur and Banna 1968; O'Neal and

Westrum 1973; Canedo et al. 2000; Hayward et al. 2014; Jörntell et al. 2014) whose descending

input is thus abolished. To the extent that the sensory response properties of CN neurons are

shaped by this descending input, then, studies of these properties without this input may be

misleading.

Second, it is unclear to what extent neural coding in cat CN/ECN will resemble its primate

counterpart because cats and primates use their upper limbs in different ways, especially their

paws/hands. In fact, the morphological organization and mechanisms of synaptic processing

differ between primates and cats (Harris et al. 1965; Biedenbach et al. 1971; Molinari et al.

1996), highlighting the need to repeat in non-human primates studies conducted in cats to

understand the organization, response properties, and circuitry in primates. Furthermore, while

ECN of cats projects solely to the cerebellum, ECN of primates also projects to the ventral posterolateral nucleus of the thalamus (Boivie & Boman, 1981). The functional implications of this divergence have yet to be determined.

In the present study, we first established the somatotopic and submodality (cutaneous vs. proprioceptive) topography of CN/ECN in anesthetized Rhesus macaques using a standard electrode microdrive. Although anatomical tracing studies have been carried out in various non-human primates (Otolemur garnetti, Aotus trivirgatus, Saimiri sciureus, Macaca radiate, Macaca mulatta) (Florence, Wall, & Kaas, 1988; Hummelsheim & Wiesendanger, 1985; Qi & Kaas, 2006), somatotopic electrophysiological mapping has not been reported and the precise location and extent of the nuclei, necessary for a chronic implant, were not provided. Second, we developed and deployed an approach to chronically implant electrode arrays in CN/ECN, which allowed us to record the responses of CN/ECN neurons in awake, behaving macaques. Third, we characterized the stability of the neuronal signals measured through the electrode arrays and the stability of the receptive fields (RFs). These results build a foundation towards exploring, for the first time, tactile and proprioceptive coding in the CN and ECN of intact, awake, and behaving animals.

Methods

Surgical approach for acute mapping procedures

All experimental protocols complied with the guidelines of the University of Chicago Animal Care and Use Committee, the Northwestern University Animal Care and Use Committee, and

the National Institutes of Health Guide for the Care and Use of Laboratory Animals. Surgical

anesthesia was induced with ketamine HCl (3 mg/kg, i.m.) and dexmedetomidine (75 µg/kg),

and maintained with Isoflurane (1%). The animal's head was held in a stereotaxic frame, and

positioned such that its neck was flexed approximately 75 degrees relative to the trunk. First, we

made a midline incision from the occipital bone to approximately segment C3. Using cautery,

we divided the posterior cervical muscles along the midline raphe and removed them from the

occipital bone and the posterior ring of segment C1 in a subperiosteal plane. Next, we exposed

the foramen magnum and the occipitocervical dura between C1 and the foramen using a

combination of gentle monopolar cautery and sharp dissection. Excess soft tissues were

removed to expose clean dura. We enlarged the foramen magnum cranially and laterally using

Kerrison rongeurs and excised the dura to provide access to the brain stem both cranially and

caudally relative to the obex. We made single electrode penetrations at various depths within the

exposed brainstem (Figure 2.1).
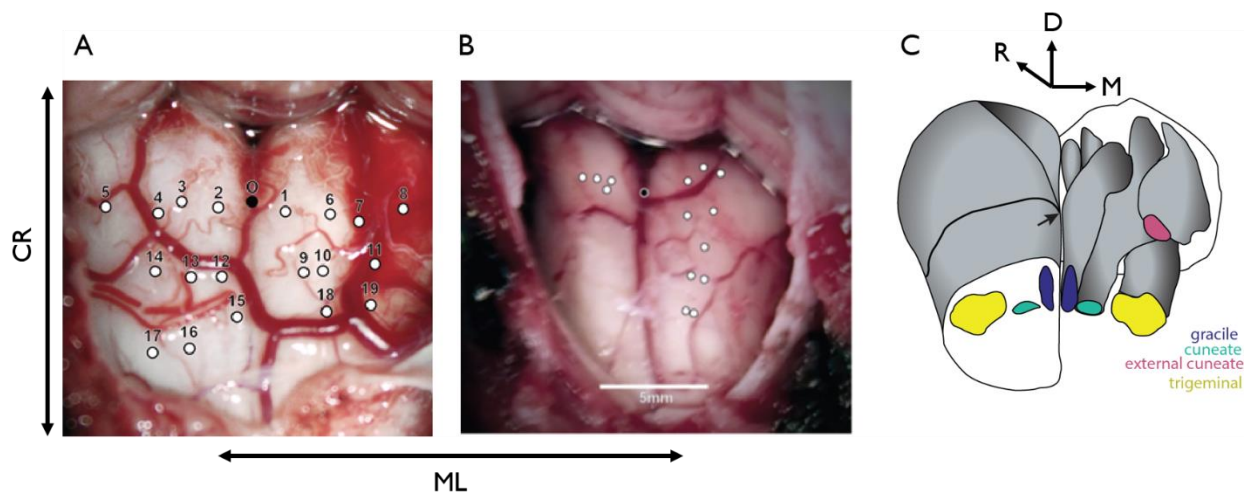
Figure 2.1: Surgical Exposure for two acute procedures. Each white circle represents a
penetration site: CR (caudal-rostral), ML (medio-lateral), D (dorsal) A: First acute experiment,
using low impedance (0.5 MOhms) electrodes, whose goal was to determine the boundaries of

gracile, cuneate, and trigeminal nuclei. B: Second acute experiment using higher impedance electrodes (1-4MOhms), in which we targeted primarily the right hemisphere to understand submodality organization and somatotopy. Black circle denotes the obex. Cerebellar tonsils are located at the top in both images. C: A reconstructed 3D view of the lower brainstem, and relative positioning of the gracile nucleus (dark blue), cuneate nucleus (light blue), external cuneate nucleus (pink), and trigeminal nucleus (yellow). The black arrow is pointing towards obex.

Surgical approach for chronic array implants

We followed a similar procedure for the chronic array implants as for the acute experiments, with a few exceptions. First, prior to the skin incision, we determined the optimal location for the array pedestal, taking into account skin healing and vulnerability to damage. We also considered the routing of the array lead between pedestal and brain stem, allowing for 1-2 cm of slack for neck movement after the animal woke up. Second, while exposure was similar to that in the acute experiments, the dura over the posterior fossa was opened with a midline linear incision, with the leaves tented back with 6-0 Prolene suture (Ethicon, Somerville, New Jersey). Third, before opening the dura, the pedestal was secured to the skull with bone screws, rostral to the occiput.

We implanted Utah Electrode Arrays (UEAs, Blackrock Microsystems Inc., Salt Lake City, UT), and Floating Microelectrode arrays (FMA, Microprobes for Life Science, Gaithersburg, MD) into the brainstem of 11 monkeys. Table 2.1 describes the type of array and design specifications for each implanted array. The FMAs, with electrodes of customized length, allowed us to access neurons with distal cutaneous RFs in the deeper aspects of the nucleus, while UEA electrodes with 1.5-mm long electrodes were well suited to the location of proprioceptive neurons with RFs on the proximal limb (see below).

Table 2.1: Array specifications for each animal.

Monkey ID	Array Type	Size (mm)	Electrode lengths	Manufacturing Impedance	Array Signal Longevity	Likely failure mode
WH	FMA HD	1.6 x 2.95	2.0-2.5 mm	0.5-0.9 MOhms	6 weeks	Wire bundle failure
TE	FMA HD	1.6 x 2.95	2.0-2.5 mm	0.3-1.1 MOhms	6 months	Wire bundle failure
PI	FMA SD	1.8 x 4	1.5-2.0 mm	0.4-0.7 MOhms	6 weeks	Wire bundle failure
BA	FMA SD	1.8 x 4	2.0-2.5mm	0.7-1.1 MOhms	3 weeks	Wire bundle failure
CU	FMA HD	1.6 x 2.95	2.0-2.5mm	0.4-1.0 MOhms	N/A	Fluid leakage
CH2	FMA SD	1.6x 2.8	1.5-3.0 mm	0.08-1.5 MOhms	<1 week	Array manufacturing defect
KR	FMA SD	1.8x 4.0	1.0- 2.0 mm	0.3- 1 MOhms	2 weeks	Array came out
MR	FMA HD	1.6x 2.8	1.25- 2.5 mm	0.6- 1.3 MOhms	N/A	Array did not insert
HA	FMA SD	1.8x 4.0	1.0-2.25 mm	0.5-1.0 MOhms	6 weeks	Wire bundle failure
LA1	FMA HD	1.6x 2.8	1.0-2.5 mm	0.5-1.0 MOhms	2 months	Wire bundle failure
OL	Utah	4.0x 4.0	1.5 mm	0.3-0.8 MOhms	1 day	Meningoencephalitis
LA2	Utah	4.0x4.0	1.5 mm	0.1-0.8 MOhms	>6 months	N/A
CH1	Utah	4.0 x 4.0	1.3 mm	0.2-0.8 MOhms	<1 week	Array came out

The insertion technique varied depending on the array: UEAs were implanted with the standard Blackrock pneumatic inserter and FMAs were inserted slowly with a stereotaxic instrument while being held by a vacuum wand (Musallam, Bak, Troyk, & Andersen, 2007; Rousche & Normann, 1998). Array insertion was often complicated by brain stem vascularization. Indeed, as a sizeable artery often courses along the dorsal brain stem across the desired location of the

implant (Figure 2.1A), we were occasionally forced to implant the array on the contralateral side to avoid vascular injury.

After array insertion, a thin layer of Tisseel fibrin dural sealant (Baxter Healthcare, Deerfield, IL) or Vetbond n-butyl cyanoacrylate (3M, St. Paul, MN) was placed over the array to stabilize it. Indeed, early implants that were not fixed with an adhesive appeared to be expelled from the brainstem shortly after implantation (Table 1; KR and CH1). The dura was closed with interrupted 6-0 Prolene sutures, taking care to cinch it around the wire bundle as tightly as possible. Due to the high risk of CSF leakage with posterior fossa procedures, and the fragile nature of the animals' dura, a layer of Duragen Plus (Integra, Plainsboro, NJ) followed by a layer of Tisseel was placed over the closed dura to further reduce the chance of a CSF fistula. Finally, muscle and skin were closed. Figure 2.3**Error! Reference source not found.**A and 2 .3B show the surgical exposure after insertion of each type of array.
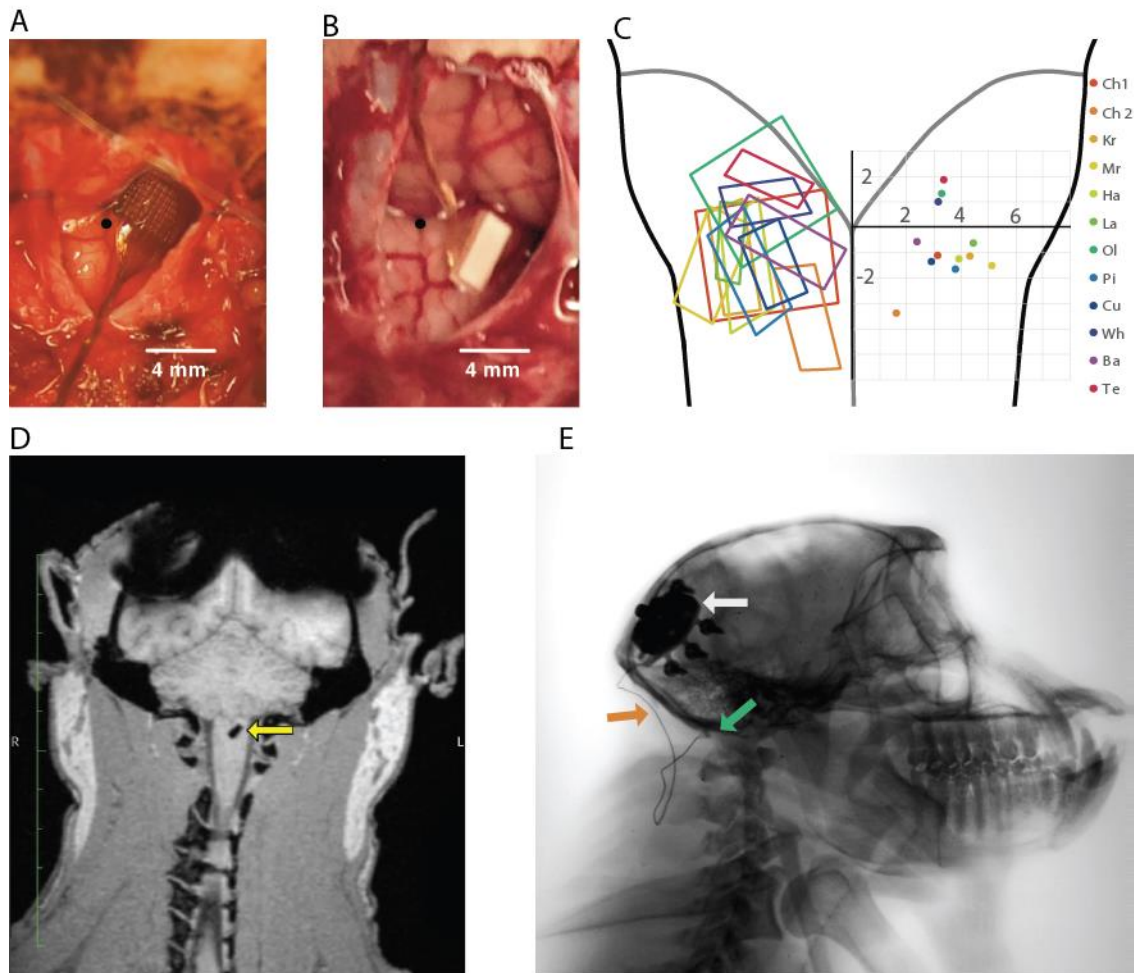
Figure 2.2: Chronic implants. A,B: Examples of an implanted UEA (A, animal Ol) and FMA (B, animal Pi). Obex is indicated by the black circle. C: Left: Approximate location of each array implant shown on a diagram of the brainstem. Right: Coordinates of the center of each array. Array locations are all shown on the same hemisphere for visualization purposes. D: 3D MRI scan 5 weeks post-implantation shows the FMA array (yellow arrow) in the brainstem of animal Ba. E: Sagittal X-ray of animal Cu shows the pedestal (white arrow), leads (orange arrow), and FMA array (green arrow) 6 weeks post-implant.

Data acquisition

In the acute experiments, neural signals were recorded using resin-coated tungsten or glass-coated platinum-iridium electrodes (FHC, Bowdoin ME) with impedances varying from 0.5 to 4 MΩ. These signals were amplified by a DAM50 amplifier (World Precision Instruments, Sarasota FL) and simultaneously played through audio speakers and displayed on an

oscilloscope. Single unit and multi-unit activity from chronically implanted electrode arrays were recorded using a Cerebus system (Blackrock Microsystems, Inc., Salt Lake City, Utah). Spikes were sorted offline using standard software (Plexon Inc., Dallas, Texas).

Receptive field mapping

While listening to the neural activity, we manipulated the animals' joints, squeezed muscles, and gently brushed the surface of the skin to determine whether the neuronal activity was driven by proprioceptive or tactile stimulation. The RFs of cutaneous units were drawn on a body diagram for later analysis. To characterize RF position of both cutaneous and proprioceptive units along the proximal-distal axis of the upper limb, we used a numeric system that defines RF location along this axis: 1- distal digits; 2- proximal digits; 3- wrist; 4-forearm; 5-elbow; 6-upper arm; 7-shoulder.

Vibrotactile stimulation

We delivered tactile stimuli to the distal pads of the digits using a stainless steel probe with a 1 mm tip diameter, driven by a custom shaker motor (Westling, Johansson, & Vallbo, 1976). We delivered sinusoidal stimuli – each 1 second long and separated by a 1-second inter-stimulus interval – at 5, 10, 20, 30, 40, 50, 100, 200, 250, and 300 Hz. Amplitudes were spaced in 10 equal logarithmic steps spanning the following ranges at each frequency: 13-250 µm for 5-50 Hz, 4–200 µm at 100 Hz, 1-100 µm at 200 Hz, 1.3 - 75 µm at 250 Hz, and 0.7-50 µm at 300 Hz. The shaker motor was calibrated before each experimental run and stimuli were presented in

pseudorandom order.

Center-out task

To study responses to passive perturbations of the arm, the monkey was trained to grasp the handle of a 2D robotic manipulandum that controlled the position of a cursor on a screen. The monkey moved the cursor to a 2 cm target in the center of the screen, held it there between 1.0 and 1.5 seconds until a force perturbation was delivered to the handle in a randomly chosen cardinal direction (forward, backward, left, right). The perturbation magnitude was 2.5 N and its duration 125 ms. Following the perturbation the monkey returned the cursor to the center of the screen to receive a liquid reward. Handle kinematics and interface forces were recorded using the Cerebus system at a sampling rate of 100 Hz. Here, we report only CN responses to the perturbation and not to active movements.

Anatomical Imaging

To confirm the position of arrays and leads after weeks of recovery, we performed x-ray on 3 animals and 3D magnetic resonance imaging on 1 animal 5-8 weeks post-implantation (Figure 2.2D and Figure 2.2E). X-ray images in the sagittal plane offer the clearest view of the full implant, including the pedestal, leads and array.

Results

We characterized the topographical organization of somatosensory brainstem nuclei (cuneate/external cuneate, gracile and trigeminal) in acute experiments and estimated the

coordinates for chronic array implantation targeting the cutaneous or proprioceptive representations of the upper limb. Without histological confirmation, we could not distinguish between CN and ECN as neurons in both nuclei exhibit similar proprioceptive responses, though ECN has been shown to contain a preponderance of proprioceptive neurons (Hummelsheim & Wiesendanger, 1985; Hummelsheim, Wiesendanger, & Wiesendanger, 1985; Niu et al., 2013; Claire L Witham & Baker, 2011). In parallel, we modified the design of electrode arrays and the implantation approach to improve their stability and longevity.

Location and topographic organization of the cuneate nucleus

During acute acute recordings, we monitored multiunit activity from 90 distinct sites in CN/ECN, 13 in gracile nucleus, and 9 in trigeminal nucleus. Proprioceptive and, especially, tactile responses were most discernable when electrode impedance was greater than 1 MΩ. Our main goal was to characterize the topography of the upper limb representation in CN/ECN. Data used to generate the response maps were pooled across the left and right brainstems of two animals (two sides from one animal, one from the other). While we strived for a consistent coordinate system across experiments, differences in surface curvature, electrode angle, and neck flexion angle may have caused some distortion in the resulting maps of the brainstem.

Borders of the observed brainstem nuclei:

Our first goal was to determine the medio-lateral extent of the CN/ECN by finding the medial border with the gracile nucleus and the lateral border with the trigeminal nucleus relative to midline. Figure 2.3A illustrates the position of upper limb (CN/ECN), lower limb (gracile), or

face units (trigeminal). The gracile nucleus spans the first 1.25-1.5 mm lateral to midline, the

CN/ECN the following 1.5-1.75 mm, and the trigeminal nucleus spans the remaining 1 mm. The

medio-lateral extent of these structures remains fairly constant along the rostro-caudal axis

(within a range of ±3mm from obex) as well as in depth. These findings are consistent with

previous anatomical studies of primate brainstem nuclei (Figure 2.1C illustrates the relative

positioning of these nuclei in lower brainstem, see also Mai and Paxinos 2011).
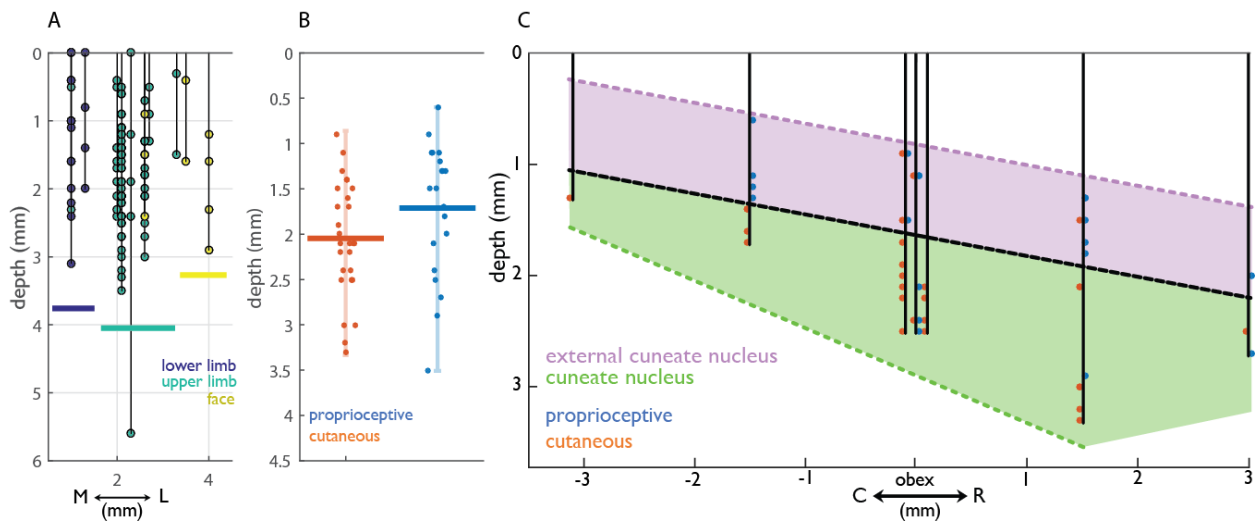
Figure 2.3: Topography of the observed brainstem nuclei. A: RF as a function of depth and medio-lateral position of the electrode tip. RFs on the lower limb (gracile) are coded in dark blue, upper limb (cuneate/external cuneate) in light blue, and face (trigeminal) in yellow. The medial and lateral borders of the upper limb units are about 1.5 and 3 mm from the midline respectively. B: Distribution of distances from the neural tissue surface for cutaneous and proprioceptive units of cuneate and external cuneate neurons. Cutaneous units tended to be deeper than proprioceptive ones. Vertical bars span the range of observed depths and horizontal bars their mean. C: Diagram of several electrode penetrations made along the rostro-caudal and dorsal-ventral (depth) axis. Black dotted line represents estimated boundary between ECN and CN, with ECN shaded in purple (proprioceptive) and CN shaded in green (majority cutaneous).

Response modality:

Next, we aimed to characterize the organization of proprioceptive and cutaneous inputs to CN/ECN and estimate the location of the boundary between the two nuclei. We found that proprioceptive units tended to be more superficial than cutaneous ones, and more frequently caudal to obex (Figure 2.3B,C). Additionally, proprioceptive units tended to be more lateral (mean distance from obex: 2.2mm, range: 1mm-3.3mm) than their tactile counterparts (mean: 2.1, range: 1mm-2.7mm), in part because the ECN is dominated by proprioceptive responses and is located more laterally.

We estimated the boundary between the ECN (majority proprioceptive) and CN (both cutaneous and proprioceptive) along the dorsal-ventral and rostro-caudal axis (Figure 2.3C). We also estimated the lateral boundary between CN and ECN to be located at ~2.7 mm, since no tactile units were observed beyond this point. These findings are consistent with previous studies in macaques and other primates (Figure 2.1C) showing that ECN is located dorsal to CN, and extends ~2mm from obex in each direction along the rostro-caudal axis (Florence et al., 1988; Hummelsheim & Wiesendanger, 1985; Hummelsheim, Wiesendanger, & Wiesendanger, 1985; Qi & Kaas, 2006).

In summary, then, gradients of submodality composition (tactile vs. proprioceptive) were most pronounced along the rostro-caudal axis and the dorsal-ventral axis (depth), as might be expected given that these define the boundary between CN and ECN (Figure 2.1C). Tactile units were most frequently observed ~2mm lateral to obex at a depth of 2mm or greater. Proprioceptive units were observed relatively uniformly across the rostro-caudal axis (±2mm to

obex), but most frequently observed superficially.

Somatotopic organization of proprioceptive and cuneate units:

Units with proximal cutaneous RFs tended to be located more superficially than those with distal ones (Figure 2.4A,B,C). The mean depth of units with RFs proximal to the elbow was approximately 1.5 mm (range of 0.6 - 2.9 mm) whereas that of units with RFs distal to the elbow was 2.4 mm (range of 1.2 - 3.5mm), consistent with previous findings in other primates (Florence et al., 1988; Qi & Kaas, 2006). A topographic progression was also observed along the rostro-caudal axis: units with distal RFs tended to be more rostral to the obex (with a mean location of -0.6 mm and a range of -3.0 to 1.5 mm) while units with proximal RFs tended to be caudal (0.6 mm with a range of -1.5 to 3.0mm) (Figure 2.4D,E,F). Somatotopic organization was similar for tactile and proprioceptive units both in depth and along the rostro-caudal axis.
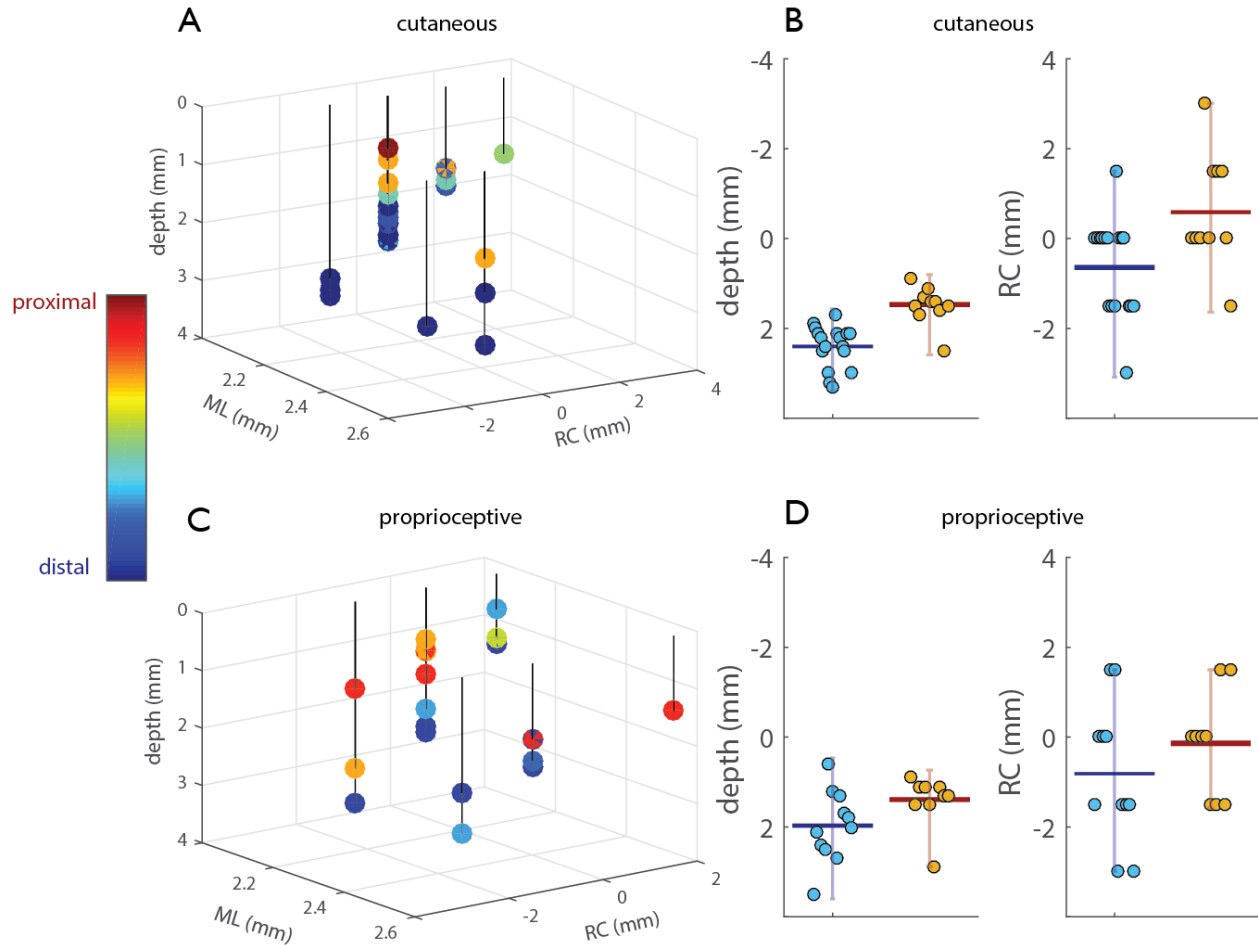
Figure 2.4: Somatotopic organization of CN. A: 3D diagram of penetrations with cutaneous RFs plotted with respect to obex and the surface. Color bar indicates the RF location. ML: medio-lateral, RC: rostro-caudal. B: Summary of cutaneous results: (Left) distal units tend to be deeper than proximal ones. Horizontal bar represents mean values, and vertical bars span the range of values. (Right) distal units tend be more cranial (negative along the RC dimension) than proximal ones. The forearm served as the boundary between distal and proximal units in the bar plots. C: 3D diagram of penetrations with proprioceptive responses with respect to obex and the surface. Color bar indicates RF location. D: Summary of proprioceptive results: (Left) distal units tend to be deeper than proximal ones. (Right) Distal units tend to be anterior to their proximal counterparts. Overall, both proprioceptive and cutaneous modalities exhibited similar somatotopic trends: proximal units were located more superficially and more posterior to the obex than distal ones.

Array performance

In total, we placed 13 arrays (4 UEAs and 9 FMAs) into the brainstem nuclei of 11 macaques

(two monkeys were implanted bilaterally in separate surgeries). The design of the arrays and the

implantation procedure evolved over time and the success rate improved progressively. Four

arrays (2 UEAs and 2 FMAs) yielded strong single-unit signals, which allowed us to collect

information about the stability of RF locations over the course of the arrays' lifespans. Of the

remaining arrays, four FMAs and one UEA yielded signals that were either limited to a few

electrodes, of poor quality, and/or of short lifespan. We were not able to record any signals from

the remaining arrays due to health complications (3/9) or complete array failure (1/9). Figure

2.2C shows the approximate locations of each array on the brainstem.

FMA Design

An advantage of FMAs is that the electrode length, material, and configuration, as well as the

lead length and pedestal shape can be specified on an array-by-array basis. We found that arrays

whose leads were manufactured with steel (rather than the standard gold) and reinforced with a

thin silicone coating around the wire bundle exhibited longer lifespans. Only TE received an

array with steel wires and silicone cable reinforcements, and this array had a signal longevity of

6 months, while all other FMAs lasted 8 weeks or less. Unlike implantation in cortex, for which

movement between pedestal and array is relatively limited, brainstem implants move

substantially relative to the pedestal, thereby stressing the leads (Buford & Davidson, 2004;

Fuchs & Luschei, 1970; Hoffman, Dubner, & Hayes, 1981). Moreover, the lead traverses neck

muscles that are constantly flexing and extending, creating additional stress. Lead breakage was

the most likely failure mode for many of our initial FMA implants.

We found that lengths of 7-9 cm were optimal for the leads in that sufficient slack was provided for movement, but not so much excess lead to adhere to muscle and other tissue (assuming that the more foreign material is implanted in the tissue, the more opportunity for adhesion). We began our studies with longer leads (up to 14 cm), and gradually shortened the leads to facilitate implantation of the array. During vacuum insertion, longer cables impose more torque on the array while lowering electrodes into neural tissue, ultimately destabilizing the array during implantation. Shortening the cable not only led to easier insertion but also improved signal longevity (monkeys WH, BA, LA1, HA). After several iterations, we converged onto specifications that yielded long lasting arrays in brainstem: shorter, silicone reinforced cables made of steel wire. TE received an array with all three design features, and signal longevity on this array substantially improved compared to all other FMA implants (Table 1). Although we did not have the same design options available with the UEAs, these arrays seem to be less susceptible to lead breakage, perhaps because of the greater number of individual leads, which results in a stronger aggregate cable.

RF stability and array longevity

First, we characterized the location of each electrode's RF in each of two FMAs over the lifetime of the arrays. Specifically, we counted the number of days over which each channel was activated by the same skin location or same joints (Figure 2.5A). The majority of upper limb units remained stable for only 1 or 2 days suggesting significant turnover of neuronal units from

day to day. Qualitative assessment of the stability of the longest lasting UEA suggests that RFs

may be more stable in these arrays. Note, however, that proximal RFs are larger than their distal

counterparts so differences in RF location – indicative of different units – may be more difficult

to identify for proximal than for distal representations.

Second, we characterized the number of channels that yielded discernible units over the lifetime

of each array as a gauge of signal stability and array longevity. By this measure, modifications

to the arrays and to the insertion procedure led to significantly improved longevity (Figure

2.4B). The more recent implants yielded units for up to 6 months whereas early arrays failed

within days or weeks (Figure 2.4B). The improved longevity can be attributed to improvements

in FMA design as described above, and to modifications to the surgical procedure to include an

adhesive that prevented arrays from being expelled from the brainstem. For both UEAs and

FMAs, we found that applying Vetbond yielded more stable arrays than did Tisseel. TE (FMA),

and LA1 (UEA) had Vetbond applied to the array post-insertion, and these arrays were

functional for the longest period of time (Table 1).

A

B
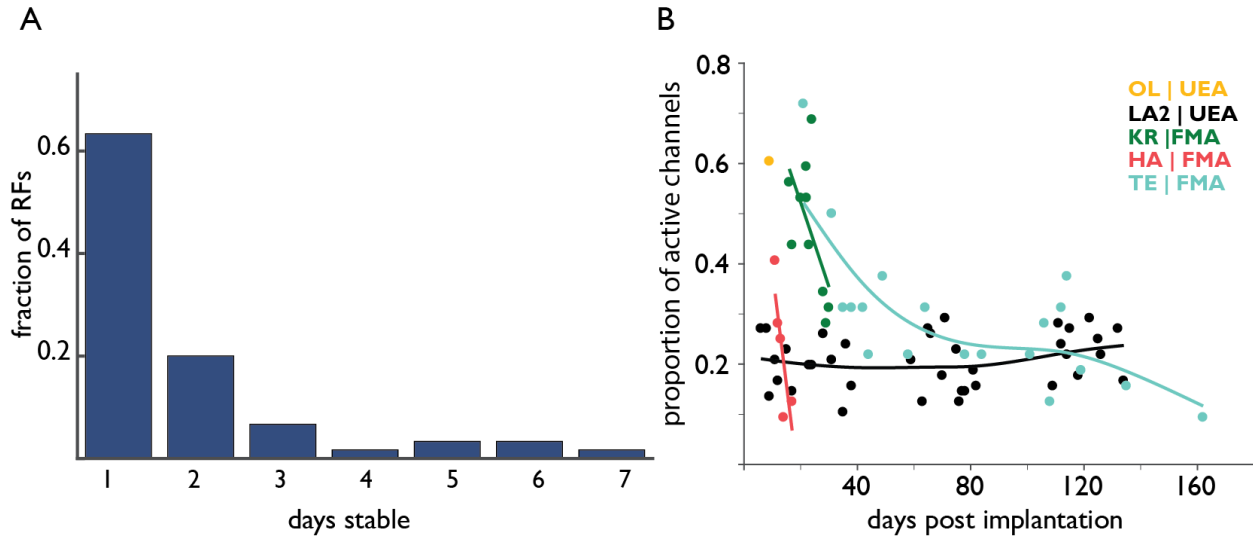
Figure 2.5: Electrode and receptive field stability. A: Number of consecutive days that observed RFs remained stable for each array. Channel RFs tended to remain stable for 1 or 2 days, with a maximum of 7 days. These data were collected over 20 sessions across two monkeys (WH and TE), whose distributions were very similar. B: Array Longevity for five electrode arrays. Points represent number of sorted neurons recorded after array implantation. Early implants (KR, HA) degraded rapidly after initial implantation. Longevity of LA(2), TE improved, as measured by number of units. One subject, OL (yellow), developed a fatal case of acute meningoencephalitis.

Single unit responses

Figure 2.6 shows the topography of the brainstem inferred from the chronically implanted

electrode arrays. Observed topographies were broadly consistent with those in the acute

experiments.

Figure 2.7 shows the responses of a cutaneous unit in CN to vibratory stimuli that varied in

frequency and amplitude. This unit exhibits phase locking – i.e., produces a spike or a burst of

spikes within a restricted portion of each stimulus cycle – as has been shown in both tactile

nerve fibers (Talbot, Darian-Smith, Kornhuber, & Mountcastle, 1968) and S1 neurons (M A

Harvey, Saal, Dammann 3rd, & Bensmaia, 2013). The frequency response profile of this unit

suggests that it receives input from Pacinian afferents. Indeed, it peaks in sensitivity at around

250-300 Hz, as do Pacinian fibers. Interestingly, however, this unit also exhibits a sustained

response to a skin indentation, a property that is only observed in slowly adapting type 1 fibers.

This combination of response properties suggests that signals from multiple submodalities

converge onto individual neurons in CN (see Saal and Bensmaia 2014b for a review).
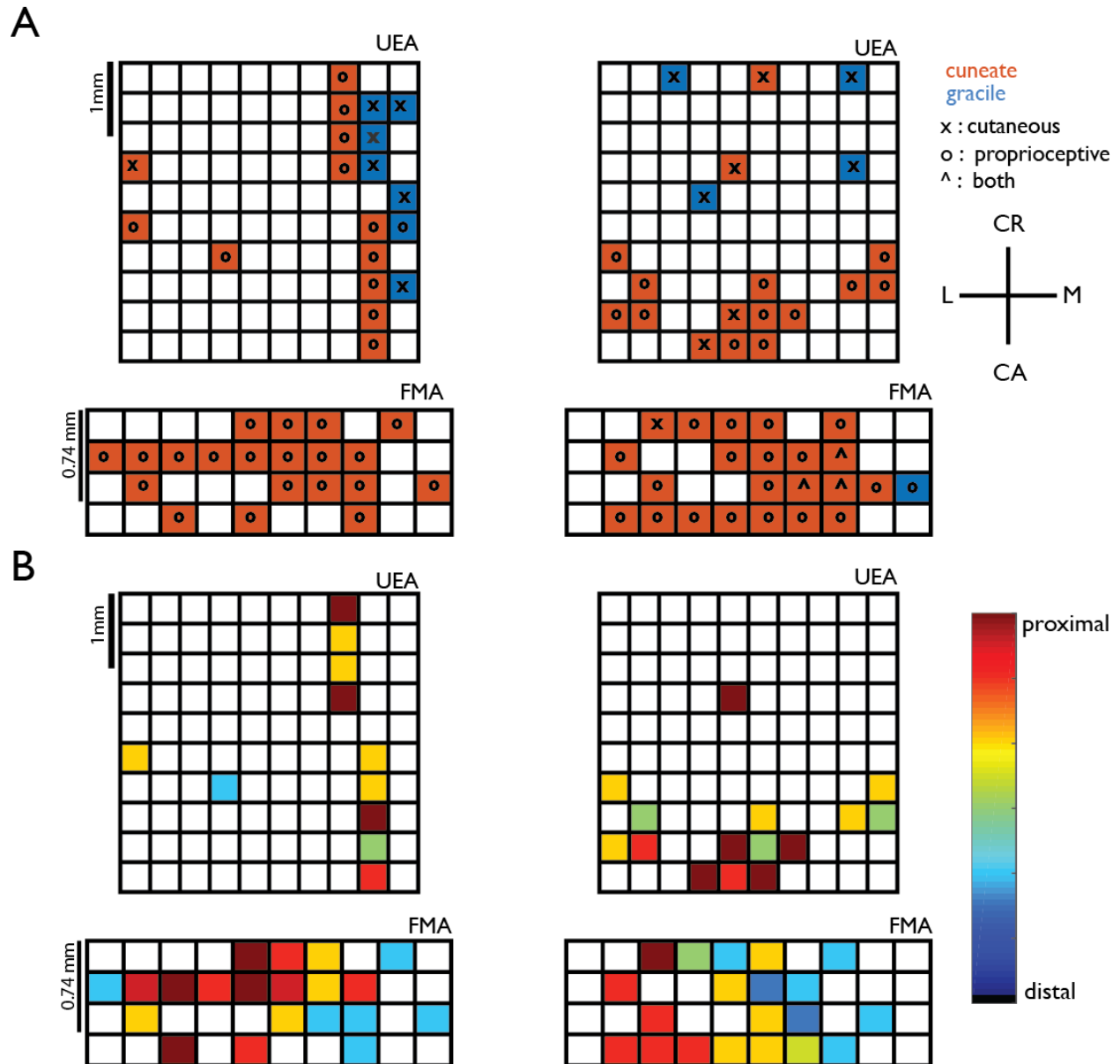
Figure 2.6: Topographical organization of the brainstem inferred from array recordings. A: Receptive field locations (M medial, L lateral, CR cranial, CA caudal) of electrodes in 2 UEAs and 2 FMAs, identified by anatomical location and modality. Most units had RFs on the upper limb (as expected since we targeted CN) and responded to proprioceptive stimulation. B: Somatotopy of upper limb proprioceptive units observed on each array. Utah arrays do not show a somatotopic trend, while FMAs show a medio-lateral trend. Distal units are observed medially, while proximal units are observed laterally. Overall, chronic arrays are able to capture proprioceptive cuneate nucleus responses (ECN), but due to the depth and/or insertion of these electrodes, relatively few cutaneous responses (CN) were observed.
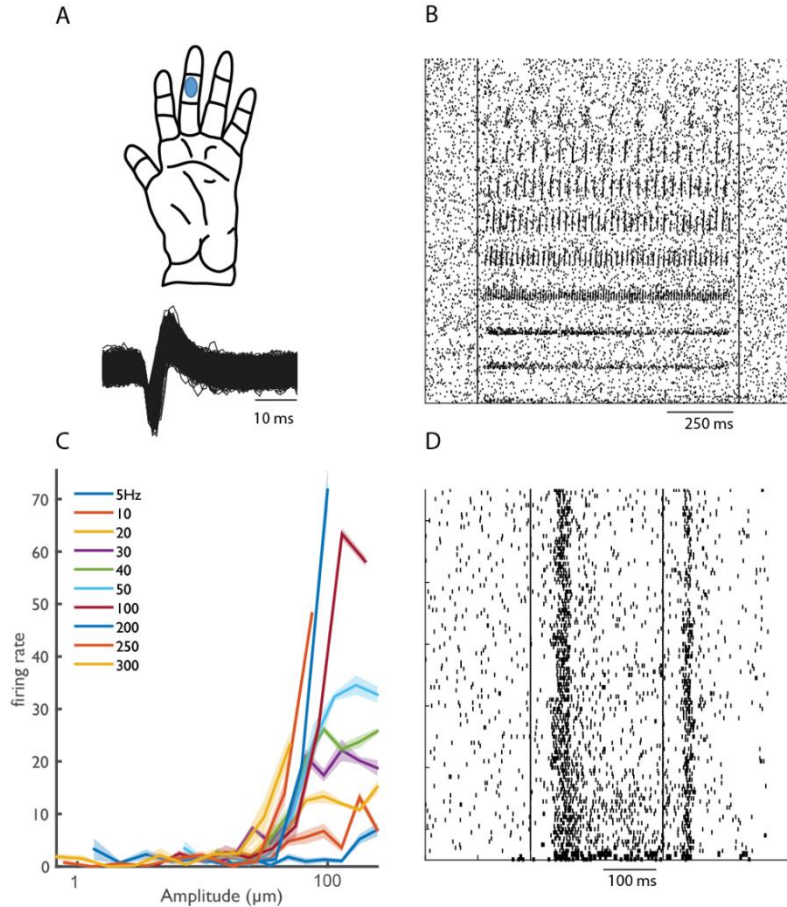
Figure 2.7: Responses of a cutaneous unit in CN. A: (Top) Receptive field center. (Bottom) Waveforms of identified action potentials. B: Responses of a CN neuron to vibrations delivered to the RF. C: Rate-intensity relationship demonstrates that this neuron's responses are frequency-dependent and peak in sensitivity at around 300 Hz, similarly to PC fibers. D: Responses of the same neuron to indentations delivered to different locations on the index fingerpad. Responses comprise both a sustained component and a strong off component: the sustained response indicates input from slowly adapting fibers and the off response indicates input from rapidly adapting fibers.

Figure 2.8 shows the responses of two CN/ECN neurons as we applied perturbations to the

monkey's hand. The first neuron (Figure 2.8B) exhibits preferential responses to force pulses in

the AP direction, with little or no response in the ML direction. Interestingly, the neuron burst at

a rate of nearly 80 Hz at both the onset and offset of force pulses either toward or away from the

body, with no sustained response. Figure 2.8C is a simultaneously recorded neuron which

exhibited a qualitatively similar response, with weaker tuning directed slightly up and to the

right.
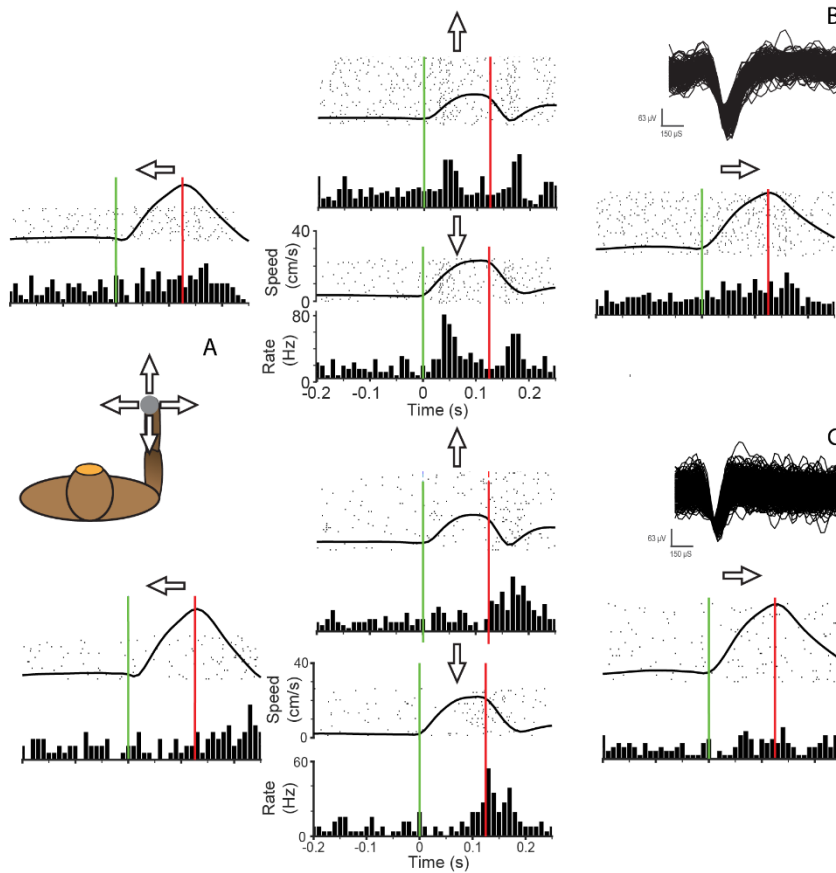
Figure 2.8: Cuneate/External cuneate neuron responses to limb perturbations. A: The monkey
was trained to hold onto a powered manipulandum which exerted forces in 4 direction from a
central point. A 125 ms bump was applied to the handle to test response of cuneate neurons. B:
Responses to bumps in each of four directions. Plots are arranged with respect to the direction of
the bump, with bump onset represented by vertical green bar. Bump offset is represented by
vertical red bar. Each row of the raster represents a single trial. A binned average firing rate is
plotted below the raster plot. The trial averaged speed of the handle (cm/s) is superimposed on
the raster. Inset: Waveforms of isolated action potentials. C: Responses to bumps evoked in
another CN/ECN neuron. Inset: Waveforms of isolated action potentials.

Discussion

Topography of the Somatosensory Brainstem Nuclei

While the organization of the somatosensory brainstem nuclei in primates has been documented in previous studies (Florence et al., 1988; Qi & Kaas, 2006), our study is the first to characterize the topographical organization of these nuclei in rhesus macaques. We find that proprioceptive units tend to be more superficial than cutaneous ones and that the CN/ECN exhibit a somatotopy both in depth and along the rostro-caudal axis: units with RFs on the proximal limb tend to be more superficial and caudal than those with distal RFs. The dorsal-ventral trends observed in rhesus macaques with regards to somatotopy and submodality distribution match those reported for other macaque species (Florence, Wall, & Kaas, 1989; Qi & Kaas, 2006), with the additional observation of somatotopic trends along the rostro-caudal or medio-lateral axes.

In the FMA recordings, we noticed a distal to proximal trend of RFs along the medio-lateral axis. That is, units with distal RFs tended to be located medially while units with proximal RFs were predominantly located laterally. This somatotopy was observed neither in the anesthetized acute experiments, nor in the UEA RF maps, and may be attributed to the curvature of the brainstem, which caused medial electrodes to penetrate deeper than others.

Implications of the topography for chronic implants

To record from digit-related units in CN is challenging due to their depth and their location rostral to the obex, which can be partially obstructed by the cerebellum. Electrode arrays must include long (>2mm) electrodes yet still allow insertion in a far rostral position along the

brainstem. Unfortunately, the angle for this insertion is often hindered by the occipital bone, even after a wide suboccipital craniectomy that extends to the transverse sinuses. Proprioceptive units with proximal RFs are more easily accessible given their superficiality and caudal location.

The boundary between CN and ECN is difficult to establish conclusively based on electrophysiological response properties because both nuclei exhibit similar proprioceptive responses (Hummelsheim, Wiesendanger, & Wiesendanger, 1985; Claire L Witham & Baker, 2011). Any implant is likely to impinge on the two nuclei given their small size, and histology will almost certainly be necessary to distinguish them post hoc.

Array design considerations

The manner in which signals recorded by the FMAs decayed over time and subsequently failed suggests either lead or connector breakage. However, the fact that some channels failed while others remained stable seems to exclude connector failure. Impedance spectroscopy indicated open circuits, consistent with lead breakage.

UEAs offer the advantage of greater coverage, more and more closely spaced electrodes, and strong leads. However, targeting cutaneous units requires longer electrodes than are currently commercially available with UEAs. Furthermore, the insertion technique for FMAs, which involves a narrow vacuum probe, facilitates rostral positioning relative to its UEA counterpart, as the pneumatic inserter required for the latter has a wider footprint. Given the rostral position

of cutaneous digit, this further favors FMAs over UEAs for studies involving the cutaneous representations of the digits.

Stability of cutaneous receptive fields

That the location of RFs turn over at a relatively rapid rate for the FMA implants (every other day approximately) suggests movement of the array within the tissue. The great stability of our most recent UEA implants is difficult to explain, unless the much greater number and density of electrodes helped to stabilize the array within the tissue. While cortical implants with either FMAs or UEAs also exhibit some neuronal turn over, its rate is much slower, with some units remaining stable for weeks or even months (Vaidya et al., 2014). The poor stability of CN implants can be attributed to the much greater mobility of the brain stem, which flexes during neck movements, a degree of freedom not present in cranial implants (Buford & Davidson, 2004; Fuchs & Luschei, 1970; Hoffman et al., 1981).

Conclusions

We have developed a strategy to record stably for single sessions from the somatosensory brainstem nuclei using chronically implanted electrode arrays. We have characterized the somatotopic and functional topography of neurons in the CN/ECN using electrophysiology, and illustrated the firing rate characteristics of several neurons in response to passive RF manipulation. Although stereotaxic coordinates cannot offer well-defined boundaries between somatosensory brainstem nuclei due to various confounding factors, the observed topographical trends will inform future array placement and design. Vibratory responses have been extensively

characterized in the periphery and cortex of rhesus macaques (Michael A. Harvey et al., 2013; Johnson & Lamb, 1981; Mountcastle, Talbot, Darian-Smith, & Kornhuber, 1967; Muniak, Ray, Hsiao, Dammann, & Bensmaia, 2008), as have responses to passive and active limb movements. The ability to collect single unit data from the CN of awake behaving primates will provide us with an opportunity to understand how these limb state representations are transformed as they ascend the neuraxis. We may also begin to understand the nature and function of the top-down modulation CN receives from cortex.

Chapter 3 – Encoding of limb state by single neurons in the cuneate nucleus of awake monkeys

Christopher Versteeg, Joshua M. Rosenow, Sliman J. Bensmaia & Lee E. Miller

Foreword

The following was adapted from a manuscript published in the Journal of Neurophysiology in May 2021.

Abstract

The cuneate nucleus (CN) is among the first sites along the neuraxis where proprioceptive signals can be integrated, transformed, and modulated. The objective of the study was to characterize the proprioceptive representations in CN. To this end, we recorded from single CN neurons in three monkeys during active reaching and passive limb perturbation. We found that many neurons exhibited responses that were tuned approximately sinusoidally to limb

movement direction, as has been found for other sensorimotor neurons. The distribution of their

preferred directions (PDs) was highly non-uniform and resembled that of muscle spindles within

individual muscles, suggesting that CN neurons typically receive inputs from only a single

muscle. We also found that the responses of proprioceptive CN neurons tended to be modestly

amplified during active reaching movements compared to passive limb perturbations, in contrast

to cutaneous CN neurons whose responses were not systematically different in the active and

passive conditions. Somatosensory signals thus seem to be subject to a "spotlighting" of

relevant sensory information rather than uniform suppression as has been suggested previously.

Introduction

Proprioception plays a critical role in our ability to move, as demonstrated by the severe deficits

that occur when it is absent (Proske & Gandevia, 2012; Sainburg et al., 1995). In the periphery,

proprioception relies on several classes of mechanoreceptors. While joint receptors and Golgi

tendon organs (GTOs) also contribute, muscle spindles are the primary receptor underlying

proprioception (Proske & Gandevia, 2012). Because each spindle signals stretch of the muscle

within which it is embedded, responses vary with movement direction, peaking for movements

that lead to the greatest stretch. This characteristic may give rise to the sinusoidal tuning curves

that have been described in somatosensory cortex (Brian M London & Miller, 2013;

Prud'homme & Kalaska, 1994). A major challenge in studying proprioception is that both

spindle sensitivity and signal transmission through the cuneate nucleus are modulated by

descending inputs (Michael Dimitriou, 2014; Ghez & Pisa, 1972) so proprioceptive responses

are liable to differ for actively generated and passively imposed limb movements.

In the present study, we sought to characterize the proprioceptive response properties of CN neurons in the context of arm movements. First, we examined the degree to which CN neurons are tuned to reach direction. Observed patterns of spatial tuning suggest that individual CN neurons receive convergent input from one or only a few muscles. Second, we investigated whether CN responses to kinematically similar movements depend on whether they are produced actively or imposed on the limb. We found that the responses of proprioceptive neurons were typically potentiated during active movement but this systematic potentiation was not observed in cutaneous neurons. We speculate about why these two streams of somatosensory information may be modulated differently during active movements.

Methods

All surgical and experimental procedures were fully consistent with the guide for the care and use of laboratory animals and approved by the institutional animal care and use committee of Northwestern University under protocol #IS00000367.

Behavioral task

We trained three monkeys (macaca mulatta, two males, one female, ages 7-10 years) to perform a modified center-out (CO) reaching task. Each monkey grasped a handle attached to two-link manipulandum constrained to a horizontal plane. The monkeys used the position of the handle to control a cursor displayed on a vertical screen. Each trial began when the monkey moved the

cursor to a target at the center of the screen. After a random delay of 0.5-1.2 seconds, an outer

target appeared in one of eight locations spaced equally on a circle at a distance ranging from

eight to 12 cm from the center target depending on the monkey (example trajectories in Figure

3.1A). Some experimental sessions with monkey Bu had only four targets, one along each of the

cardinal directions. Following a tone cue and the disappearance of the center target, the monkey

had two seconds to reach to the outer target and hold it for a random interval between 0.1 and

0.2 seconds. If the monkey correctly performed these steps, it received a liquid reward.

On some trials, we imposed a force perturbation (either 2.0 or 2.5N, depending on the size of the

monkey) during the center-hold period which pushed the hand in one of the eight target

directions with kinematics that roughly matched that of the initial, active reaches (Figure 3.1A).

The robot delivered the force for 125 ms, begun prior to the appearance of the outer target, but

after the monkey had been holding for at least 0.3 seconds (examples in Figure 3.1B). In the

passive trials, we confined our analyses of the neural responses (shown in Figure 3.1C and D for

active and passive conditions, respectively) to a 130 ms window beginning at bump onset to

exclude the potential reafferent input due to voluntary movement. We analyzed active reaches

tor 400 ms beyond movement onset, unless otherwise noted. To determine movement onset for

active reaches, we found the time between the go cue and the end of the trial at which the handle

acceleration crossed half its maximum, then walked backwards until we found a hand speed

minimum.
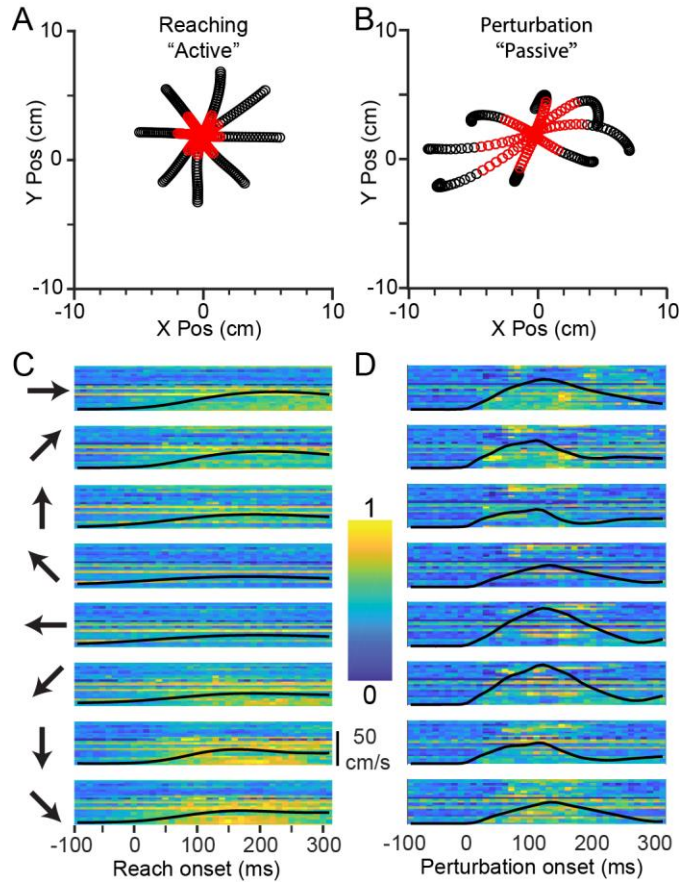
Figure 3.1: CN activity during Center-Out reaching and limb perturbation. A: X/Y plot of mean handle position during reaching (-100 ms to +300 ms from movement onset), averaged across ~120 trials per direction for monkey Sn. Red symbols are in the window from 0 ms to 130 ms. B: Corresponding plot during perturbation trials. Significant asymmetries can be seen due to the non-uniform impedance of the hand. C: Neural firing rates during reaching in 8 directions, indicated by the arrows to the left of the plots. Each row of pixels represents a single CN neuron, with color indicating the normalized firing rate. The black line superimposed on the image is the speed of the hand, normalized to the fastest hand speed in either the active or passive condition. D: Firing rates during passive trials, as in panel C.

Data collection

We implanted 96-channel iridium-oxide arrays (Blackrock Microsystems) with an electrode length of 1.5 mm in three monkeys. We targeted all implants for the right CN, which receives inputs from the right arm. Detailed surgical procedures have been described previously (Suresh

et al., 2017). For monkey Bu, we used a standard 10x10 shank array. For two subsequent

monkeys, we maximized the area of CN sampled by implanting 8x12 shank rectangular arrays,

thereby avoiding most of the gracile and trigeminal nuclei which lie medial and lateral to CN,

respectively (Figure 3.2A). Receptive field mappings revealed areas of each array receiving

inputs from the lower limb (gracile) and face (trigeminal). We used this somatotopic

organization, which was conserved across time, to eliminate from consideration neurons with

receptive fields not on the upper limb and torso.
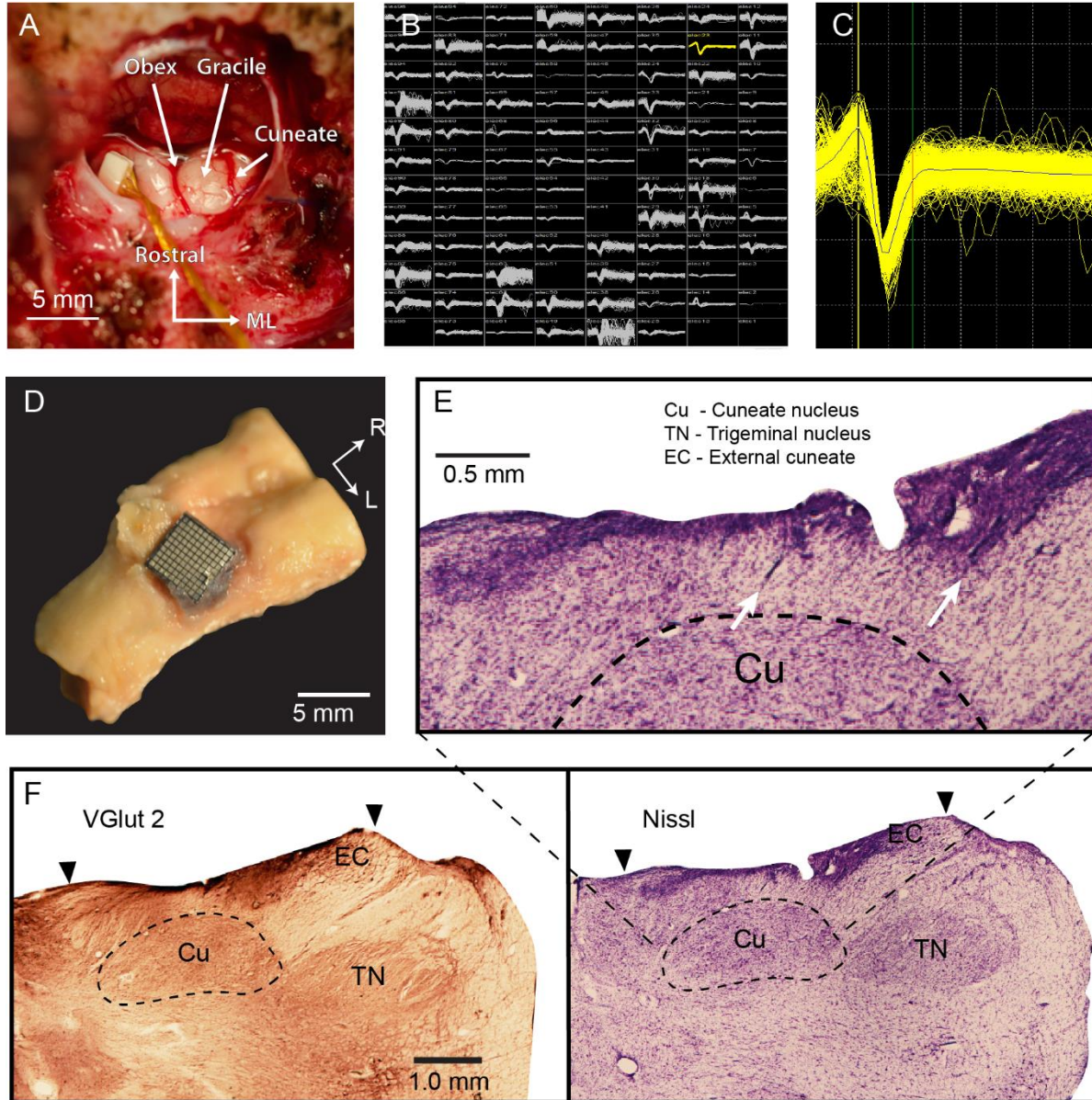
Figure 3.2: Electrode arrays implanted in dorsal brainstem yield single neuron recordings from the cuneate nucleus. A: Intraoperative exposure of the dorsal brainstem and cuneate nucleus following implantation of a Floating Microelectrode Array (Microprobes for Life Sciences) in an early monkey, not used in this study. The obex and cerebellar tonsils are in the center of the image. Gracile nucleus is the structure immediately lateral to the midline, with the main CN further lateral. B: Screenshot of the recordings across an implanted Utah array (monkey Sn). C: An example single neuron from monkey Sn. D: Histological examinations of monkey La showed that the implant successfully targeted the main CN. Brainstem with the Utah array in place. E: Arrows mark electrode tracks leading into the main CN. F: Staining by Vglut2 (left) and Nissl (right) sharply delineate the boundaries of the CN and trigeminal nuclei. Main CN (Cu) begins at ~0.5 mm depth and extends to ~2 mm. External cuneate (EC) is more lateral and

shallower. Trigeminal nucleus is farther lateral. Black arrows indicate the mediolateral extent of the Utah array.

We simultaneously recorded cursor position, timestamps indicating trial events, and neural data while the monkey performed the task. We bandpass filtered the neural recordings between 250 Hz and 5000 Hz, and set a voltage threshold manually on each channel to record single neuron activity in 1.6 ms snippets surrounding each threshold crossing (Figure 3.2B,C). We sorted the snippets in Offline Sorter (Plexon Inc.) using waveshape and interspike interval to isolate single neurons. Neurons in CN can fire spike doublets at approximately millisecond intervals. During these high-frequency bursts, the waveshape changes, causing two clearly separable clusters in Offline Sorter. Cross-correlograms between the spike times of snippets in two such clusters have a characteristic profile, with smaller of the two waveforms reliably lagging the larger waveform (supplementary fig 1, https://figshare.com/s/038f93c114ba056d729e). We combined all the waveforms in these pairs of clusters to avoid double counting single neurons. We placed all the sorted spikes into 10 ms wide bins and convolved the resulting counts with a 20 ms, noncausal Gaussian kernel to produce a smoothly varying firing-rate signal for subsequent analyses.

Histology

To confirm that our implantation procedure was appropriate to target the main CN, we performed histology on one monkey (monkey La, not included in this paper due to low neuron yield; monkeys Sn and Cr are still in use in other experiments) that had a CN implant like that of monkey Bu. The monkey was deeply anesthetized and perfused with saline followed by

paraformaldehyde solution. We removed the brainstem with the array in place (Figure 3.2D), then removed the array and placed the brainstem in 5% Normal Buffered Formalin (NBF) for several weeks. The tissue was then placed in 30% sucrose in 0.1M Phosphate Buffer (PB) until it sunk. The dura and microelectrode array implant were removed, and the brainstem was blocked and mounted on a freezing microtome and sectioned coronally into 50µm sections. Tissue intended for immunohistochemical processing by VGluT2 staining was placed in 0.1M Tris-Buffered Saline with 0.1% sodium azide, while tissue for Nissl staining was placed in 5% Formalin.

Immunohistochemistry
The brainstem tissue was rinsed 3x5min in 0.1M Phosphate-Buffered Saline (PBS), and quenched for 10 min in 3% hydrogen peroxide in PBS. All processing was performed at room temperature. Sections were rinsed 3x5min in PBS, blocked for 2 hrs in 5% horse serum with 0.05% Tritin X-100 in PBS, and incubated overnight in the primary antibody (MsαVGluT2, Millipore, #MAB5504, 1:5000, binding specific to vGluT2 receptors (Balaram, Young, & Kaas, 2014)) diluted in blocking solution. The tissue was then rinsed 3x5min in PBS, and placed in the secondary antibody solution (HsαMs, Vector Labs, 1:500) diluted in blocking solution for 1hr 45min, rinsed 3x5min in PBS, and incubated in the avidin-biotin complex in PBS for 2 hrs. Sections were rinsed 3x5min in PBS, developed in a solution of 0.5% DAB, 0.05% nickel ammonium sulfate and hydrogen peroxide in 0.1M PB and given a final rinse in PBS. Sections were mounted on gelatin-coated slides, dried, and cover slipped with DPX.   A representativevGluT2 labeled CN section is shown in Figure 3.2F.

Nissl Staining

Sections were mounted out of 0.1M PB onto gelatin-coated slides and left to dry overnight. The tissue was then placed in a 1:1 chloroform and ethanol solution and sent through an ascending ethanol series into xylenes for a 15min incubation. The tissue was then put through a descending ethanol series into water and placed into the Nissl substance for 15min, followed by differentiation in 70% ethanol with acetic acid, and back through the ascending ethanol series into xylenes. The sections were cover slipped out of xylenes in DPX. A representative Nissl stained CN section is shown in Figure 3.2E,F)

Receptive field mapping

During our experiments, we found some neurons that responded to body segments other than the proximal arm and upper torso. To exclude these neurons from our analysis of limb movement, we mapped the receptive fields (RFs) of neurons under light ketamine or dexmedetomidine sedation after all reported experimental sessions. These RF mappings typically took one to two hours, limited by sedation time and animal tolerance for manual mapping. We excluded from our analyses all neurons that had receptive fields on the forearm, hand, legs, lower torso and head or face. We also removed neurons that had a stereotypical bimodal passive tuning curve that was indicative of receptive fields on the hand (for example, see supplementary fig 2, https://figshare.com/s/cbebb1957388bf75b5c4). Gross somatotopic arrangement of RFs was consistent across long time periods (Figure 3.3), allowing us to target electrodes that reliably had proximal limb RFs.

To find neurons with apparent cutaneous input, we brushed the skin around the arm and torso while listening to pulses from discriminated action potentials. Cutaneous receptive fields were of highly variable size; some responded to brushing of skin over large areas, while others had focal receptive fields, often on the hand. Due to methodological limitations, we did not test for Aδ receptive fields, joint receptor afferents, or Golgi tendon organ input.

To find putative spindle afferents, we began with passive arm movements to determine articulations in which the neuronal firing rate increased and used that information to guide palpation of muscles that lengthened during those articulations. We then applied 100-Hz vibration to the belly of these muscles, using either an electrodynamic LDS V101 shaker (BRÜEL & KJÆR) or smaller vibration motors. This stimulus has been shown to activate primary muscle spindle afferents (Fallon & Macefield, 2007; Proske & Gandevia, 2012). Often, CN neurons responded only to vibration of small regions of the muscle belly.

We classified a neuron as a putative recipient of muscle spindle input ("spindle-receiving") if it responded to the lengthening, and either vibration or palpation of a given muscle, but not to stroking of the skin overlying the muscle. When testing a putative muscle spindle-receiving neuron, we vibrated the muscle through different patches of skin (by manually displacing the lax skin) to confirm that the response was caused by vibration of the muscle and not the overlying skin. We found occasional neurons that responded to vibration of more than one muscle, typically adjacent synergist wrist flexors. Whether this was due to convergence of multiple muscle receptors onto a single CN neuron or vibration spreading to adjacent muscles is difficult

to determine with certainty. We defined any neuron that consistently and selectively responded to passive movements of the limb, but with an RF that we were not able to localize to a single muscle or cutaneous field as "muscle-like". This included the spindle-receiving neurons.

Motion tracking

In one monkey, we used three video cameras to record the movements of the monkey's arm. We triggered frame collection with a 30 Hz pulse transmitted from our data collection system, simultaneously recorded as an analog input for post-hoc alignment of neural, task, and video data. We used a publicly available package (DeepLabCut (A. Mathis et al., 2018)) to infer 10 locations on the monkey's arm after training on ~200 hand-labelled reference images. We reconstructed 3D coordinates of each location based on four separate camera views. Based on the output from DeepLabCut, we used Opensim (Delp et al., 2007) and a 3D musculoskeletal model of a macaque arm with 7 degrees-of-freedom (Chan & Moran, 2006) to compute the lengths and velocities of 39 muscles. We binned these data at 10 ms and aligned them in time with the neural data.

Spatial tuning curves and preferred directions

We calculated the mean firing rate and its 95% confidence interval for each neuron across trials in a 130 ms period beginning at perturbation onset, or in active trials, the 200 ms surrounding the peak hand speed in each direction. In addition to the classic method of fitting a sinusoid to trial-averaged data (A P Georgopoulos et al., 1982; Prud'homme & Kalaska, 1994), our lab has begun to compute preferred directions (PDs) by fitting models from hand velocity to the

smoothed firing rates of each neuron using Poisson Generalized Linear Models (GLMs) (Chowdhury et al., 2020). This latter approach is sensitive to variability in reach kinematics across trials and can be applied to random-target reaching tasks as well as center-out tasks. Here, we concatenated all trials and placed the data is 50 ms bins. In Eq 1, λ and α represent the time-varying and baseline firing rates (spikes/sec), respectively, of a given neuron. β is the weight vector for the x and y components of velocity. We computed a PD from the GLM by taking the inverse tangent of the ratio of the y and x velocity weight vectors, β. We used bootstrap sampling across data points to generate 95% confidence intervals on the PD.

$$\lambda = e^{\alpha + \beta x} \qquad (1)$$

$$pseudoR^2 = 1 - \frac{ln\hat{L}(M_{Full})}{ln\hat{L}(M_{Intercept})} \qquad (2)$$

Neural tuning metrics

We classified neurons as "Active Tuned" if there were statistically significant differences in an F-test across reaching directions with a cutoff of $p < 0.01$. Similarly, neurons were "Passive Tuned" if they met the same criterion for bump-evoked responses. Neurons could be "Active Tuned", "Passive Tuned", or both. We considered neurons "Sinusoidally Tuned" if the PD confidence interval had a total width of 90 degrees or less. Neurons could be "Active

Sinusoidally Tuned", "Passive Sinusoidally Tuned" or both.

We found the time a neuron modulated relative to movement onset for each target direction (supplementary figure 3, https://figshare.com/s/5fbfea294e9725a7375d) by computing the trial-averaged firing rate in 10 ms bins from 100 ms prior, to 200 ms after movement onset. We found the first time at which this average rate was outside the 99.9 percentile of the baseline firing rate (from 150 ms to 100 ms prior to movement onset) for two consecutive bins. We computed the latency for passive movements in a similar manner, using a baseline window from 100 to 50 ms prior to perturbation onset, testing for changes from 50 ms prior to the bump to 100 ms after the bump.

Analysis of simulated spindle-receiving CN neurons

To determine the extent to which the representation of movement direction within CN resembles that of the periphery, we compared the spatial tuning of CN neurons to that expected from their apparent muscle spindle inputs. This process had several steps. We computed typical length changes of arm muscles while a monkey performed the CO task using motion tracking data from a single session of monkey Sn. We simulated spindle firing rates by passing the lengthening velocity of each muscle through a power law with coefficient of 0.5 (J. C. Houk et al., 1981). We set firing rates during muscle shortening to zero. We scaled each spindle output to a firing rate of 50 Hz at near-maximal lengthening speed (90th percentile). Treating this rate as the time-varying λ of a Poisson distribution, we sampled randomly to generate firing rates for each simulated spindle on each trial. Finally, we used a linear model to determine PDs for the

simulated spindles from the velocity of the hand as we did for CN neurons.

We computed the PDs for simulated CN neurons that each received input from a single randomly chosen muscle spindle from muscles distributed throughout the proximal arm. The number of muscle spindles in each muscle is roughly proportional to the square root of the muscle's mass (Banks & Stacey, 1988). We estimated the mass of each muscle by the multiplying the pulling force (proportional to cross-sectional area) by the length of the muscle, both of which were included in our musculoskeletal model. Thus, we assumed that the number of muscle spindles in each muscle was proportional to the square root of its pulling force times the length of the muscle. We simulated 1000 muscle spindle-receiving CN neurons, apportioned across the muscles on this basis. From this population, we computed PD distributions based on the kinematics for active reaches.

Sensitivity analyses

To estimate the sensitivity of CN neurons to hand movements, we used the x and y components of hand velocity as input to linear models that predicted the smoothed firing rate of each neuron. The length of the weight vector was that neuron's sensitivity to velocity and quantifies the expected change in firing rate for an increase of one cm/s in the direction of the neuron's velocity PD.

Due to the anisotropy of the limb and idiosyncrasies of a monkey's task performance, the perturbations did not produce kinematics perfectly matching those of the reach. If firing rates

are a nonlinear function of speed, such as the power law observed in muscle spindles (J. C.

Houk et al., 1981), mismatched movement speeds across conditions would bias the apparent

sensitivity. To address this potential confounding factor, we matched the input velocity

domains of the data used to train the models. We found separate static 2D distributions of firing

rates as a function of velocity for the active and passive trials. For each reach-velocity datapoint,

we found the distance to the nearest passive datapoint, in an approach analogous to a nearest

neighbor method. If this distance was greater than 3 cm/s, we excluded the active point, as it had

no near neighbors. We repeated this process to exclude passive data that did not have active

neighbors. The result was training data in which the active and passive movements had matched

velocity domains. The data windowing did not substantially alter the results of the sensitivity

analyses; we demonstrate the data windowing and its effects on the results of this analysis in

supplementary figure 4 (https://figshare.com/s/897eb744ba2ff3f2971c).

To compute whether a neuron's movement sensitivity differed significantly between the active

and passive conditions, we bootstrapped, across trials, a confidence interval on the difference

between active and passive sensitivities for each neuron. If the mean of this metric was positive

and the 95% confidence interval did not include zero, the neuron was more sensitive in the

active condition; if the mean was negative and the 95% confidence interval did not include zero,

the neuron was significantly less sensitive.

Results

We recorded the responses of neurons with receptive fields (cutaneous or proprioceptive) on the proximal arm while the animals performed a modified Center-Out reaching task that included force pulse perturbations applied to the robot handle during the center-hold period. Unless otherwise specified, the data were obtained in two sessions with each monkey, separated by at least three weeks to reduce the likelihood of double-counted neurons.

Somatotopic organization of CN is similar across monkeys

First, we examined the somatotopic organization of the CN by systematically mapping the receptive field types and locations across the arrays. Using intra-operative photos of array placement, we found the coordinates of each array relative to the obex. We then plotted the most common RF location (i.e., legs, trunk etc.; Figure 3.3A) and modality (muscle-like, cutaneous; Figure 3.3B) for each electrode). Receptive field locations varied systematically along the minor axis cutting through CN (dotted arrows in Figure 3.3A, projected onto axis in 3.3C). This progression reflects the transition from the gracile nucleus to CN, and finally to the trigeminal nucleus. RF locations on the arm were largely conserved along the major axis, possibly corresponding to the CN subnucleus known to receive primary inputs from distal cutaneous receptors (Loutit et al., 2021). These results are consistent with our histological results from one monkey (Fig 3.2F), which indicate that the array likely penetrated through the external CN, to record from rostral portions of the main CN. We could not confirm this independently for all monkeys, for which histology has not been completed. The orientation of the major and minor axes departs from strictly mediolateral because of the sharply lateral bend of the brainstem and

nuclei just rostral to the obex. RF type varied along the major axis, with muscle-like response properties slightly more common farther from the obex (fig 3.3B,D).
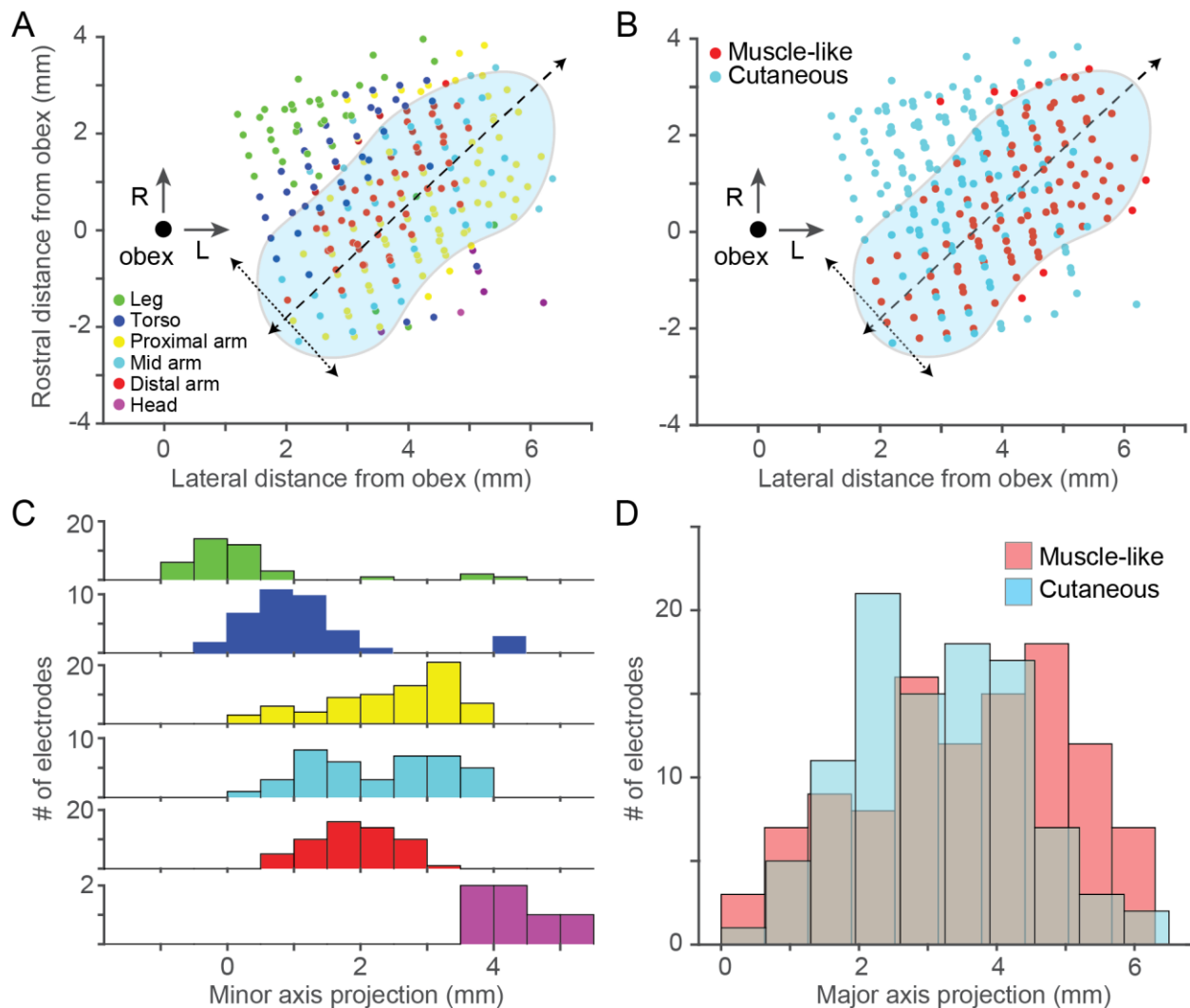
Figure 3.3: Receptive field location and modality across monkeys. A: Scatter plot of receptive field locations as a function of the location of the recording site relative to obex (large black point). Each point represents a recording site in the dorsal medulla from one monkey. Color of points denotes the most common receptive field location for a given electrode. Approximate location of CN is show in blue, with its major (dashed) and minor (dotted) CN axes overlaid. RF locations appear to vary primarily along the minor axis. "Proximal arm" included shoulder related receptive fields, "Mid arm" included RFs around the elbow, and "Distal arm" included all forearm and hand related RFs. B: Modality as a function of electrode location. As in A, symbol color indicates the most common modality. C: Histogram of receptive field location

along the minor axis in A, relative to the obex. RFs progressed systematically along minor axis from lower limb (green) to head/face (purple). D: Histogram of receptive field type along the major axis. There was a weak bias for muscle-like RFs away from the obex.

Localized vibratory stimulation robustly activates CN neurons

Having identified joints that appeared to be within the RF of a given CN neuron, we characterized the spindle input to that neuron by applying vibration to the belly of muscles that articulate that joint. Figure 3.4 shows the response of a CN neuron to vibration of the brachialis muscle, presumably due to the activation of its muscle spindles. As in this example, neural responses typically increased and became phase locked with the vibration. We found that many of these spindle-receiving neurons required the vibration be delivered quite precisely within a given muscle to be effective, suggesting that CN neurons may not even receive input from spindles throughout a given muscle.

Next, we examined the degree to which CN neurons receive input from multiple muscles. In most cases, CN neurons responded to passive manipulation (or vibration) of a single joint or muscle. In a few cases (<10), we found evidence that signals from multiple (typically agonist) muscles converged onto a single CN neuron. We never found neurons that responded to muscles that were not in near proximity to one another nor did we find neurons that exhibited both cutaneous and proprioceptive responses, though due to time constraints on sensory mappings, convergence may be broader than our mappings suggest.
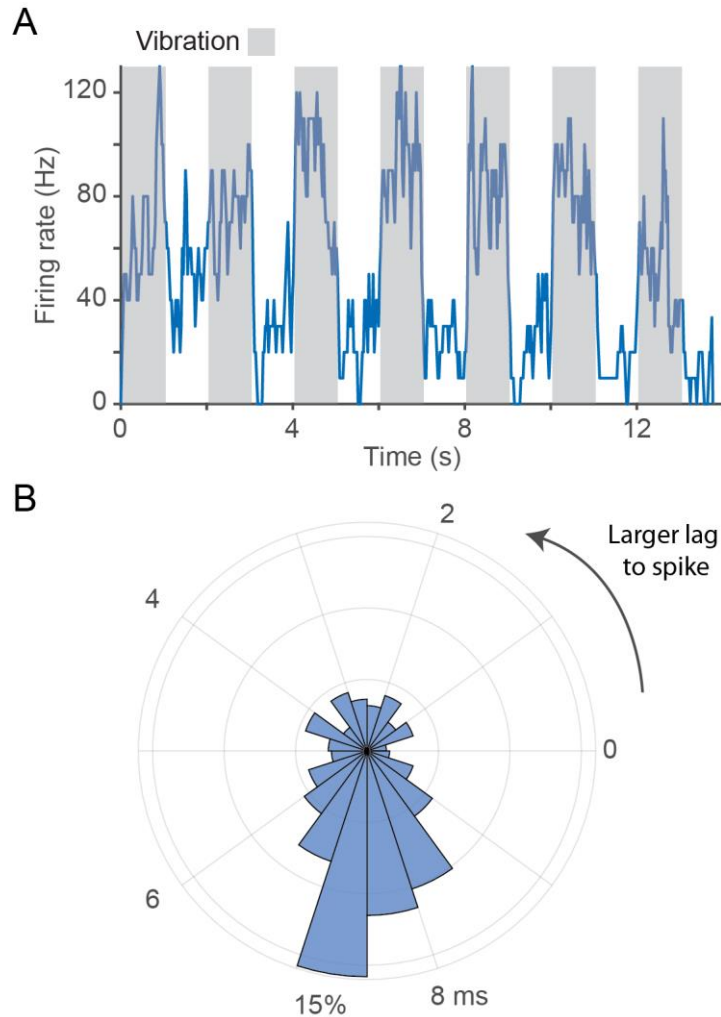
Figure 3.4: Responses to muscle vibration of a spindle-receiving neuron. A: Response of a CN neuron to 100-Hz vibration applied to the brachialis muscle belly. Grey regions indicate the stimulation epoch. The neuron's firing rate rose quickly to 100 Hz and returned to baseline immediately when the vibration stopped. B: Phase locking between the vibration peaks and action potentials. We computed a phase histogram between the peak voltage applied to the stimulation and evoked spikes. The peak at ~7.5 ms indicates that the vibrator peak led this neuron's spikes with a reliable latency. Some of the breadth of the peak is certainly due to the sinusoidal nature of the stimulus.

CN neurons are tuned to movement direction

Figure 3.5 shows the responses of two representative CN neurons measured during ~50 reaches

in each of eight directions, a cutaneous neuron with an RF on the axilla (Fig. 3.5A,B) and a

spindle-receiving neuron with an RF on the triceps muscle (Fig 3.5C,D). The firing rates of both neurons varied with movement directions, peaking for a single target direction, with similar tuning during reaching and passive limb displacement.

During active reaching movements, trial-averaged firing rates of muscle-like neurons in CN were generally well fit by a cosine tuning model (A P Georgopoulos et al., 1982; Prud'homme & Kalaska, 1994), with average fits of r = 0.76. Cutaneous neurons yielded, on average, a cosine fit of 0.62, which was not statistically different from the muscle-like population (t-test p-value ≈ 0.10). These values are very similar to those reported previously for neurons in motor and somatosensory cortices (A P Georgopoulos et al., 1982; Prud'homme & Kalaska, 1994) (See supplemental figure 5 (https://figshare.com/s/e1def22f5231e0bd99a7) and supplemental Table 1 (https://figshare.com/s/7dd159e0d7a0d19f1942)). For compiled firing rate, sensitivity, and latency metrics, see supplemental figure 6 (https://figshare.com/s/aa1a3eb97a8c93cea13a).

Other neurons exhibited idiosyncratic responses, including unexpected dynamics at movement onset, (supplementary figure 7, https://figshare.com/s/a60ab3de2b78d5a73d98), potential GTO inputs (supplementary figure 8, https://figshare.com/s/e0a76ff42af5a92628af), cutaneous responses from the hand (supplementary figure 2, https://figshare.com/s/cbebb1957388bf75b5c4) and forearm (supplementary figure 9, https://figshare.com/s/7829094100f94971ed4e).
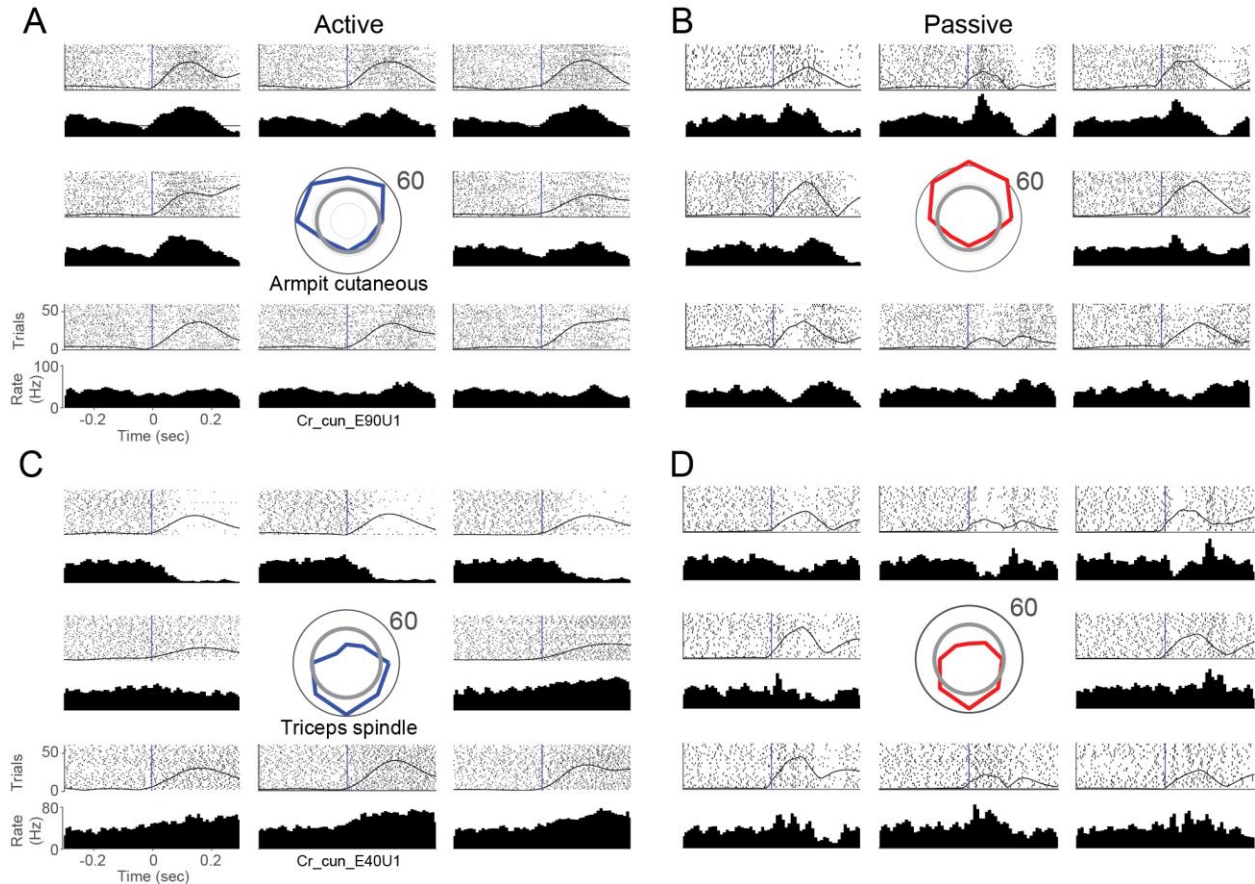
Figure 3.5: CN neurons respond robustly to active and passive arm movements. A: Responses of a CN neuron during active reaches in eight directions. RF mapping revealed that the neuron received input from cutaneous receptors in the axilla. The tuning curve (centered, blue) indicates the firing rate averaged across the 130 ms after movement onset in each direction. The grey circle illustrates the baseline rate before movement. Rasters and histograms are positioned relative to the tuning curve, to correspond to the direction of movement. The black vertical lines indicate movement onset. The hand speed is represented as a solid black line imposed over the rasters. B: Same neuron as A, for passively evoked arm movements. Passive tuning curve plotted in red at center. C,D: A second neuron, presented as in A, B, that appeared to receive input from receptors in the triceps muscle spindle.

Distribution of CN PDs can be predicted from single-muscle receptor inputs

Next, we examined the distribution of PDs across the population of CN neurons and found it to

be highly non-uniform (Figure 3.6A,B): A large proportion of PDs fell within a single lobe

pointed toward the body (near -90°) in both the active and passive conditions. This observation

was consistent across monkeys (supplemental figure 10,

https://figshare.com/s/2327936f84bf9a5a2d17). To shed light on this result, we simulated a

population of CN neurons, each with spindle input from a single muscle, inspired by the very

limited convergence we found for vibration-evoked responses in muscle-like neurons (see

Methods). The resulting distribution of simulated PDs featured a mode at -90°, much like that

that of the CN neurons, but also another mode at 90° (Figure 3.6C).

This strongly bimodal distribution of simulated spindle-driven neurons reflects the

biomechanical non-uniformity of muscles, which predominantly drive arm movements toward

and away from the body. A consequence of this anisotropy in muscle pulling directions is that

we can push and pull objects with greater strength than we can move them from side to side.

The lack of neurons with PDs pointing away from the body suggests that we recorded neurons

with a somatotopically biased set of RFs, namely a preponderance of neurons driven by

lengthening of elbow extensors and shoulder flexors and lacking neurons driven by their

complements. When we limited the inputs to our simulated neurons based on the mapped RFs of

our recorded CN neurons, the two PD distributions matched more closely (Figure 3.6D,E). Even

at the single-neuron level there was a reasonable correspondence between the PD of the

recorded neurons and their modeled counterparts. While prediction accuracy was poorer for CN

neurons that received inputs from muscles in the back (which tend to be multi-layered, broad,

and biomechanically dissimilar), accuracy for CN neurons that received inputs from the arm

was high (supplementary figure 11 https://figshare.com/s/94078b422bd069857c1a). These

results are consistent with the view that CN neurons receive input primarily from individual

muscles.
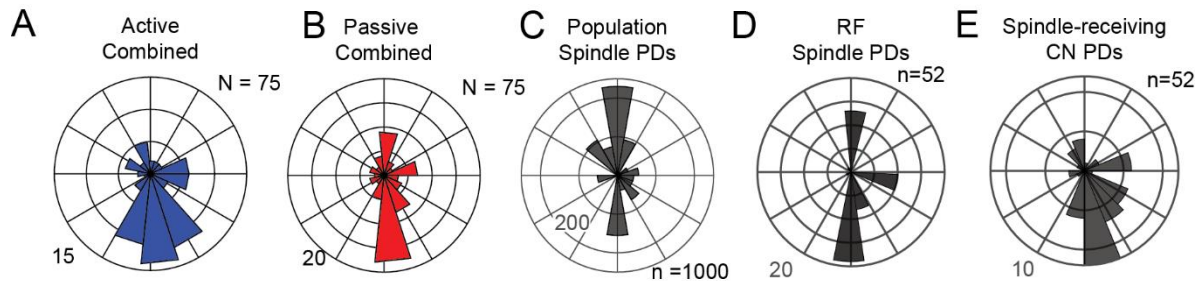
Figure 3.6: Preferred direction distributions for simulated and actual CN neurons. A: Polar histogram of active PDs combined across monkeys (N= 75 neurons). Outer circle represents 15 neurons with PDs in that bin. All subsequent plots in this figure have the same layout as A. Neurons included in this figure were sinusoidally tuned in both active and passive conditions, from CN regions of the array, and appeared to receive inputs from the upper trunk, shoulder or proximal arm. B: Passive PD distribution for CN neurons. C: PD distribution for all 1000 simulated CN neurons receiving input from a muscle spindle of a single randomly chosen muscle in the proximal arm. D: PD distribution for simulated CN neurons, having inputs corresponding to those actually mapped for recorded neurons. E) Actual PD distribution of the same spindle-receiving neurons in D (n = 52).

Directional tuning of active and passive responses are similar

Next, we examined the directional tuning during actively generated movements and compared it to directional tuning during imposed limb perturbations, focusing on neurons that exhibited sinusoidal directional tuning. First, we found that the depth of modulation was correlated across conditions: Neurons that were strongly tuned in the active condition were also tuned in the passive one (Figure 3.7A). Second, we found that PDs were typically consistent across the two conditions (Figure 3.7B), with more than 50% of neurons exhibiting active and passive PDs that differed by less than 30º (Figure 3.7C). From these data, we conclude that CN neurons convey information about direction that is largely consistent regardless of whether limb movements are generated actively or imposed.
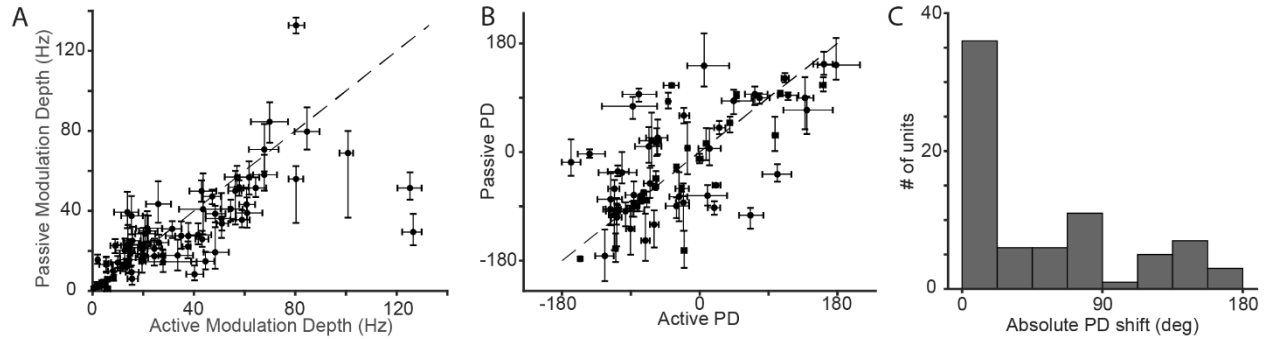
Figure 3.7: CN neurons have similar active and passive tuning. A: Each point represents the modulation depth of a neuron in the passive condition plotted against its active modulation depth. Error bars denote the bootstrapped 95% confidence interval of the modulation depth computed across trials. Neurons in the figure have the same inclusion criteria as those of Fig 6A. B: Each point represents the active and passive tuning direction for single proximal limb CN neurons that were sinusoidally tuned in both conditions. The black dashed line is the unity line. The error bars denote the bootstrapped 95% confidence interval on the PD. C: Histogram of the absolute angle between active PDs and passive PDs.

Response strength differs in the active and passive conditions

CN responses to tactile stimulation have been shown to be suppressed during movement (Ghez & Pisa, 1972; He, Suresh, Versteeg, Rosenow, & Bensmaia, 2019), a phenomenon that likely accounts in part for the documented decrease in cutaneous sensitivity during movement (Williams & Chapman, 2000, 2002; Williams, Shenasa, & Chapman, 1998). With this in mind, we examined the degree to which such a gating phenomenon occurred in our sample of CN responses. Specifically, we compared the strength of the response evoked in CN neurons in the active vs. passive movement conditions. As the kinematics were not identical in the two conditions, we selected a subset of datapoints for further analysis that had matching velocity across the two conditions. Furthermore, we focused the analysis on the responses of 65 neurons whose responses were sinusoidally tuned for at least one of the two conditions, 48 of which

were muscle-like and the rest cutaneous.

Of the 48 muscle-like neurons, 21 were potentiated during active reaching and 7 were attenuated; the remaining 20 produced responses that did not differ significantly in the two conditions (Figure 3.8A). Among the muscle-like neurons, the results were similar whether or not they were spindle-receiving. Of 17 cutaneous neurons with RFs on the upper torso and proximal arm, 3 were significantly potentiated, another 4 were attenuated, and the remainder were not significantly affected. To quantify the degree of potentiation or attenuation, we projected the responses onto a "potentiation axis" orthogonal to the unity line on Figure 3.8B. Positive projections indicate potentiation, while negative projections indicate attenuation. As a population, muscle-like neurons were potentiated during reaching, while cutaneous neurons were not (Figure 3.8C; two-sided t-test $p = 0.037$ for proprioceptive neurons, $p = 0.96$ for cutaneous neurons). We found that spindle-receiving neurons as well as the more general class of muscle-like neurons were similarly potentiated. Among 38 spindle-receiving neurons, 15 were potentiated and 6 were attenuated, while for the 10 muscle-like (but not spindle-receiving) neurons, 6 were potentiated and only 1 was attenuated. Two examples of these neurons are shown in Supp. Fig 8. These neurons included three with possible GTO inputs, which may explain their bias towards potentiation. We also examined the consistency of the potentiation, which varied considerably across neurons for all monkeys and found the potentiation was quite consistent across the first and second halves of experimental sessions (Figure 3.8D). Both the sign and magnitude of the potentiation were well preserved for virtually all neurons, cutaneous as well as muscle-like.
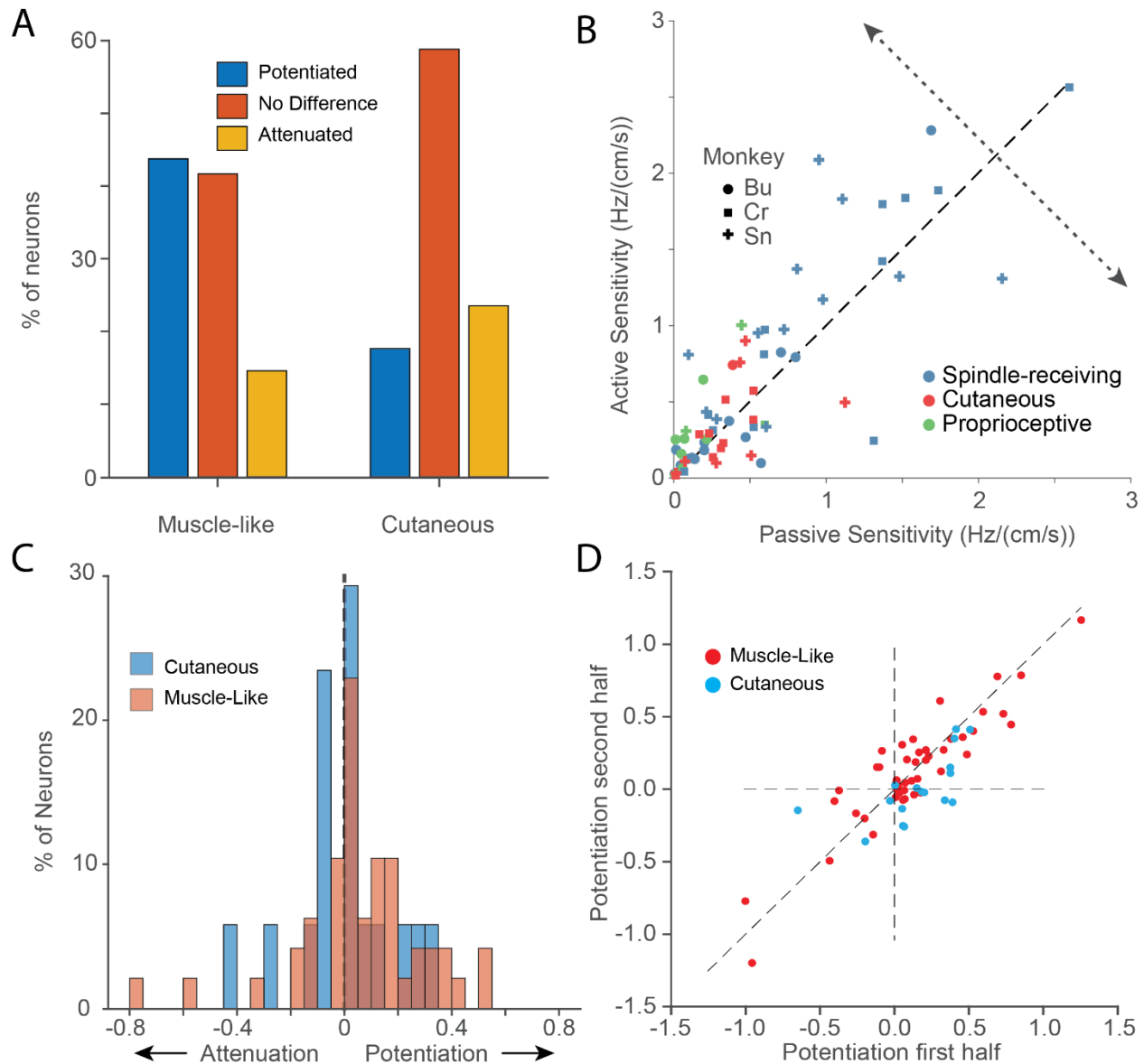
Figure 3.8: Sensitivity of neurons is modulated by movement context. A: Distribution of sensitivity changes with reaching across all neurons by modality (across two experimental sessions from each monkey, n = 48). B: Scatter plot of active sensitivity as a function of passive sensitivity for CN neurons that were sinusoidally tuned in either condition, and with RFs that didn't include the distal arm. The potentiation axis (dotted line) indicates change in sensitivity of active reaching vs. passive perturbation. Symbol shape indicates the monkey from which the neuron was recorded. Symbol color indicates the sensory modality of the neuron. C: Magnitude of the potentiation across neurons. While muscle-like neurons (red, top subplot) yielded positive gains (two-sided t-test, n = 48, p = 0.037), cutaneous neurons were not more significantly more prone to potentiation or attenuation (blue, bottom sub-plot, two-sided t-test, n = 17, p = 0.96).)

D: Scatter plot of the potentiation effect in the second half of a given experimental session plotted against that in the first half, for all monkeys.

Discussion

In this study, we examined the representation of arm movements – actively generated and passively imposed – in the CN of three monkeys. First, we found that CN neurons are strongly activated during both types of movement, typically with sinusoidal directional tuning that is largely conserved between the two conditions. Second, our inability to drive CN neurons with vibrations applied to more than one muscle, and the similarity of actual CN preferred directions to those derived from the simulated spindle responses of single muscles, suggest that most CN neurons receive input from a single muscle. Third, while directional tuning is similar in the active and passive conditions for muscle-like CN neurons, their sensitivity to movement is potentiated during active reaching. This potentiation is not observed in cutaneous neurons.

Convergence of multiple muscles onto CN neurons is limited

We never observed cross-modal convergence and found only infrequent convergence from multiple muscles. Those few neurons that appeared to have multi-muscle RFs received inputs from multiple forearm muscles. It may be that forearm muscles have higher levels of convergence than other muscle groups. It is possible that this finding reflects greater mechanical coupling between the parallel forearm muscles (Hummelsheim & Wiesendanger, 1985), but the precise placement of the vibrator, even within a single muscle, required to evoke firing argues against this interpretation. Previous studies have reported receptive fields in rostral CN spanning multiple joints (Cheema et al., 1983). Whether these RFs resulted from single biarticular

muscles rather than convergence across muscles is not clear.

Prior studies investigating whether afferent signals from multiple muscles converge onto individual CN neurons have yielded contradictory results. One study found that CN neurons typically respond to stretch of only one forearm muscle (Hummelsheim & Wiesendanger, 1985), with only about 25% of neurons exhibiting convergence from another muscle. In contrast, another study found that 87% of CN neurons could be excited by electrical stimulation of more than one peripheral nerve. A high percentage responded even to stimulation of both superficial and deep radial nerves (purely tactile and proprioceptive, respectively) suggesting cross modal in addition to cross-muscle convergence (C. L. Witham & Baker, 2011). A more recent study helps to reconcile these findings; Bengtsson et al. found that while CN neurons often receive input from a large number of afferents, only a small number of them strongly activate CN; the majority are "silent synapses" (Bengtsson, Brasselet, Johansson, Arleo, & Jörntell, 2013b). The high levels of convergence observed with peripheral nerve stimulation may result from nonphysiological levels of synchronous inputs.

This evidence of limited convergence onto CN is supported by our ability to predict the PDs of individual spindle-receiving neurons based on the single dominant muscle in their receptive field. This was true both at the single-neuron level (primarily for CN neurons that received inputs from the arm; supplementary figure 11, https://figshare.com/s/94078b422bd069857c1a) as well as the population level, with one caveat. While the major node of the CN PD distribution pointing toward the body closely matched that of the simulated distribution. The latter had an

additional prominent lobe pointing away from the body, which was only weakly represented in the CN distribution. This bimodal PD distribution was predicted previously for both muscle spindles (Sandbrink et al., 2020) and neurons in primary motor cortex (Lillicrap & Scott, 2013). The discrepancy between simulated and actual CN PD distributions may be explained by a sampling bias introduced by the fixed depth of the recording electrodes. Consistent with this idea, somatotopic organization in DCN-complex nuclei has been observed not only along the mediolateral and rostro caudal axes but also in depth (Loutit et al., 2021; Suresh et al., 2017). Previous investigations have found proprioceptive CN neurons over 3.5 mm deep compared to our 1.5 mm, suggesting that we may be sampling less than half of the depth-extent of CN with this array design.

For the most part, active and passive PDs were similar for CN neurons, with more than 50% differing by less than 30°. There were occasional discrepancies, which likely arise from a combination of factors including PD estimation uncertainty (Stevenson et al., 2011), altered descending drive (including gamma drive, sup. figure 7, https://figshare.com/s/a60ab3de2b78d5a73d98) or convergence from unmodeled receptors, such as GTOs (sup. figure 8, https://figshare.com/s/e0a76ff42af5a92628af).

Modulation of CN response sensitivity during active and passive arm movements

Tactile perceptual sensitivity is attenuated during self-generated movement (Juravle, Binsted, & Spence, 2017a; Schmidt, Schady, & Torebjörk, 1990). Consistent with this observation, the magnitude of evoked potentials in somatosensory cortex is also reduced during reaching

(Morita, Petersen, & Nielsen, 1998). This attenuation has been shown to occur at least in part at the level of CN, where experiments in cats showed that CN output is attenuated both by stimulation of the motor cortices (Andersen, Eccles, Oshima, et al., 1964) and during active stepping movements (Ghez & Pisa, 1972). These effects are at least partially mediated by presynaptic inhibition in the cuneate (Andersen, Eccles, Schmidt, et al., 1964a). These observations led to the hypothesis that afferent signals might be attenuated to reduce sensory noise, particularly during rapid, ballistic movements intended to be executed without feedback (Cohen & Starr, 1987; Morita et al., 1998). However, more recent studies reveal a more nuanced picture: particular CN responses are potentiated when stimulation is applied to a cortical site with an RF that matches that of CN and attenuated when the RFs do not match (Palmeri, Bellomo, Giuffrida, & Sapienza, 1999). We found that about 40% of all CN muscle-like neurons were potentiated in the active condition, while only 15% were attenuated (though some quite markedly).

The responses of cutaneous nerve fibers have been shown to carry limb-kinematic information comparable to that of muscle spindles (Edin, 1992). Furthermore, activation of cutaneous afferents in a manner that mimics that occurring during arm movement biases the conscious perception of hand location (Collins et al., 2005; Edin & Johansson, 1995). To the extent that cutaneous signals complement muscle-derived ones to support proprioception, one might expect that cutaneous signals would also be potentiated during active movements. In our experiments, changes in sensitivity of cutaneous neurons were less common than those of muscle-like neurons and were equally likely to be attenuation as potentiation. These widely varied patterns

of altered sensitivity, and their consistency within experimental sessions (Figure 3.8C), suggest that they are not random, but rather fine-tuned across muscles and receptors, perhaps functionally "spotlighting" relevant information. There may also be differential effects on sensitivity depending on the location of the RF. More distal tactile RFs may have different sensitivity than the proximal, primarily proprioceptive, RFs included in this analysis.

CN neurons receive input both directly from peripheral receptors and by way of spinal interneurons in laminae 3-7. One study estimates that in the rat, between 30-40% of dorsal column afferents to CN are these second-order neurons (Giesler et al., 1984; Loutit et al., 2021). Thus, gain modulation in CN might have a spinal origin. One study found cutaneous afferent input to cervical spinal interneurons to be consistently attenuated during active movements, while proprioceptive information was potentiated (Confais, Kim, Tomatsu, Takei, & Seki, 2017a). That study differed from ours in the location of the receptive fields, ours focusing on neurons with proximal limb RFs, and the earlier study, the hand and distal arm. The discrepancy between our studies may result from the very different roles of distal cutaneous neurons for stereognosis and object interactions, and proximal arm neurons (both cutaneous and muscle) for control of reaching and a sense of limb position and movement. Importantly, our experiments could not distinguish between altered gamma drive, spinal modulation of spinal transmission, or descending inputs to CN as the source for the amplification of proprioception in our recordings.

CN responses: A lens into gamma drive

The influence of gamma drive on spindle responses during active reaching movements is understood only qualitatively (Michael Dimitriou & Edin, 2008; Proske & Gandevia, 2012). Our ability to record CN neurons during reaching may provide an indirect view of gamma modulation of spindle activity. In the passive condition, many spindle-receiving CN neurons reduced their firing for non-preferred directions, responses presumably associated with shortening of the muscle in their RF. However, these same neurons often did not have decreased rates during active movement in the same directions, suggesting that gamma drive may have prevented the spindles from falling silent. In fact, we often saw transient increases in the firing rate in these anti-preferred directions near movement onset (supplementary figure 7, https://figshare.com/s/a60ab3de2b78d5a73d98). These effects are consistent with increased gamma drive, though we cannot rule out other effects of descending modulatory input to the spinal cord or CN.

Use of CN as a neural interface site for somatosensory replacement

With the increasing sophistication of efferent brain computer interfaces that can allow paralyzed patients to move (Collinger, Gaunt, & Schwartz, 2018; Hochberg et al., 2006; Lee et al., 2018), attention has swung to the complementary problem: restoring touch and proprioception to these patients by activating the somatosensory system electrically (Bensmaia & Miller, 2014b; Flesher et al., 2016; Tabot et al., 2013). Somatosensory cortical stimulation has been used in both intact monkeys and paralyzed patients to elicit somatosensory percepts. Humans with electrode arrays implanted in the primary somatosensory cortex report strong, repeatable

sensations from stimulation, including pressure, tingling, and vibration. However, proprioceptive-like percepts have been rare or absent (Collinger et al., 2018; Flesher et al., 2016; Lee et al., 2018). Likewise, targeted muscle reinnervation (TMR) and peripheral nerve stimulation have shown promise in restoring sensation in limb amputees (Horch, Meek, Taylor, & Hutchinson, 2011; Schiefer, Graczyk, Sidik, Tan, & Tyler, 2018; Tan et al., 2014), in part because the simpler coding and additional peripheral processing may simplify stimulus paradigms.

For spinal injury patients, the most peripheral site above the lesion is the CN, making it an appealing option to consider as a site of stimulation for sensory replacement (Loutit & Potas, 2020). We found a somatotopy across each array that was consistent across monkeys. Neurons were segregated both by modality (rostral and ventral subnuclei) and receptive field location, similar to earlier descriptions (Loutit et al., 2021). This somatotopic representation may allow for coherent proprioceptive percepts to be evoked via electrical stimulation. One drawback to CN as a site of proprioceptive replacement is the potential for damage to the dorsal columns or other medullary nuclei. While deafferentation is not a major concern for a person with a spinal cord injury who lacks sensation, CN lies close to medullary regions critical for homeostatic regulation, such as the dorsal respiratory group (Berger, 1977). Attempts to restore sensation in the medulla need to take care to minimize trauma to the surrounding tissue, perhaps with lower stiffness or non-penetrating electrodes.

Chapter 4 – Cuneate nucleus: the somatosensory gateway to the brain

Christopher Versteeg, Raeed H. Chowdhury, and Lee E. Miller

Foreword

The following was adapted from a manuscript published in the Current Opinion in Physiology in April 2021. In it, I review some previous results from my CN recordings, and compare the sensory gain and convergence in CN to previously recorded signals in somatosensory area 2. I then present a high-level overview of the current understanding of CN in the proprioceptive pathway.

Abstract

Much remains unknown about the transformation of proprioceptive afferent input from the periphery to the cortex. Until recently, the only recordings from neurons in the cuneate nucleus (CN) were from anesthetized animals. We are beginning to learn more about how the sense of proprioception is transformed as it propagates centrally. Recent recordings from microelectrode arrays chronically implanted in CN have revealed that CN neurons with muscle-like properties have a greater sensitivity to active reaching movements than to passive limb displacement, and we find that these neurons have receptive fields that resemble single muscles. In this review, we focus on the varied uses of proprioceptive input and the possible role of CN in processing this information.

Introduction:

Proprioception is generated by a variety of receptors that encode mechanical strain and deformation caused by the movement of all parts of the body, including the trunk, head and limbs. Chief among these receptors are muscle spindles that encode muscle length and the speed of length change (Proske & Gandevia, 2012). Golgi tendon organs that respond to active muscle force, joint receptors responding to loads and extreme positions, and skin receptors activated by movement-related stretch of the skin (J. Houk & Simon, 1967). This diverse set of receptors supplies information throughout the cerebral cortex and cerebellum and underlies all aspects of proprioception, from simple spinal reflexes to complex supraspinal reflexes as well as the planning and execution of voluntary movements. Information from these same receptors is also necessary for the conscious perception of the position and motion of our limbs, a perception that remains largely in the background (Proske & Gandevia, 2012) causing it to be referred to colloquially as the "hidden" sixth sense.

A significant portion of afferents from these receptors project directly or indirectly to a caudal brainstem region referred to as the dorsal column nuclei (DCN) complex (Loutit et al., 2021; Mountcastle, 2011). This complex of nuclei is in an ideal position to regulate these inputs. Early work examining their structure and function was primarily conducted on cat models, almost always while under sedation (Andersen, Eccles, Oshima, et al., 1964; Andersen, Eccles, Schmidt, et al., 1964a; Cooke, Larson, Oscarsson, & Sjölund, 1971; Rosén & Sjölund, 1973), with notable exceptions (Ghez & Pisa, 1972).

We have recently begun to record in awake monkeys from the cuneate nucleus (CN) (Suresh et al., 2017), the portion of the DCN that carries signals from the arms to the thalamus (Rosén & Sjölund, 1973). Such recordings now allow us to make observations that were previously impossible under sedation. For example, our results show that the sensitivity of many CN neurons differs for actively generated reaches and passive limb displacements of the arm. Those neurons that appear to receive input from muscle spindles are typically more sensitive during active movement. Furthermore, we found that the tuning of CN neurons for movements in different directions is quite similar to what we would expect from receptors of a single muscle, matching the results of previous studies using single muscle stretches (Hummelsheim & Wiesendanger, 1985; Rosén & Sjölund, 1973) but contrasting with a study using electrical stimulation of peripheral nerves (C. L. Witham & Baker, 2011). In this review, we will attempt to reconcile the apparent inconsistencies in the previous literature, focusing on two major areas: proprioceptive gain modulation and convergence of afferent input in DCN. In doing so, we hope to provide a perspective from which to examine previous DCN research and to design new studies to illuminate how proprioceptive information is processed as it moves from the periphery to the brain.

Proprioceptive gain modulation in the cuneate nucleus:

Sensory gating, or the attenuation of afferent input, is a feature of many sensory systems (Azim & Seki, 2019). During saccadic eye movements, visual information is attenuated to avoid blurred images caused by the movement of the eye (Binda & Morrone, 2018; Bremmer, Kubischik, Hoffmann, & Krekelberg, 2009; Crevecoeur & Kording, 2017; Holt, 1903).

Similarly, tactile sensations arising during active touch are significantly weaker than the same stimuli presented passively (Cohen & Starr, 1987; Schmidt et al., 1990). These observations have led to the hypothesis that the nervous system turns down the gain on sensory receptors when the information they are transmitting is likely to be noisy (Ghez & Pisa, 1972). As the somatosensory gateway to the brain, neurons in the DCN complex are a logical site of proprioceptive gating.

Consistent with the sensory gating hypothesis, CN receives descending signals from the somatosensory and motor cortices (Andersen, Eccles, Schmidt, et al., 1964a; Leiras, Velo, Martín-Cora, & Canedo, 2010; Loutit et al., 2021). Their effect on afferent transmission has been the subject of experiments conducted mostly in anesthetized cats. Stimulation of these cortical areas leads to both excitatory and inhibitory effects, though early studies focused primarily on the inhibitory ones (Aguilar, Rivadulla, Soto, & Canedo, 2003; Andersen, Eccles, Oshima, et al., 1964; Andersen, Eccles, Schmidt, et al., 1964a). Much like the effect of cortical stimulation, the afferent volley from stimulating the second of two peripheral nerves in close succession is markedly attenuated, suggesting that inhibitory circuitry within CN also contributes to the attenuation of afferent signals (Andersen, Eccles, Oshima, et al., 1964).

The potential functional role of this afferent attenuation was studied more directly by recording medial lemniscus field potentials evoked by stimulation of the tactile superficial radial nerve in cats (Ghez & Pisa, 1972). The resulting afferent volleys, which would have been generated by axons supplying RFs throughout the forearm and paw were attenuated during stepping. Without

finer spatial resolution, it would have been difficult to see combined enhancement and attenuation of the effects, if it were there. As a means to determine the mechanism giving rise to the attenuation they applied Wall's technique (Wall, 1958), which measures the amplitude of the antidromic potential in the peripheral nerve in response to CN stimulation. This amplitude is correlated with the extent of depolarization in the presynaptic terminal, called primary afferent depolarization (PAD), itself an indirect measure of presynaptic inhibition. In these experiments, PAD increased in a velocity-dependent manner throughout a step, suggesting that presynaptic effects on the inputs to CN mediate at least some of the sensory gating of tactile signals.

The problem of the blurring of retinal images during rapid eye movements was recognized already in the 11th century by the Persian scholar Alhazen (Saliba & Sabra, 1992). Over 100 years ago, Holt proposed that vision is simply suppressed during saccades (Holt, 1903), but we now know that a more selective filtering of visual input occurs (Binda & Morrone, 2018). The sensation of a shirtsleeve sliding over the skin during reaching may be analogous to blurred vision during a saccade, contributing noise that the somatosensory system might appropriately attenuate. However, uniformly gating all somatosensory signals during movement, including muscle length changes or unexpected object contact, could cause blindness to critical sources of feedback. In CN, perhaps as in the visual system, there is evidence of gain modulation that is more complex than simple gating (Leiras et al., 2010; Palmeri et al., 1999). The experiments described above that yielded predominantly inhibitory effects in CN (Andersen, Eccles, Oshima, et al., 1964) relied on broadly distributed cortical stimulation. In other experiments that matched the receptive field of the stimulated cortical area to that of the CN neuron, the effect was

typically excitatory. As the receptive fields became more dissimilar, the effect of stimulation was more likely to be inhibitory (Palmeri et al., 1999), leading to a "spotlighting" effect.

While these results were for CN neurons with cutaneous receptive fields, the idea of more flexible gain modulation might well apply broadly across the somatosensory system. We investigated this question with extracellular recordings from implanted electrode arrays that allowed us to record single CN neurons from awake, behaving monkeys. We compared the movement sensitivity of CN neurons during reaching to that of passive limb perturbations. Figure 4.1A shows the response of one example neuron that appeared to receive input from the anterior deltoid. We fit sinusoidal tuning curves to the responses and found the neuron's preferred direction (PD) using simple linear models (A P Georgopoulos et al., 1982).

In addition to deriving the PD of each neuron, these linear models allowed us to infer the sensitivity of each neuron's firing rate to the speed of movement. We compared these inferred sensitivities between the active and passive conditions. The slope of the fitted lines in Figure 4.1B represents the sensitivity for both active (blue) and passive (orange) limb movements. In this example, the sensitivity of the active movements was larger (1.3 Hz/(cm/s)) than that of the of the passive condition (0.8 Hz/(cm/s)). Across all muscle-like CN neurons (those that had receptive fields that resembled muscles with no tactile response), the active sensitivity tended to be greater than the passive sensitivity (Figure 4.1C, filled circles). To make statistical comparisons between active and passive sensitivity, we used bootstrapping to estimate the confidence interval of the sensitivity difference for each neuron (Efron & Tibshirani, 1986). We

then counted those neurons with significantly enhanced or attenuated sensitivity. Across three monkeys, the sensitivity of muscle-like CN neurons was more than twice as likely to be enhanced during active reaching than attenuated (Figure 4.1D, black bars). There was no such bias in CN neurons with tactile receptive fields (Figure 4.1D, gray bars). We also performed this analysis for neurons recorded under the same conditions from area 2, a mixed cutaneous and proprioceptive area of cerebral cortex. We found that unlike CN, area 2 neuron sensitivities were somewhat more likely to be attenuated during active movement than enhanced (open symbols and bars, Figure 4.1 C, D), in contrast with an earlier study whose methods didn't take into account differences in kinematics and found no significant difference across conditions (Brian M London & Miller, 2013). This may reflect additional attenuation that occurs after signals pass through CN, for which there is some evidence (Chapman, Jiang, & Lamarre, 1988; Dale & Cullen, 2019). The functional role of this added inhibition is not clear.
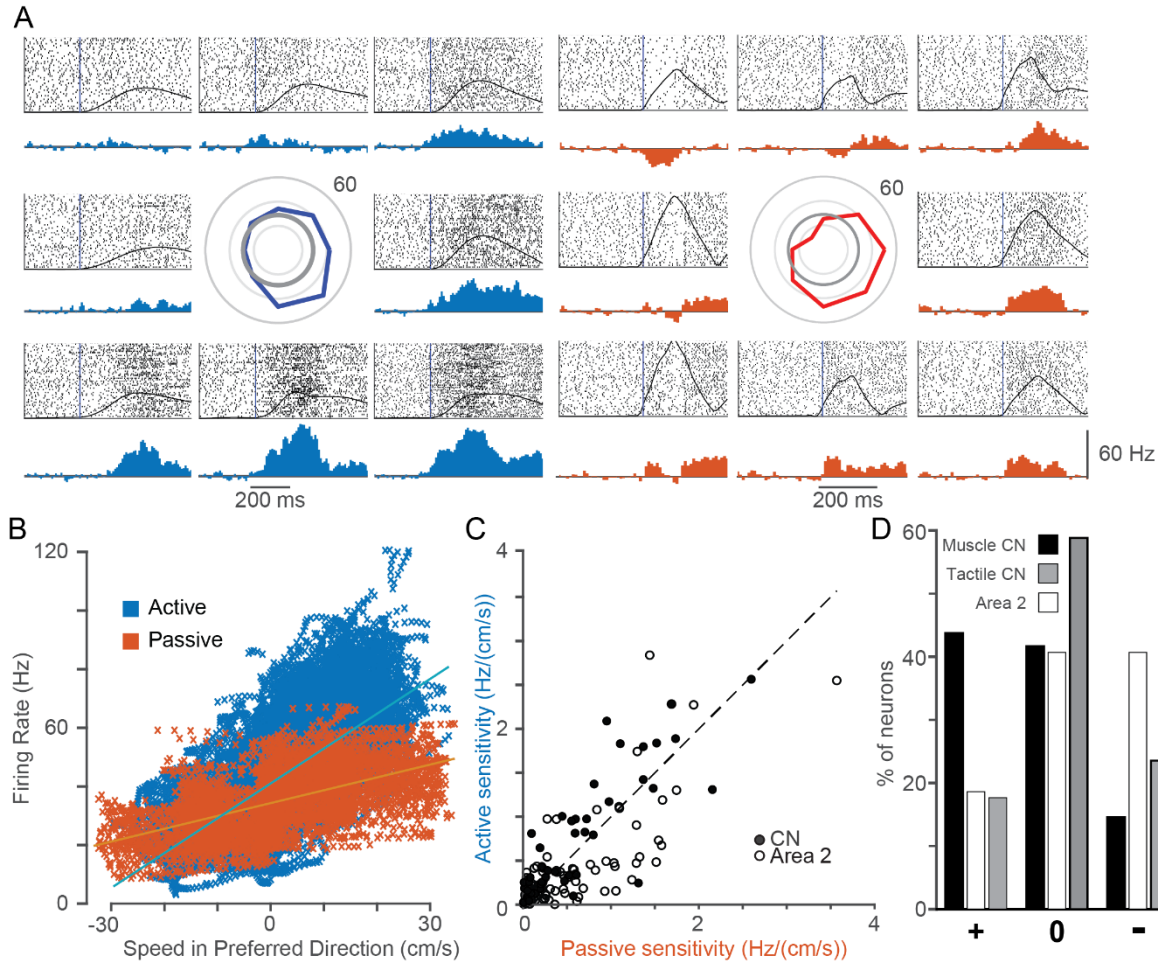
Figure 4.1: CN neurons with muscle-like inputs tend to respond more strongly to reaching movements than to passive arm perturbations. A: Responses recorded from a single CN neuron that appeared to receive input from muscle spindles in the anterior deltoid. The monkey grasped the handle of a planar manipulandum and made "center-out" movements in eight directions (left group of eight responses). We applied force perturbations in the same eight directions when the hand was at rest in the center-hold position prior to 50% of the movements (right group of responses). Raster plots (above) and trial-averaged firing rate histograms (below) are shown for each movement direction, positioned relative to the center of each group of plots. In the center of the plots is the tuning curve of the neuron. Overlaid on the raster plots are trial averaged hand speed traces for each direction. B: Scatter plot relating the firing rate of the example neuron in A to the hand speed in the PD. Each data point represents a single 10 ms time bin, color coded by condition. Blue and orange lines represent the best linear model fit from hand velocity to firing rate. C: Summary of the active and passive sensitivity of spindle-receiving CN neurons (filled circles, three monkeys, 48 neurons) and somatosensory cortical area 2 (open circles, two monkeys, 86 neurons) neurons. D: Percentage of neurons with sensitivity that was significantly

enhanced (+), was unchanged (0), or was attenuated (-) in the active case compared to the passive case.

Gain modulation in CN could arise from multiple sources including descending modulatory input to CN, altered gamma drive to muscle spindles, and altered transmission of the afferent input through spinal interneurons. Muscle spindles receive descending gamma drive that directly modulates their sensitivity (A. Prochazka et al., 1985a). During locomotion, gamma drive is modulated substantially, particularly so during less stereotypic gait (Bennett et al., 1996; Ellaway, Taylor, & Durbaba, 2015b). Although gamma drive has the potential to explain the context-dependence that we observe in CN, its modulation during reaching has not been well studied and extrapolating to reaching from quadrupedal locomotion in cats is problematic (K. E. Jones, Wessberg, & Vallbo, 2001). Experiments using methods insensitive to gamma drive, such as measurement of PAD, have found similar enhancement in proprioceptive spinal interneurons (Confais et al., 2017a), evidence that reach-related enhancement is likely not wholly due to alterations in gamma drive. Experiments designed to further identify the site or sites of proprioceptive gain modulation would make an important contribution to our understanding of this system.

Functionally, gain modulation serves at least two purposes. First, it can enhance or attenuate the intensity of the conscious experience of a sensation, as demonstrated in previous psychophysical studies (Juravle, Binsted, & Spence, 2017b; Schmidt et al., 1990). Perhaps more importantly, sensory gain must be optimized for motor control. For example, the gain of the stretch reflex is reduced in muscles that would otherwise oppose the generation of fast movements (Adams &

Hicks, 2005) . Throughout the gait cycle of normal walking, the stretch reflex is maximal during

stance and completely suppress in the transition from stance to swing (Sinkjær, Andersen, &

Larsen, 1996). Recently, groups have begun to investigate the consequences of disrupting these

gain-modulating pathways, leading to profound motor deficits, including oscillatory movements

that are consistent with an underdamped feedback control system (Fink et al., 2014). Gain

modulation at every level of the somatosensory neuraxis (including fusimotor drive to the

spindles) likely underlies the flexibility of multiple hierarchical feedback control loops (Kurtzer

et al., 2008; Nashed et al., 2014; Pruszynski et al., 2011a; Scott, 2004, 2016; Scott, Cluff,

Lowrey, & Takei, 2015; Weiler et al., 2019).

Convergence properties in CN and area 2

In addition to selective modulation of gain, sensory afferent pathways may also combine inputs

across space and differing modalities. The evidence for such convergence in CN is mixed. In

one study, 87% of CN neurons responded to electrical stimulation of more than one peripheral

nerve, even across modalities (C. L. Witham & Baker, 2011). Other experiments, in which

individual muscles were stretched, found very little convergence (Hummelsheim &

Wiesendanger, 1985; Rosén & Sjölund, 1973).

We estimated the extent of convergence in CN with two complementary methods: mapping

receptive fields using vibratory stimuli and examining the spatial tuning of single CN neurons

during passive arm movements. A good fraction (~50%) of neurons in CN that appeared to have

muscle-like receptive fields from manual testing responded robustly to ~100 Hz muscle

vibration, a stimulus that strongly activates muscle spindles (Figure 4.2A). Figure 4.2B shows a

neuron with a phase-locked response to vibration with a lag of ~8 ms from the peak voltage

driving the vibrator. Despite these strong responses from individual muscles, it was quite rare

that a given CN neuron could be driven by vibration of more than one muscle. Attempts to

evoke similar responses in area 2 were uniformly unsuccessful. We speculated that the inability

to drive area 2 neurons may be due to their receiving convergent input not only from multiple

muscles but also cutaneous afferents, thereby diluting the effect of the spindle input from a

single vibrated muscle. It would be informative to repeat this experiment in thalamus and

somatosensory cortical area 3a, as both regions have neurons which receive exclusively muscle

inputs.
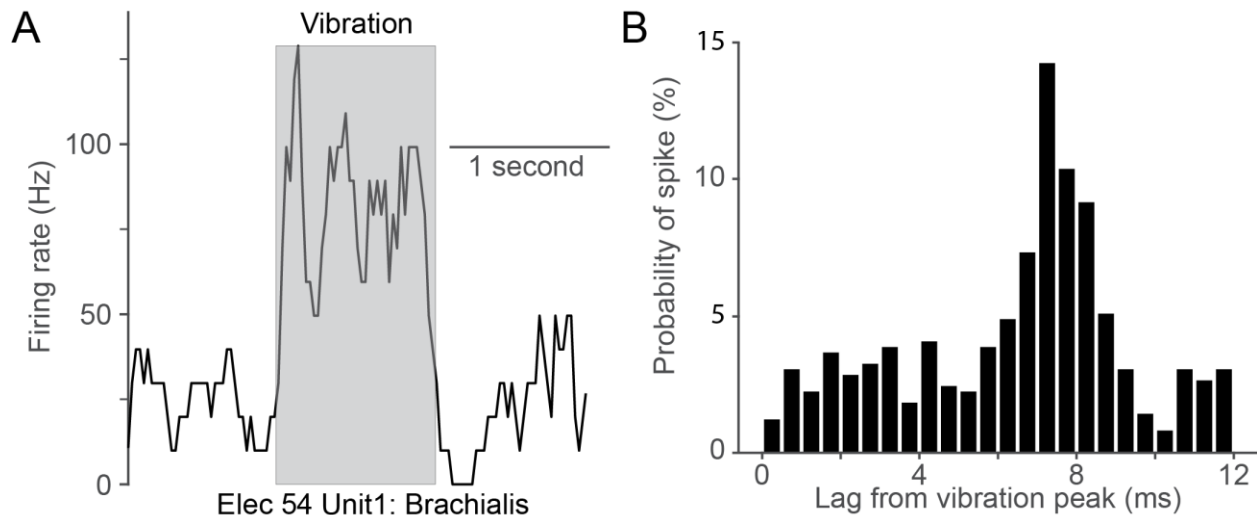
Figure 4.2: Neurons in CN are strongly activated by 100 Hz sinusoidal vibration. A: Example CN response to vibration of brachialis. During 100 Hz vibration (grey box), firing rates increased to ~100 Hz, and returned to baseline immediately after stimulation ended. B: Time-dependent probability of the occurrence of the first spike after peak indentation suggests that this example CN neuron was phase-locked to the vibration.

We found a striking nonuniformity in the distribution of CN PDs (Figure 4.3A) and asked whether it might also be evidence of limited convergence. To this end, we used DeepLabCut, a markerless motion tracking system (A. Mathis et al., 2018), an OpenSim musculoskeletal model (Chan & Moran, 2006; Delp et al., 2007), and a simple model of the spindle response to muscle length change (a one-half power law mapping muscle lengthening to firing rate (J. C. Houk et al., 1981)) to simulate the activity of muscle spindles throughout the 18 major muscles of the arm during the passive limb movements. These simulated muscle spindle PDs were also highly nonuniform, falling primarily along the axis towards and away from the body, qualitatively like that of CN (Figure 4.3B). We reasoned that convergence of multiple muscles would cause a significantly more uniform distribution.

However, when we analyzed area 2 similarly, we found those PD distributions to be only slightly more uniform than CN, but not statistically so (Figure 4.3C). This was unexpected, given our intuition about convergence and an earlier report of a PD distribution in area 2 that was by eye, more nearly uniform (Prud'homme & Kalaska, 1994). Accordingly, we simulated the PD distributions neurons receiving convergent excitatory and inhibitory inputs from the spindles of different numbers of muscles, examining the changes in distribution with increasing convergence. While this slightly increased the distribution uniformity, the change was considerably less than we anticipated (Figure 4.3D) indicating that this tool is too crude to address the question of convergence with any precision.
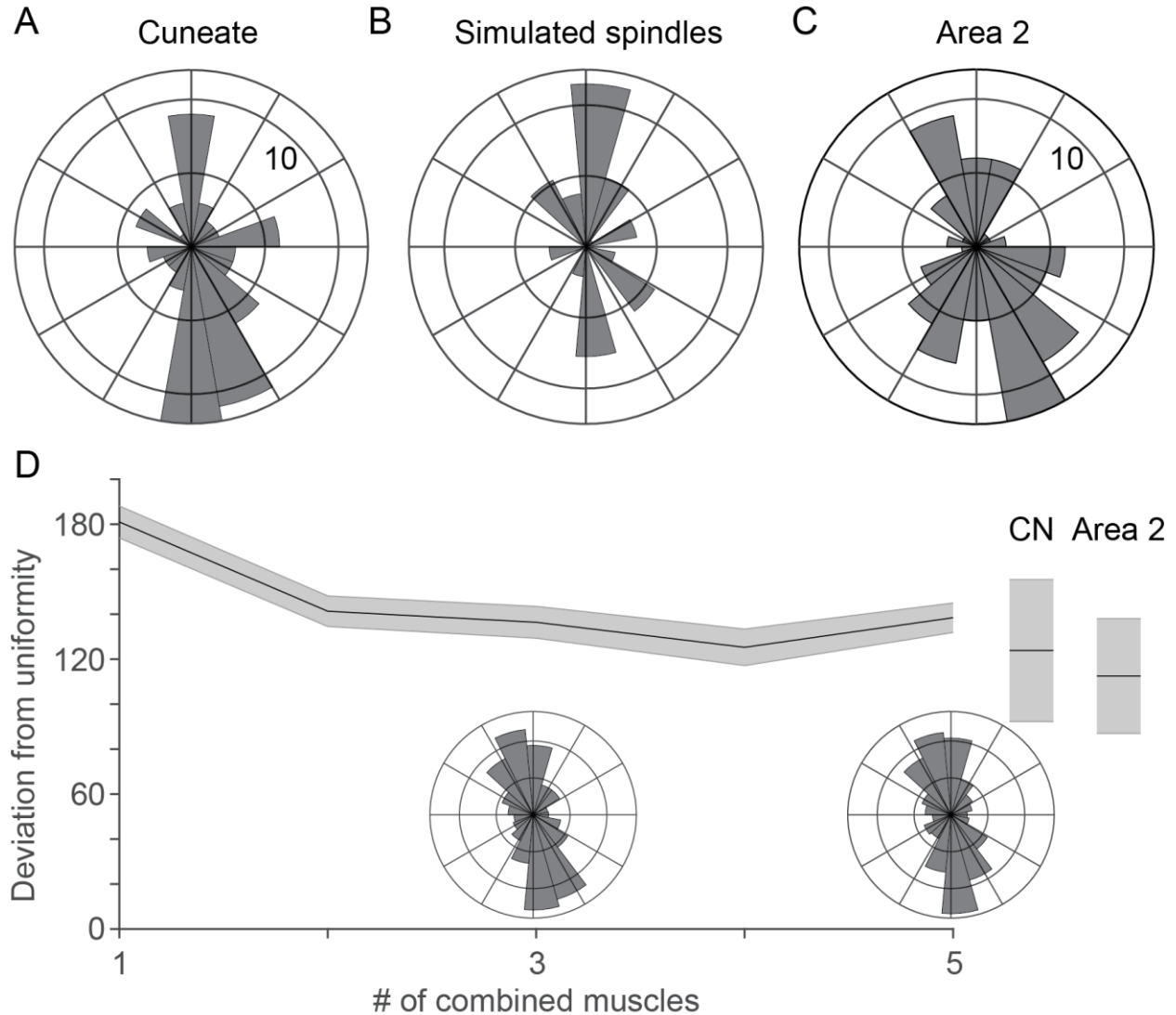
Figure 4.3: Both CN and area 2 appear to inherit strongly bimodal distributions of preferred direction from the biomechanics of the arm during passive limb displacement. A: Distribution of CN preferred directions during passive arm movements. B: PD distribution from a population of simulated proximal arm muscle spindles. C: Distribution of PDs for area 2 neurons for passive arm movements. D: Convergence of simulated muscle spindle afferents from multiple muscles slightly decreases mean absolute deviation from uniformity. Inset polar histograms show the PD distribution for simulated spindles from different numbers of muscles. Deviation from nonuniformity for actual CN and area 2 distributions plotted at the extreme of the plot. Shaded areas indicate one standard deviation of the mean across bootstrap iterations.

Proprioceptive neuroscience is in need of better tools to precisely measure and control the

relevant movement-related variables. Unlike vision or touch, which offer the means to activate

receptors with nearly arbitrary spatial and temporal patterns (Killebrew et al., 2007; Korenberg

& Naka, 1988), the mechanics of the muscles of the limb cause virtually unavoidable

correlations during natural movements (Mollazadeh, Aggarwal, Thakor, & Schieber, 2014;

Santello, Flanders, & Soechting, 1998). Opto- and chemogenetic methods are promising,

potentially allowing for fine-grained experimental circuit dissection and control of afferent

signals during behavior (M. W. Mathis et al., 2017; B. Sauerbrei et al., 2018; K. S. Smith,

Bucci, Luikart, & Mahler, 2016; Tashima et al., 2018), including targeted activation of muscle

spindle afferents (Kubota et al., 2019).

Proprioceptive streams and their relevance to motor control

For a "hidden" sense, proprioception plays several vital roles. Proprioceptive inputs to the

anterior and posterior parietal cortices, as well as to the secondary somatosensory cortex in the

superior bank of the Sylvian fissure, contribute individually to a variety of disparate functions,

including movement planning, online movement correction, as well as the conscious perception

of limb state (Pavlides et al., 1993; Rushworth et al., 1997; Wolpert, Goodbody, et al., 1998).

The ideal location of the dorsal column nuclei to combine and modulate these inputs for the

diverse function they subserve (Loutit et al., 2021) is the final topic of this review.

Area 2 is the earliest cortical area with a large proportion of neurons having combined cutaneous

and muscle inputs. For this reason, some consider it not to belong with areas 3a, 3b, and 1 as

part of S1. The confluence of these inputs within hand area 2 is thought to be important for

stereognosis, for which a knowledge of hand conformation combined with object contact points is critical (Gardner et al., 2007; Rincon-Gonzalez, Warren, Meller, & Helms Tillery, 2011; Yau, Kim, Thakur, & Bensmaia, 2016). The role of arm area 2 is less obvious, but its conjunction of tactile and proprioceptive information may be important in localizing the limb relative to nearby objects in the environment. Its strong connections to area 5 in the posterior parietal cortex reinforce this possibility (Padberg, Cooke, Cerkevich, Kaas, & Krubitzer, 2018).

The posterior parietal cortex (PPC), including area 5, is considered "multimodal association cortex", neither strictly sensory nor motor, and related to multiple interoceptive and exteroceptive sensory modalities. Interestingly, area 2 neurons retain a prominent force component (Prud'homme & Kalaska, 1994) which is eliminated in area 5, perhaps to accommodate the multimodal convergence with vision in area 7 (Hamel-Pâquet, Sergio, & Kalaska, 2006). In humans, a stroke causing a lesion in the right PPC can cause a profound neglect of the left side of the body. More precise ablations in area 5 of monkeys impair reaching in darkness but not in light, while area 7 lesions have the opposite effect: reaching in the light is impaired, but not in darkness (Rushworth et al., 1997). A human patient with a lesion in area 5 "loses" her arm when it leaves her view for more than a few seconds, but it returns when it becomes visible again (Wolpert, Goodbody, et al., 1998). This apparent role of PPC in updating limb position is closely related to its contribution to movement planning and may also involve the secondary somatosensory cortex.

The descending connections to CN from the sensorimotor cortex suggest that CN has a key role in flexibly modulating the gain of somatosensory input, although this would not rule out other lower-level mechanisms. Such gain modulation could serve to focus attention on a class of receptors or a portion of the limb under different behavioral contexts, and may also be necessary to generate complex, context-dependent reflex activity. Experiments to monitor the inputs to CN, for example in the dorsal root ganglia, under similar behavioral conditions, will be an important next step in understanding this processing.

Our own results, including sensory mappings of proprioceptive CN neurons and recording of their activity during behavior, point to a CN that receives potent connections from only a small number of afferent inputs. This finding is not altogether surprising—recent evidence shows that only a small number of synapses (4-8 for cutaneous receptors) dominate the firing of CN neurons despite far larger numbers of synapses observed anatomically on these neurons (Bengtsson et al., 2013b). This anatomical rather than physiological observation may also underlie the discrepancy with the much broader convergence estimates based on electrical stimulation that might synchronously recruit more of these afferents (C. L. Witham & Baker, 2011). The purpose of this apparently broad, yet weak convergence from the periphery is still an open question. One possible answer is that it may enable greater plasticity in sensory processing. Much like the analogous pruning process in the cerebral cortex, CN has many inputs that are lost late in development as descending corticobulbar fibers invade the dorsal column nuclei (Fisher & Clowry, 2009). Furthermore, recent studies have shown that the change in cortical representation observed after loss of peripheral input (Jain, Qi, Collins, & Kaas, 2008)

has its origin in dorsal column remapping (Kambi et al., 2014). These observations suggest that both in development and in recovery from injury, CN may optimize the strength of its diverse peripheral inputs for the proprioceptive functions carried out by more central brain structures.

Summary

Figure 4.4 presents a high-level summary of the convergence and sensitivity properties of somatic sensation presented in this review. In the periphery, the sensitivity of muscle spindles, the main receptor considered in this review, is modulated in a complex, behavior-dependent manner by descending gamma drive. Golgi tendon organs, which signal force, and cutaneous receptors lack this descending control. Additional mechanisms within the spinal cord allow the sensitivity to all somatosensory modalities to be modulated. As a general rule, muscle afferent input is primarily enhanced during active movement, while cutaneous input is attenuated. Gain modulation in the spinal cord is critically important for spinal motor circuitry to produce controlled movements. Within the main cuneate nucleus, this modality-dependent movement sensitivity is largely maintained. At this first site for convergence between afferents in the brain, there appears to be quite low behaviorally-relevant convergence between muscle inputs during typical movements, although there is some evidence that multiple cutaneous submodalities (i.e., rapidly adapting and slowly adapting receptors) may converge on single CN neurons (Suresh et al., 2017). There is also evidence of a larger number of latent synapses during development and recruited in response to injury that may only contribute meaningfully to firing when they are activated with an unusually high intensity, such as by electrical stimulation of the peripheral nerve. Finally, neurons within area 2 of the somatosensory cortex are the first neurons in the

cortical somatosensory pathway for which there is clear evidence of broad convergence across muscle and tactile modalities. Its anatomical position between the single-modality primary somatosensory areas and the even more broadly convergent receptive fields of posterior parietal cortex suggest an early role in the development of an internal body map for planning and controlling movement. How the more uniform (relative to CN) attenuation of input during movement might relate to such a functional role remains unclear.
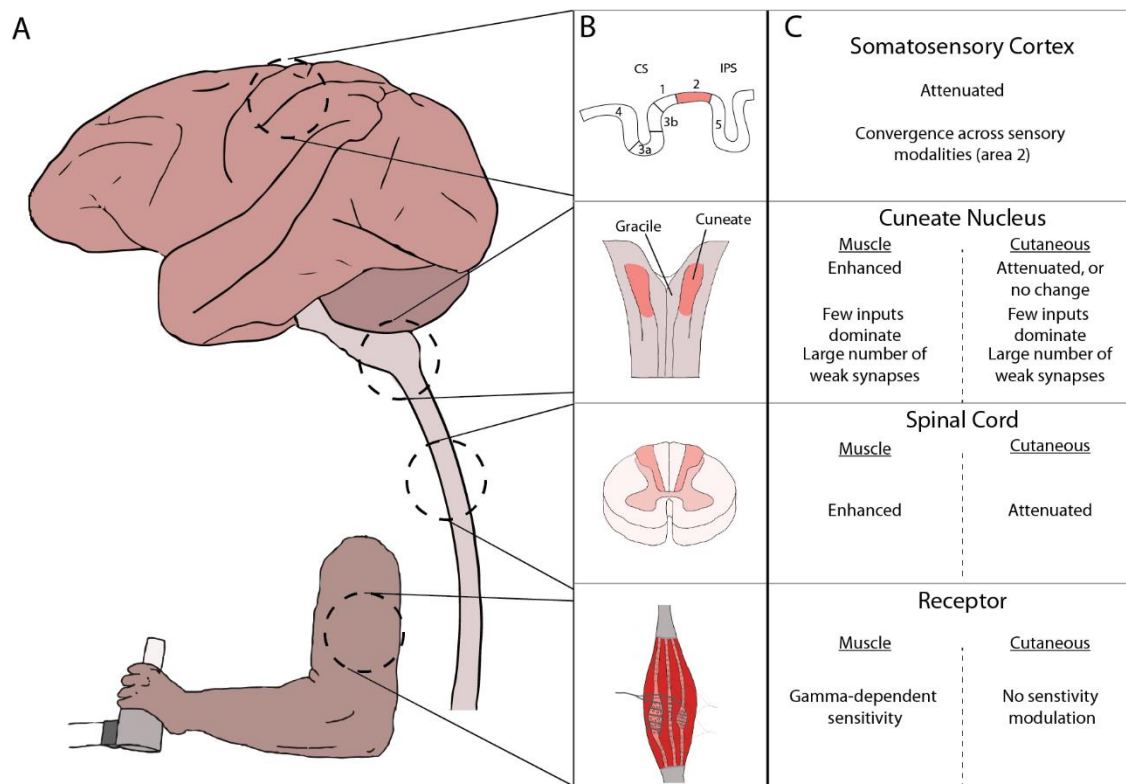
Figure 4.4: Overview of convergence and sensitivity properties along the somatosensory neuraxis A: Diagram of somatosensory areas discussed in this review. From top to bottom, in dashed circles: somatosensory cortex (adapted from a Scalable Brain Atlas of the macaque brain (Bakker, Tiesinga, & Kötter, 2015), dorsal column nuclei, spinal cord, and muscle receptors. Those areas most relevant to this review are expanded in B: and highlighted in light red. C: Summaries of the convergence and sensitivity in each of these areas. For brevity, we condensed a complex literature to the primary direction of sensitivity modulation ("attenuated" or "enhanced"), together with a similarly high-level overview of the convergence at each region.

See text and references for more nuanced detail.

Chapter 5 – Dynamical Feedback Control: Motor cortex as an optimal feedback controller built using neural dynamics

Foreword:

To understand for what purpose CN processes proprioception, we must understand how the motor system uses proprioceptive information to generate movement. This manuscript emerged as an attempt to reconcile the existing theoretical framework of neural dynamical systems (which does not typically consider proprioceptive inputs) with the apparent criticality of proprioceptive feedback for motor control. We are preparing a shortened version of this manuscript for submission to the Journal of Neurophysiology.

Introduction:

Many of the questions that we ask about the brain are determined by the framework through which we view its behavior. Questions that are entirely sensible under one paradigm may be meaningless in another; for example, under a Lamarckian view of evolution, the question "Does this change increase reproductive fitness?" is answered with a resounding "Who cares?". What is considered a reasonable question can change depending on your viewpoint (Kaiser, 2012).

Two major conceptual frameworks have guided recent study of the motor system, optimal feedback control (OFC) and neural dynamical systems (NDS). The former posits that the brain generates movement through a control system built from a feedback controller, a forward

model, and a state estimator (Scott, 2004; Shadmehr & Krakauer, 2008). The brain can adjust

feedback gains according to planning and context, thereby altering the transformation of state

estimates (combinations of both actual afferent sensory signals and predicted ones) into motor

output. OFC presents an algorithm-level description of how the motor system might generate

controlled movements but is agnostic to how this algorithm is implemented.

In contrast, the dynamical systems framework posits that motor cortical areas are autonomous

pattern-generating circuits whose firing patterns emerge in large part due to intrinsic dynamics

of the network (Shenoy et al., 2013). Under the dynamical systems hypothesis, the neural state

evolves according to this dynamical landscape, much like a ball rolling predictably along a (N-

dimensional) curved track. Here, contextual and planning inputs from premotor areas encode

different movements simply by setting different starting points: different tracks for the neural

state space ball to roll down. NDS presents both an algorithm-level (pattern-generation) and an

implementation-level (dynamics of neural circuits) description of movement generation.

These two frameworks offer different high-level perspectives on the question of how the brain

controls movement, each with its own advantages and limitations. Questions that OFC models

pose, such as "what are the feedback gains that produce this movement?" do not seem

interpretable under NDS. Conversely, common questions in NDS, such as "what does the

dynamical landscape of this neural circuit look like?" cannot easily be posed in the framework

of OFC. These fields have rich bodies of research that attempt to explain the same system while

operating largely independently of one another. Without a common language, knowledge from

one field cannot easily transfer. To bridge this gap, I propose a hybrid model called Dynamical Feedback Control (DFC), that provides a common language for dynamics and feedback control and a unifying framework for algorithmic and implementation-level descriptions of the motor system. To do this, DFC proposes that the algorithm of OFC is implemented by the dynamics of motor cortical circuits.

I am greatly indebted to prior experimental and theoretical work in the development of this model. I relied heavily on previous conceptions of the motor system, especially from the neuroanatomy reviewed here (Shadmehr & Krakauer, 2008). In particular, I would like to highlight the contributions of the Shadmehr and Krakauer groups, Scott and Pruszynski groups, recent optogenetic work studying neural dynamics from Hantman and Svoboda, and pioneering analyses of neural data from Kaufman and Churchland.

To introduce this model, I will begin by giving brief reviews of OFC and NDS. This overview is not meant to be comprehensive as more complete reviews of both already exist (Scott, 2004; Shadmehr & Krakauer, 2008; Shenoy et al., 2013). My goal with these introductory sections is to convince the reader that 1) the brain embodies the major components of an optimal feedback control system, and 2) neural dynamics offers a powerful tool for describing how neural circuits perform computation. From these two concepts, I will then build up intuition for how feedback controllers in motor cortex could be implemented by the intrinsic dynamics of sensorimotor areas. I close with an example experiment that tests the key predictions of DFC and demonstrates that the DFC model can answer questions posed in the language of both OFC and

NDS frameworks.

OFC Model:

Features of OFC:

There are many ways that a movement can be "optimal", such as minimum distance travelled, minimum jerk, or minimum energy. A major feature of the OFC optimality is a rule known as the minimum intervention principle (Todorov & Jordan, 2002). The minimum intervention principle states that a good control system should correct only task-relevant parameters, while allowing parameters that are irrelevant to vary (Todorov & Jordan, 2002).

The uncontrolled manifold task is a case in point. In one version of this task, a subject is instructed to exert force onto two buttons using different fingers (F1 and F2). The sum of the forces must be controlled using any combination of F1 and F2. For example, the subject could exert all the force with either finger if they so desired. In this task, there is a "task-relevant" dimension of control (F1+F2) and a "task-null" dimension of control (F1-F2). The minimum intervention principle predicts that an optimal controller should allow variance in the task-null dimension to achieve tighter control in the task-relevant dimension (Figure 5.1A).

Human behavior generally follows the minimum intervention principle. In very early studies of motor psychophysics, Bernstein found that while the trajectories of hammer strokes were highly variable, position at the time of the hammer-strike was remarkably precise, suggesting that the trajectory was irrelevant as long as it produced an accurate strike (Biryukova & Sirotkina,

2020). Across a wide variety of tasks, this seems to be a principle of human movement: Task-null dimensions have large variance while task-relevant dimensions are well controlled. Any implementation of OFC needs to account for this feature.

Components of the OFC model:

Optimal feedback control theories have been around for decades (Todorov & Jordan, 2002), but in recent years a common picture has emerged. Modern OFC proposes that different regions of the brain build four major components necessary to generate movement: a planning module, a feedback controller, a forward model, and a state estimator (Shadmehr & Krakauer, 2008). I will discuss the connections between these components and then briefly describe the evidence that all (except the planning module) are housed in specific locations in the brain.

Figure 5.1B depicts one prevailing model for OFC. In this model, the planning module sets feedback controller gains that are specific to the desired movement and context. The feedback controller transmits a motor command to the muscles, a copy of which ("efference copy") is sent to the forward model. The forward model computes the predicted sensory consequence ("sensory prediction") given the outgoing motor command and the current state of the limb. The ensuing movement generates actual sensory signals ("reafference") that travel from the periphery to the brain. The state estimator combines the predicted and reafferent signals, weighted by their relative confidences, to produce an estimate of the state of the limb. This state estimate passes through the feedback controller which sends new motor output to the plant (the body part being controlled) and forward model, and the cycle repeats itself. The ability of the

feedback controller to rapidly adopt different sets of feedback gains, designated by inputs from the planning module, underlies the expansive and context-dependent repertoire of movements that the brain can produce.

There is substantial evidence that these components exist in different areas of the brain (Figure 5.1C, D). The behavior of the cerebellum has many of the hallmarks of a forward model, the motor cortex appears able to enact feedback control policy (potentially with dual proprioceptive and visual controllers; Figure 5.1C, D), and the state estimator may be constructed by circuits in early proprioceptive cortex (Figure 5.1C) and posterior parietal cortex (Figure 5.1D). As the planning module accounts for a wide variety of cost and reward signals, it is unlikely that this component can be localized to any single area, but instead includes a wide-ranging set of inputs to motor cortex from premotor and prefrontal areas, as well as the basal ganglia that collectively determine a specific feedback controller.
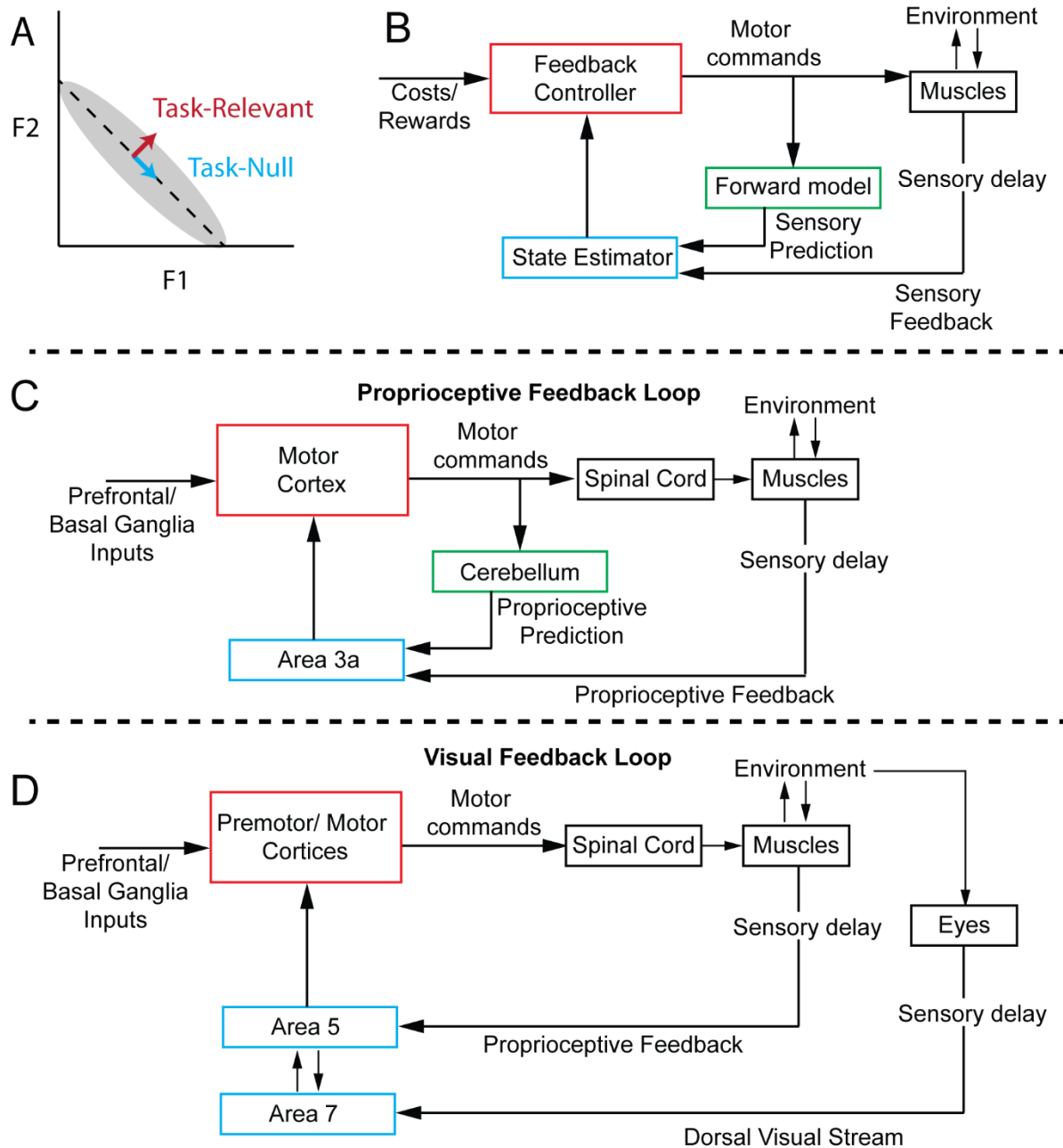
Figure 5.1: Features and neural correlates of Optimal Feedback Control for reaching. A: Diagram of Uncontrolled Manifold (UCM). X and Y axes denote forces applied by a single finger. Dotted line represents control value (F1+F2). Grey region represents variance of controller. Variance is smaller along task-relevant (red) than task-null (blue) dimensions. B: Model of optimal feedback control system, consisting of feedback controller (red), forward model (green), state estimator (blue), and musculoskeletal system. Colors denote the role of brain areas in the subsequent portions of the figure. C: Proposed proprioceptive feedback control loop. Motor cortex acts as a feedback controller, cerebellum a forward model, and area

3a a state estimator. D: Proposed visual feedback control loop. Premotor and motor cortices are the feedback controller, area 5 and area 7 jointly construct a visual/proprioceptive model of the arm.

Cerebellum as a forward model:

Forward models, at a high level, take in copies of motor commands and predict their sensory consequences. Forward models are necessary for control systems that include substantial feedback delays; running the feedback controller on delayed sensory information (~40-50 ms for signals from the distal arm) can produce oscillations about the setpoint (Kawato, 1999; Wolpert, Miall, & Kawato, 1998). Providing predicted sensory consequences to the feedback controller while waiting for actual sensory feedback can mitigate this problem.

Among its other functions, many studies point to the cerebellum as the neural implementation of a forward model (Figure 5.2A (Shadmehr, 2020)). Here, the inputs take the form of mossy fibers, and the deep cerebellar nuclei provide the predicted sensory signals. Sensory prediction errors trigger updates to the forward model (through Purkinje cell complex spikes), which alter the synaptic weights of the parallel fibers onto Purkinje cells. For further review, see (Shadmehr, 2020). Under the OFC model, disruptions to the cerebellum should cause motor output to behave as though it has only lagged sensory information.

Transcranial magnetic stimulation (TMS) can be used to disrupt processes in circumscribed regions of the brain and test how the loss of function affects behavior. Human subjects have undergone TMS to the cerebellum while making a two-segment reaching movement (R. Chris Miall, Christensen, Cain, & Stanley, 2007). In the first segment, the subject moved their hand to

the right prior to making a second, cued segment to a distant target (Figure 5.2B, blue line to yellow square). The time of the cue (which varied randomly across trials) caused the angle of the second reaching segment to vary. For instance, if the cue happened early, the second segment was almost directly away from the body. On trials with longer latency cues, the second segment required a significant leftward compensation.

On TMS trials, the trajectory of the second segment did not point toward the target: instead, it pointed toward where the target *would've* been more than 100 ms in the past (Figure 5.2B, red line). Disrupting the cerebellum did not eliminate the second segment but caused it to proceed as though it were acting on out-of-date sensory information, evidence that the cerebellum is indeed providing a sensory prediction *and* that the controller can use lagged sensory information when the prediction is unavailable (or obviously inaccurate, as is presumably the case for TMS). This experiment supports the existence of *both* a forward model in the cerebellum *and* a state estimator somewhere else in the brain that combines predicted and actual sensory information to compute a single state estimate for use by the controller.

The evidence for the cerebellum as a forward model extends well beyond the few studies described in detail here. Cerebellar patients exhibit motor oscillations reminiscent of feedback controllers with sensory conduction delays. They do not show anticipatory increases in grip force during a predictable ball-drop task (Nowak, Timmann, & Hermsdörfer, 2007; Serrien & Wiesendanger, 1999). A major clinical sign of cerebellar damage is difficulty in coordinating movements that involve multiple joints (Izawa et al., 2012; Nowak et al., 2007), which may

reflect difficulties in predicting the interaction torques arising between mechanically-coupled

limb segments (Bastian, Martin, Keating, & Thach, 1996).
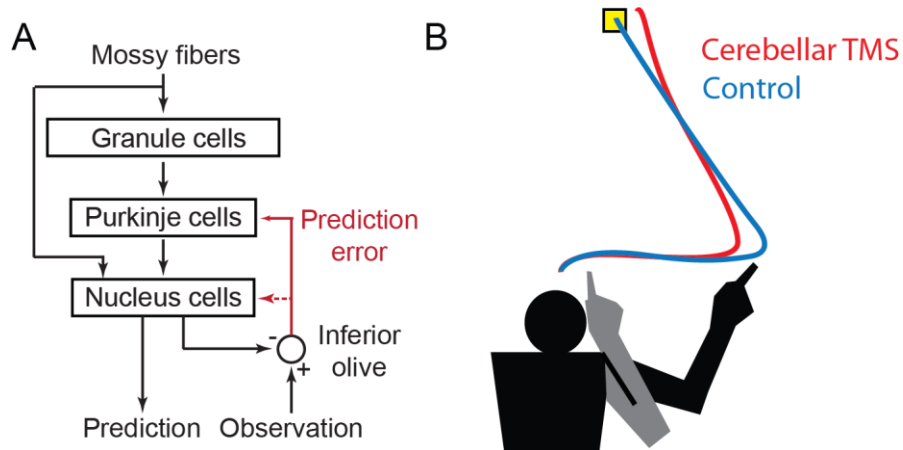
Figure 5.2: Cerebellum as a forward model. A: Model of cerebellum that generates a prediction of sensory input using efference copy. Adapted from (Shadmehr, 2020), figure 1B. B: Cerebellar transcranial magnetic stimulation caused trajectories (red trace) that behave as though they are operating on lagged somatosensory information, while control reaches (blue trace) are correctly directed to target (yellow square) (adapted from Miall et al. 2007, figure 1A, D).

Motor cortex as a feedback controller:

At a high level, a feedback controller maps from states to actions that drive the system to some

desired location in state space. In the case of the control of reaching, this feedback controller

maps a state estimate derived from prediction, vision, and proprioception to muscle activation

that produces the desired movement. In this section, I will review the evidence that M1 houses a

controller that maps sensory input states to motor output, such that these sensory-motor

mappings accomplish a behavioral goal.

To perform the feedback control presented in Figure 5.1B, the candidate brain region must 1) receive sensory inputs 2) project to the muscles and 3) send an efference copy signal to the forward model. Motor cortical neurons receive substantial somatosensory and visual inputs (Cross, Cook, & Scott, 2021; Pavlides et al., 1993). Primates have direct projections from motor cortex to motor neurons in the ventral horn of the spinal cord (Maertens De Noordhout et al., 1999). The cortico-ponto-cerebellar loop is thought to provide the cerebellum with efference copy inputs (Ramnani, 2006). Thus, motor cortex presents a promising location for the feedback controller.

Before discussing voluntary control of the limb, I will give a brief overview of reflexes, whose mapping from sensation to action occurs faster than is possible by voluntary choice. Many different loops exist along the neuraxis, but in general, more complex reflex actions are accomplished more centrally, and therefore have longer latencies (Scott, 2016). Some of these reflex arcs traverse the cortex before returning to the muscles. The fastest of these transcortical reflexes is capable of obstacle avoidance and rapid (<100ms) target switching in response to proprioceptive perturbations (Figure 5.3A, B (Nashed et al., 2014)). Still longer latency reflexes can compensate for perturbations of visual information, such as cursor or target displacement (Desmurget et al., 1999; Michael Dimitriou, Wolpert, & Franklin, 2013).

These transcortical reflexes can incorporate abstract features of a task, such as obstacles and multiple potential targets. In the experiment shown in Figure 5.3A, subjects were asked to make a reach from the open black circle to one of the colored circles positioned away from the body.

They were instructed to avoid an obstacle, the filled black circle. On some trials, the experimenters bumped the subject's hand to the left, and the subject corrected their reach to avoid the obstacle. Typical trajectories of the leftward and rightward corrections are plotted in red and blue respectively. On trials when the hand happened to be further to the left, the subjects tended to move around the obstacle to the left (red), while on trials when the hand happened to be further to the right, the subjects tended to move around the obstacle to the right (blue). The elbow extensor activation differed between these two conditions in less than 100 ms (Figure 5.3B). Given the low latency of this motor activity, the subjects did not voluntarily choose which target to reach to; rather, the mapping from sensory state (arm kinematics and kinetics) to motor output (EMG) was apparently pre-computed to flexibly respond to the perturbation (Figure 5.3A, green arrows represent hypothetical endpoint force production as a function of hand position).
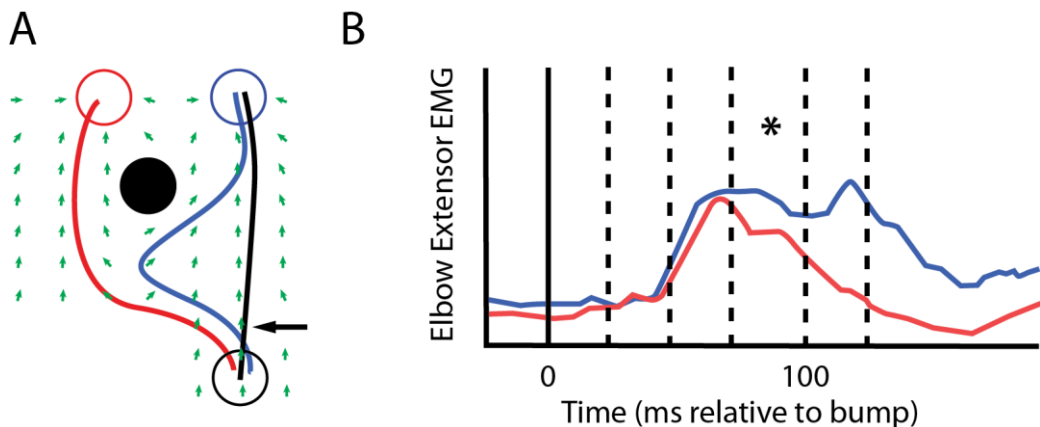
Figure 5.3: Transcortical feedback controllers can rapidly redirect reaching between targets. Adapted from Nashed et al., 2014, figures 2B and 6B A: Human subjects were asked to reach from black circle to either of two outer targets (red and blue circles) while avoiding an obstacle (filled black circle). Occasionally, a leftward bump perturbation displaced the hand (black arrow). Schematic of perturbed trajectories (colored lines) and unperturbed trajectory (black line) are shown. Some reaches were corrected towards the right target, curving around the black obstacle (blue trace). On other trials, the trajectory curved to the left target (red trace). Given the short latency of the response, the mapping from sensory state to force (green arrows) is likely

precomputed. Green force field arrows are for visualization and not necessarily the forces that the subjects produced. B: Mean elbow extensor muscle activity for right (blue) and left targets (red). Statistically significant differences occurred less than 100 ms after bump was applied (*). Dashed lines represent different phases of the reflex response.

There is evidence that these transcortical reflexes travel through M1 (Asanuma, 1975; Zarzecki & Asanuma, 1979). Alterations of transcortical reflexes are accompanied by corresponding changes in firing rates of M1 neurons, evidence that these reflexes are built in the motor cortex (Pruszynski et al., 2011b). TMS over motor cortex of humans can potentiate the strength of an evoked transcortical reflex, suggesting that motor cortex is causally related to the reflexive feedback controller and not simply correlated with reflexes generated from a different brain region (Pruszynski et al., 2011b).

A recent hypothesis posits a single sensory-motor mapping shared between voluntary and reflexive control of the arm (Scott et al., 2015). Supporting this hypothesis is the observation that adaptation of reflexes causes a corresponding adaptation of voluntary reaches (Maeda et al., 2018; Pruszynski, 2014; Scott et al., 2015). Conversely, learning to reach in an altered force environment causes adaptation of reflexes (Maeda et al., 2018). This bidirectional transfer of motor learning suggests that learning updates are not simply applied concurrently to two separate models for voluntary and reflex control, but instead that they share neural circuitry.

Motor cortex builds transcortical reflexes; those reflexes and voluntary control seem to share a model. Therefore, the precomputed sensory-motor mapping for reflexes described above (Figure 5.3A, green arrows) may also be used to generate voluntary movements. To explain, I will return to the task described in Figure 5.3A. Consider an unperturbed trial in which the subject

reaches from the black starting circle to the blue target (black line). The force generated at the

handle (green arrow) depends on the location of the hand; at the start of the movement, the

subject should exert a force away from the body. Motor cortex could generate the voluntary

reach simply by following the contour of the sensory-motor mapping (the string of green

arrows) leading to the blue target. If the hand is perturbed (as in blue and red traces), a different

region of the same force generation landscape could correct for that error. By precomputing the

sensory-motor mapping across all likely states, a single model in M1 could plan both

unperturbed voluntary reaches and transcortical reflexes.

There may, however, be separate feedback controllers that map proprioceptive and visual

sensory information to motor output. Signatures of learning found in PMd during curl field

adaptation are not seen during visuomotor rotations, suggesting that the proprioceptive and

visual controllers are separate (Perich, Gallego, & Miller, 2018). Supporting this hypothesis,

TMS used to disrupt the posterior parietal cortex eliminates the ability of human subjects to

correct for jumps of a visual target while leaving the initial reach unaffected (Desmurget et al.,

1999).

Area 3a and Areas 5/7 as state estimators:

State estimators combine different sources of information into a single estimate based on the

confidence in each information stream; for instance, a pilot might rely on instruments when

flying at night but look through the windshield when flying on a clear day. State estimators in

the brain need to generate coherent estimates from three main streams of information: sensory

predictions, proprioceptive information, and visual information. Current evidence points to there being a proprioceptive state estimator in area 3a, and a separate visual/proprioceptive state estimator in areas 5/7.

Any proprioceptive state estimator should satisfy three criteria; 1) It should project strongly to M1. 2) It should receive lagged proprioceptive signals from the periphery. 3) It should receive proprioceptive predictions from the cerebellum.

Area 3a is a strong candidate for the proprioceptive state estimator, combining predicted and actual proprioceptive signals weighted by their relative confidences into a single proprioceptive state that is sent to motor cortex. Area 3a projects strongly to M1 (Huffman & Krubitzer, 2001a). Area 3a receives substantial proprioceptive input from the limbs (E. G. Jones & Porter, 1980; Phillips et al., 1971; Yumiya et al., 1974). While there is no direct evidence that area 3a receives predicted proprioceptive signals, area 3a does receive its primary thalamic inputs not from somatosensory thalamus (VPL and VPS), but instead from cerebellar thalamus (VL) (Padberg et al., 2009). Recordings in mice show that VL neurons encode *both* sensory predictions *and* actual somatosensory signals (Dooley et al., 2021), suggesting that area 3a receives cerebellar predictions from VL. Unfortunately, no one has recorded from neurons in area 3a during tasks that vary the relative confidence of predicted and actual proprioceptive information, so there is not yet definitive evidence that the signals sent to M1 from area 3a are a combined state estimate.

Combining predicted and actual proprioceptive information into a single state estimate could be a simple mechanism for motor cortex to use a single sensory-motor mapping for voluntary and reflexive control (Figure 5.3 A, green arrows). When predicted proprioceptive information is accurate, as in a well-learned task with no perturbations, the state estimator provides the feedback controller with predicted signals, thereby bypassing the sensory conduction delay (black trajectory in Figure 5.3A). In contrast, when predicted somatosensory information is inaccurate, such as when experimenters apply external bumps to the hand, the state estimator provides the feedback controller with lagged, actual sensory inputs (red and blue lines in Figure 5.3A). Intriguingly, a shared sensory-motor mapping across voluntary and reflexive movements would blur the line between volitional and reflexively generated motor activity.

For visual-proprioceptive state estimation, posterior parietal cortex is a likely candidate, specifically areas 5/7. TMS of this area disrupts visually based transcortical reflexes (Desmurget et al., 1999). Lesions to area 7 in humans impair visually guided reaching, causing one patient to "lose" her arm when she could not see it for a period of time (Wolpert, Goodbody, et al., 1998). Selective ablations of area 5 impair a monkey's ability to reach in darkness but not in light, while ablations to area 7 impair the ability to reach in light but not darkness (Rushworth et al., 1997). The combination of these studies suggests that area 5 generates a proprioceptive model of the arm, while area 7 generates a visual model. A multisensory integrator that consolidates these two sensory streams may create a second state estimate in the posterior parietal cortices.

High-level tests for OFC:

One recent study pulled the major portions of the OFC model together in a single experiment (Takei, Lomber, Cook, & Scott, 2021). They used selective cooling to turn off different regions of the monkey brain that corresponded to blocks of the OFC model in Figure 5.1A. The effects of cooling area 5 resembled disruption of a state estimator, while the effects of cooling motor cortex resembled the reduction of feedback gains in a feedback controller. Using this OFC model, they were able to recapitulate the effects of cooling on two different blocks of the OFC system. To make such precise predictions that are confirmed under such a complex experiment gives strong support to the OFC model.

The combination of these diverse studies is compelling. From human psychophysics and TMS to lesion studies, from anatomy to modeling, to targeted cooling and recordings from single neurons, a huge variety of studies all point in the same direction; the motor system is a feedback system. It has at least one feedback controller in the motor cortices, the cerebellum is the forward model, and there are likely state estimators in area 3a and areas 5/7. But unfortunately, knowing that motor cortex is a feedback controller does not tell us how the brain *builds* the feedback controller. Feedback controllers could be implemented with op-amps, software on a computer, or vacuum tubes. Neural feedback controllers must be implemented with neurons. How?

Neural Dynamical Systems:

The fundamental property of a dynamical system is that the state of the system at some time in the future is determined, in part, by its current state (Sussillo, 2014). For instance, the state of a pendulum (its angle and angular velocity) determines its future state by the equations of motion. Similarly, the current state of a neural network (the vector of its instantaneous firing rates) helps to determine its future state via a state update function. This state update function is presumably an emergent property of how the neurons in the ensemble are connected; different patterns of connectivity and synaptic strength can produce different dynamics (Sussillo, 2014). The concept of dynamical systems presents a mechanism for neural networks to generate patterns of activity that produce movement (Shenoy et al., 2013). In this section, I will review the basic concepts that underlie the dynamical systems hypothesis, including dimensionality, latent spaces, and null and potent spaces.

Neural population analyses:

Discerning how ensembles of neurons perform computation is one of the critical challenges facing the fields of both neuroscience and artificial intelligence. Firing rates of neurons, in the brain and in artificial neural networks have complex properties that are often difficult to interpret. Their temporal fluctuations often do not neatly match any observable task-related variable (Russo et al., 2018; Sussillo & Barak, 2013; Sussillo, Churchland, Kaufman, & Shenoy, 2015). This difficulty in interpreting single neuron activations has led to the adoption of population level analyses that attempt to understand the network through a lower-dimensional "latent space" (see Figure 5.4A for a simple example). Methods such as principal components

analysis and Gaussian-process factor analysis have been fruitfully applied to neural data to

uncover the latent space of recordings from motor cortex (Cunningham & Ghahramani, 2014;

Cunningham & Yu, 2014; Yu et al., 2009). By applying dimensionality-reduction tools,

researchers have demonstrated that a large percentage of the firing rate variance of a population

of neurons can be explained by many, *many* fewer latent dimensions than the total number of

neurons in the circuit (P. Gao & Ganguli, 2015). Further, the movement of the neural state

within these latent spaces is often quite similar across trials as though it were playing out a

pattern (Pandarinath et al., 2018; Shenoy et al., 2013).
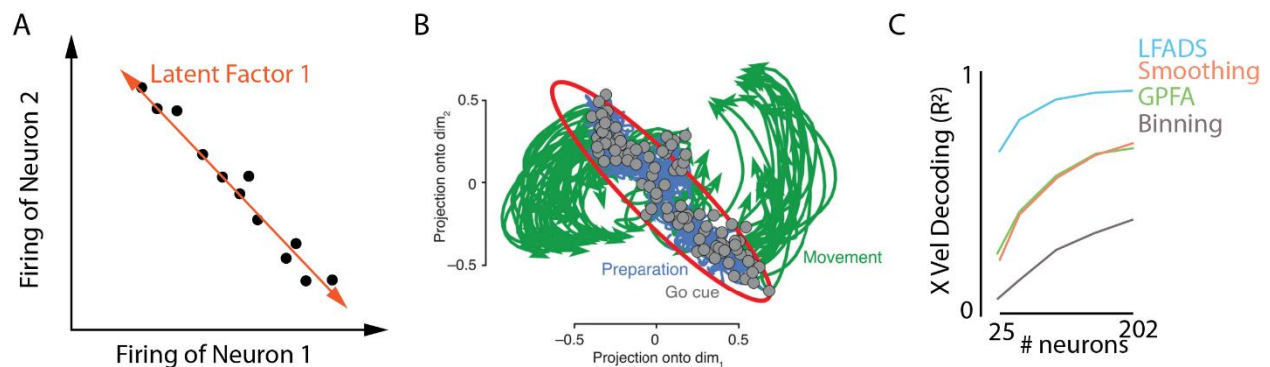
Figure 5.4: The concepts of latent spaces and neural dynamics are useful to understand how ensembles of neurons behave. A: Example of dimensionality reduction used to reduce the number of coordinates needed to describe a system. In this case, the majority of variance of the two firing rates can be explained by a single linear dimension (orange), reducing the number of coordinates from two to one. B: Low-dimensional trajectories of neural activity. Preparatory activity (blue) falls on a line determined by specifics of the motor plan. The trajectories of the neural state play out based on those initial conditions (green). Adapted from (Kaufman, Churchland, Ryu, & Shenoy, 2014), Figure 3B. C: Latent factor analysis via dynamical systems (LFADS, cyan curve) can decode kinematics from neural state much more accurately than smoothing (orange), Gaussian process factor analysis (GPFA, green), or simple binning of spikes (grey). Adapted from (Pandarinath et al., 2018), figure 2E.

Preparatory activity as setting of initial conditions of a dynamical system:

An interesting feature of recordings from motor cortex is the substantial modulation of neural activity following target presentation but prior to movement onset. It has long been a puzzle why this activity does not activate muscles. Hypotheses such as motor gating have been put forward to explain how the nervous system might prevent early, aberrant movements caused by this planning activity (Benjamin, Staras, & Kemenes, 2010; Duque & Ivry, 2009).

Dimensionality analysis offers an alternate hypothesis. Because there are *many* more neurons than muscles, there exists a "null space" for any linear mapping between motor cortex and muscles. A null-space from M1 to muscles is simply the set of directions along which the M1 neural state can move without changing muscle activity. In contrast, the "output-potent space" is the set of directions that do change the muscle activity. Mathematically, there is a high bound on the output-potent space dimensionality from motor cortex to muscles that is approximately equal to the number of muscles. Because there are only about 50 muscles in the arm and millions of M1 neurons, the vast majority of directions that M1 neural state can move are "output-null", having no effect on muscle activation. The logical question: is it possible the preparatory activity is restricted to the null-space?

By fitting linear models relating the M1 activity to EMG signals, Kaufman et al., demonstrated that most of the preparatory activity is indeed, output-null (Figure 5.4B) (Kaufman et al., 2014). Beyond that, they found that how the neural state developed over time depended on where along this "preparatory" dimension the neural state sat at the time of the go-cue. They interpreted this

as evidence that preparatory activity in M1 is setting initial conditions for a dynamical system (Shenoy et al., 2013). Analogous to a ball rolling down a hill according to the contours of the landscape, the neural state moves as determined by the dynamics of the circuit. By choosing an appropriate initial condition, the resulting dynamics generate a pattern in the output-potent space that produces muscle activity during the movement. Different movements could be selected simply by choosing different initial conditions.

Recent advances in neural dynamical systems

Since these observations, dynamical models have made pivotal contributions to how we understand the computations performed by neurons in the brain. Changing dynamics can encode changing probability distributions and speeds of behavior (Ma & Jazayeri, 2014; Wang, Narain, Hosseini, & Jazayeri, 2017). RNNs trained to produce EMG data can explain features of M1 neural activity during reaching (Sussillo et al., 2015). Techniques that leverage the dynamics of neural recordings can extract information about the neural state with remarkable accuracy relative to less sophisticated techniques (Figure 5.4C (Pandarinath et al., 2018; Sussillo, Jozefowicz, Abbott, & Pandarinath, 2016)). Stable latent dynamics of a neural circuit have even allowed the alignment of neural spaces between distinct populations of neurons across days (Wimalasena, Miller, & Pandarinath, 2020).

Recently, causal manipulations have proven that dynamics are an important feature of these networks, and not simply the result of patterned inputs to motor areas. Karel Svoboda's lab discovered a preparatory dimension in the brains of mice trained to perform a left-right lick

choice task (Inagaki, Fontolan, Romani, & Svoboda, 2019). As in monkey M1, the neural state

settled to a location on a preparatory dimension that encoded the plan to lick left or to lick right.

Using optogenetic tools, these researchers were able to "kick" the neural state in a random

direction. Often the neural state returned to its original location, but sometimes it settled at a

different point on the "choice dimension". On trials where the state settled on the "switched

choice" side, the mouse made the choice predicted by the neural state, not that of the initial

preparatory period. This study demonstrates that when the mice prepare to execute this

behavior, the dynamical landscapes for *both* lick directions exist in the brain, not just the chosen

direction. The initial conditions in the dynamical landscape of these motor circuits determines

the resulting movement.

Dynamical systems and sensory feedback:

There are, however, shortcomings to the dynamical view of the motor system. First, given the

evidence laid out in the first section suggesting that motor cortex acts as a feedback controller,

there is a glaring omission in NDS. In most conceptions of the dynamical systems hypothesis,

sensory feedback takes a backseat to intrinsic dynamics. Unfortunately, it is difficult from

neural recordings alone to distinguish an independent dynamical system from a feedforward

network that receives inputs from a dynamical system. What proportion of the "dynamics" that

we see in M1 are due to its own intrinsic dynamics, versus dynamics "inherited" from sensory

input?

A recent study from the Hantman lab gives convincing evidence that dynamics in M1 rely on inputs from the motor thalamus (B. A. Sauerbrei et al., 2019), a hub for somatosensory and cerebellar information (Dooley et al., 2021). In this experiment, they trained mice to reach out, retrieve a food pellet, and bring it to their mouths. Recordings from the motor cortex revealed robust dynamical motifs that were consistent across trials. Using optogenetic techniques, they inactivated the inputs to motor cortex from the motor thalamus (presumably analogous to primate VL). This inactivation eliminated the dynamics normally seen in motor cortical neural activity during this task. With this failure to produce the standard dynamics came a corresponding failure to execute the reaching movement. The dynamics in motor cortex are apparently contingent on thalamic inputs, at least in the mouse.

While these data are difficult to reconcile with a concept of M1 as an intrinsic dynamical system, they are predictable from the optimal feedback control hypothesis. Without sensory inputs from VL (including both sensory predictions and lagged proprioceptive inputs), the sensory state will essentially be "null". The brain has never received zero input from every sensor in the arm before, so it wouldn't have learned how to transform that state into motor output.

Dynamical Feedback Control:

Now we arrive at a significant discrepancy between these two frameworks; in OFC, sensory inputs are critical to the generation of motor activity, while in NDS those same sensory inputs are often ignored, even though without these inputs the dynamics in motor cortex fall apart. If

motor cortex doesn't generate patterns with its intrinsic dynamics, as suggested by the algorithmic level of NDS, what are the dynamics that we see in M1 doing?

To solve this dilemma, I propose that circuits in motor cortex instantiate a feedback controller, in accordance with the evidence presented in section 2 of this review. I propose that inputs from the state estimator project to a subspace of M1 neural activity called the "sensory-potent space", for which there is a complementary "non-sensory space", the set of M1 dimensions that receive no sensory inputs. By moving specific sensory-potent dimensions of M1 into output-potent dimensions, M1 dynamics could approximate a specific set of feedback gains. In this scheme, the dynamics that we see in the neural state during movement are not intrinsic, but contingent dynamics; contingent on the sensory inputs entering motor cortex. When thalamic inputs are removed (as by Sauerbrei et al.), the dynamics fall apart.

But how does motor cortex find dynamics that generate one *particular* movement from the huge number available in our behavioral repertoire? It doesn't seem possible that the motor cortex can *change* its dynamics significantly in the short time it takes to prepare a movement, as that would potentially require changing synaptic weights. I instead propose that inputs that encode the associated costs and task requirements (from the planning module) move the neural state to regions where the dynamics embody different mappings from state to motor output. The brain can quickly choose and execute movements by moving the M1 neural state to a different region of state space with a dynamical landscape that approximates sensory-motor mappings

appropriate to the task.

A simple dynamical feedback controller:

At this point, a simple example will help to illustrate the model. For this, I will take the simplest

motor loop available in the human body, the stretch reflex of the quadriceps muscle composed

of two neurons: the primary muscle spindle afferent (Ia) from a quadriceps muscle spindle

(Figure 5.5A, blue), and the α-motor neuron to the quadriceps muscle (Figure 5.5A, orange).

The Ia afferent signals the lengthening velocity of the quadriceps muscle. The α-motor neuron

firing rate determines the activation of the quadriceps muscle. The stretch reflex is a simple

monosynaptic connection between these two neurons, such that increases in the Ia firing rate

increases the firing rate of the α-motor neuron. Put simply, stretching the quadriceps causes the

quadriceps to activate.

This circuit is a very simple feedback loop (Figure 5.5B). Given a sensory input from the muscle

spindle, the circuit produces a motor output in the motor neuron. The synaptic weight of the

connection between the 1a afferent and the α-motor neuron acts as a feedback gain on the

sensory information.

This circuit is also a very simple dynamical system. At time t, the Ia afferent fires an action

potential due to a stretch. At time t+1 the α-motor neuron fires an action potential in response to

synaptic input from the 1a afferent. The neural state develops according to the dynamics

dictated by the simple monosynaptic circuit (Figure 5.5B, black lines furthest into the page).

Inputs to this dynamical system come into the 1a afferent through the environment, and there is a predictable dynamical transformation that moves the neural state from the sensory to the motor dimension of the 2D neural state.

In practice, the stretch reflex must be more complex than this simple example suggests; we must have some way of inactivating it, lest attempts to move recruit the reflex and brake the movement. Evolution has devised a way to add context to this reflex, to make it "know" when a perturbation is self-generated or external. To our simple 2D system we add a third dimension, a presynaptic inhibitory axon (denoted Inhibition) that inhibits the 1a presynaptic terminal (Figure 5.5A, green (Meunier & Pierrot-Deseilligny, 1989)).

The circuit is still a feedback loop, only now the gain depends on where the neural state sits along the Inhibition dimension (Figure 5.5B). When Inhibition is zero, the stretch reflex occurs with its normal gain. When Inhibition is large, the stretch reflex does not occur, as the gain is zero. When Inhibition is intermediate, the reflex occurs with a modest gain. We have built a feedback circuit with a modular gain that depends on preparatory activity along the Inhibition dimension.

The circuit is also now a slightly more complex dynamical system. At time t, the projection of the neural state along the 1a afferent dimension moves into dimension of the α-motor neuron with dynamics determined by the placement of the projection of the neural state onto the Inhibition dimension which serves as the context. When Inhibition is zero, the dynamical

landscape resembles the dynamics of the 1a-α circuit. When Inhibition is large, the dynamics are

eliminated; there is no movement from the 1a dimension to the α dimension (Figure 5.5B, flat

black trace). Intermediate values of Inhibition produce intermediate dynamical landscapes,

where 1a moves into α, but with a smaller projection onto the motor dimension (Figure 5.5B,

middle black trace). Finding the dynamics within the Ia- α plane at different values of Inhibition

is equivalent to finding the feedback gain for that transformation.

This simple example illustrates the key components of the DFC model. Its actual instantiation in

the brain includes more complex and higher-dimensional versions of the motor-potent, sensory-

potent, and context dimensions (Figure 5.5C). There exists some output-potent subspace in M1

which transmits signals to the muscles through the spinal cord, analogous to the α dimension.

There *also* exists some somatosensory subspace into which the state estimator projects a

combination of actual and predicted proprioceptive information, analogous to the 1a dimension.

Inputs from (at least) the basal ganglia and premotor areas provide inputs analogous to the

Inhibition. We might designate these inputs context and planning subspaces, depending on what

information they encode. The extremely high number of non-sensory and output-null

dimensions in the network provide many "scratch" dimensions on which dynamics can be

sculpted to produce appropriate sets of feedback gains. By designating a location within the

context/planning subspace, these inputs set the initial conditions of a dynamical system with

specific transformations from sensory to motor dimensions (Figure 5.5C). Equivalently, this

preparatory activity sets the feedback gains of a complex sensorimotor transformation, thereby

implementing the feedback controller predicted by OFC.
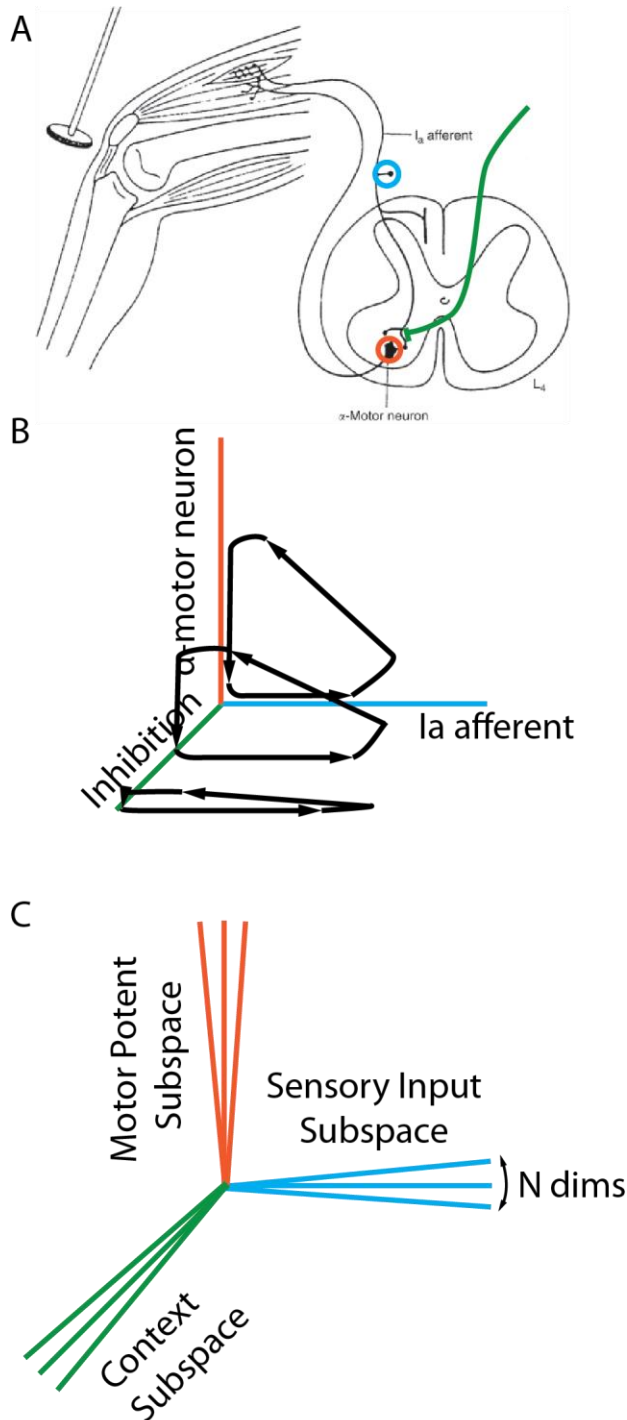
Figure 5.5: Stretch reflex as a simple dynamical feedback controller. A: Schematic diagram of the stretch reflex. Tap to patellar tendon activates Ia afferent (blue circle). α-motor neuron (orange circle) controls muscle activity of quadriceps muscle. Descending presynaptic inhibitory axon (green), affects the strength of the synapse between the Ia afferent and the α-motor neuron. B: Dynamical landscape of this simple circuit. Red axis denotes the firing rate of the α-motor neuron, blue axis the 1a afferent firing rate, and green axis the firing rate of the presynaptic inhibitory neuron. Solid black lines show the movement in state space during a tendon tap at different levels of Inhibition. Dynamics, and thereby gain, change as you move along the Inhibition axis. C: Generalization of this model to motor cortex, with α-motor neuron firing rate replaced by an M-dimensional output-potent subspace and Ia afferent dimension replaced by an N-dimensional sensory-potent subspace. Inhibition dimension is replaced by a C-dimensional context and planning input subspace. Sensory-motor transformations are analogous to those of the stretch reflex, with the blue dimensions moving into red dimensions by the dynamics at the specific location along the green dimensions.

Dynamical Feedback Control: How it works

How do you make a reach under the DFC model? For this, I consider only the proprioceptive control loop in Figure 5.1 C.

In this section, I will consider as a prototypical example a two-direction reaching task. A monkey holds his hand in the center of a workspace, and I present a target in one of two directions: left or right. The monkey plans a movement but delays execution until receiving an auditory go-cue.

Before the go-cue, as the monkey sees the target, inputs from premotor areas and basal ganglia push motor cortex into a preparatory state that depends on the motor plan and costs/rewards, respectively (Z. Gao et al., 2018; Kaufman et al., 2014; N. Li, Daie, Svoboda, & Druckmann, 2016). Movements along these preparatory dimensions place the neural state in a region whose local dynamics approximate a feedback controller meeting the requirements of this task. This neural state remains in this preparatory location until the auditory cue pushes the neural state off the preparatory subspace, initiating its movement into the output-potent dimension.

As the neural state moves into the output-potent dimensions for each muscle, motor cortex sends signals to the ventral horn of the spinal cord to initiate movement, and to the cerebellum. The cerebellum uses these efference copy inputs to predict the sensory consequences of the motor commands. These predicted proprioceptive signals travel to area 3a; at the time of movement initiation, the lagged signals have not yet arrived to area 3a, so the prediction projects into the sensory-potent dimensions of M1.

After signal conduction delay, movement-related somatosensory signals from muscle spindles and Golgi tendon organs arrive at the state estimator in 3a. Area 3a integrates these lagged

somatosensory signals with the predicted cerebellar signals to produce a combined state estimate, which projects into the sensory-potent dimensions of M1. Motor cortex transforms this combined state estimate into motor commands with gains determined by the intrinsic dynamics of the cortical circuit. Thus, the movement unfurls through a recurrent loop connecting M1 to the periphery; motor outputs generate sensory inputs generate motor outputs. The dynamics that we observe in M1 firing rates are therefore the coupled dynamics of the motor cortex and the arm.

Reaches to the left and right require different mappings from state to action. In DFC, the preparatory neural state moves along planning dimensions into different dynamical landscapes for these two reach directions. The dynamics in these regions of state space, learned previously, build the sensory-motor mappings that generate different movements. Importantly, these dynamics can map arbitrary sensory dimensions to arbitrary motor dimensions. By mapping task-relevant, but not task-null, sensory-potent dimensions onto corrective output-potent motor dimensions, the dynamics of M1 could correct only those errors that will hurt task performance, i.e., the minimum intervention principle hypothesized by OFC.

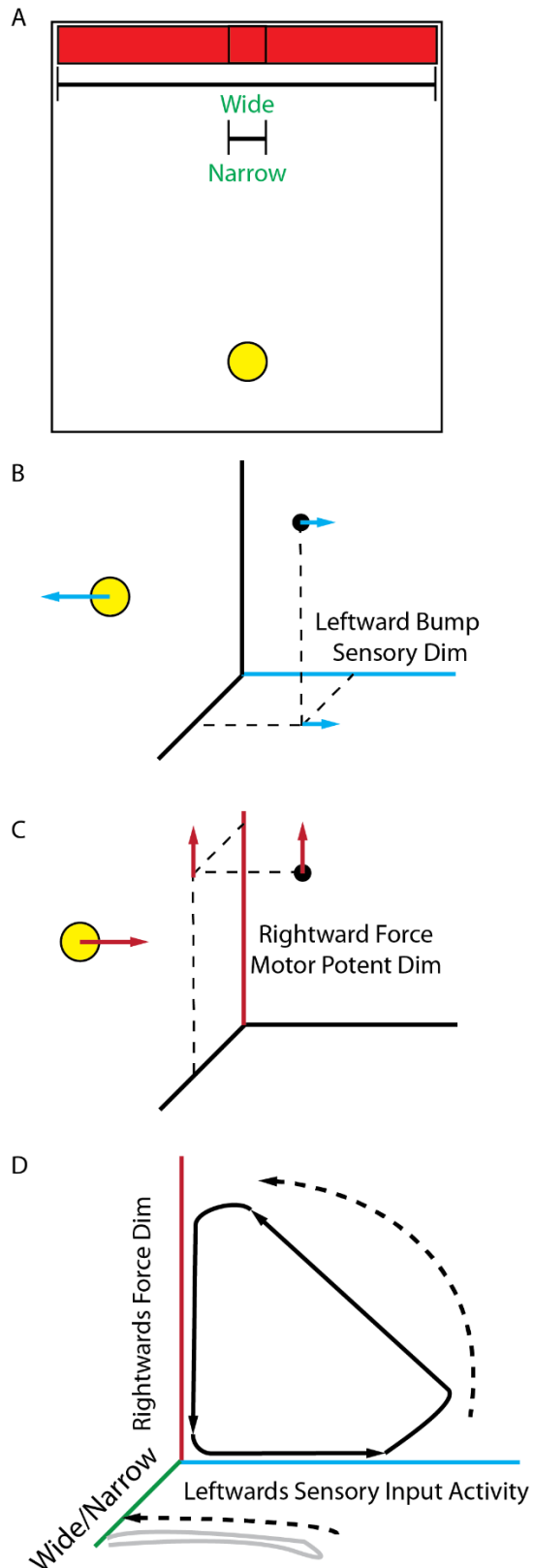## Implications of Dynamical Feedback Control

This is a very complex model of the motor system, but can it be used to make falsifiable predictions? Unlike other models of neural dynamics, this combined perspective allows researchers to ask Optimal Feedback Control questions in the language of Neural Dynamical Systems. In this section I will give some example questions and walk through how DFC helps

design experiments that yield results interpretable under both OFC and NDS.

What feedback transformation occurs during reaching?

There are two key predictions of this model. First, motor cortical dynamics should implement a sensory-motor transformation, a movement of the M1 neural state from sensory-potent dimensions into output-potent dimensions. The resulting projection of the neural state onto the M1 output-potent dimensions should predict the actual motor activity, suggesting that these dynamics are an important source of the descending command to muscles. Second, the dynamics of this transformation should change with the task requirements, not by modifying the surrounding dynamical landscape, but by moving the neural state along context dimensions to a *different* dynamical landscape. Confirmation of these two predictions would provide strong evidence of the utility of DFC as a multi-level description of the feedback control implemented by motor cortex.

The task that I propose is a modified 2D reaching task. I provide visual feedback about the location of a monkey's hand with a cursor on a screen. The monkey begins a trial by holding a robotic manipulandum in a target near to the body aligned with the center of the screen. We then show the monkey a target in line with the body center, but away from the body. The target can either be narrow or wide, randomly chosen across trials. Narrow targets are square and have a width equal to the diameter of the cursor. Wide targets are rectangular, with a major axis that spans the entire upper screen edge and a minor axis that is equal to the diameter of the cursor. After a random delay interval, we provide an auditory cue to the monkey that signals to make a reach. After acquiring the target, the monkey receives a liquid reward. On some trials, we apply

A

Wide

Narrow

B

Leftward Bump
Sensory Dim

C

Rightward Force
Motor Potent Dim

D

Rightwards Force Dim

Wide/Narrow

Leftwards Sensory Input Activity

a bump perturbation perpendicular to the straight-line trajectory (i.e., left or right) to push the monkey's hand. We record from motor cortex while a well-trained monkey performs this task (Figure 5.6A).

Figure 5.6: Example experiment under Dynamical Feedback Control (DFC) model. A: Task diagram. Narrow and wide targets represented by red square and rectangle, respectively. Yellow circle represents the cursor. B: Hand (yellow circle) is bumped to the left by a force applied at the handle (blue arrow) which will perturb the neural state (black dot) along the sensory input dimension that encodes leftward hand movements (blue arrow). Black axes represent the high-dimensional neural space in M1. C: We find the direction in the non-sensory neural state space that relates the neural state to the force at the handle (the output-potent subspace, red axis). Black axes represent the non-sensory subspace of M1 activity. D: Diagram of expected results (analogous to Figure 5.5B). Activity in the leftward movement sensory-potent dimension should move into the rightward force-generating output-potent dimension when the target is narrow (near origin on green axis) but not when it is wide (out-of-page on green axis). Dynamics of sensory-motor transformation are denoted by dashed lines.

To find the sensory-motor mapping in M1, we need to know which dimensions are sensory-potent and which are output-potent. We can map the dimensions of the sensory-potent subspace by recording M1 activity during perturbations of the

monkey's hand at rest. Bumping the hand left will generate neural activity in the sensory-potent M1 dimension for leftward movements (Figure 5.6B), and likewise, for rightward movements.

If we were to ignore the sensory inputs to M1, we could map the output-potent dimension for leftward and rightward force by fitting a model from the full neural space to the handle force; however, we know that sensory inputs and force outputs are likely highly correlated (exerting a force to the right often causes rightward movement). Instead, we exclude the previously identified sensory subspace activity (Figure 5.6B) from the neural space, then fit a model that relates the remaining M1 space to forces generated at the handle during isometric force production. This will give us a motor subspace that maps neural activity to right and left force generation and is orthogonal to the sensory subspace (Figure 5.6C).

We can use these low-D sensory and motor subspaces to examine the dynamics of the network during the task. Specifically, we want to project the neural activity onto the plane defined by a single sensory dimension and a single motor dimension. The pair of dimensions that we pick should be related; for example, we expect that an error in a task-relevant sensory dimension ("I've been bumped to the left") should be transformed into a projection of the neural state onto the output-potent dimension that corrects the error ("I exert a force to the right") (Figure 5.6D). The dynamics projected onto this plane will show how the sensory dimension moves into the motor dimension, or through the OFC lens, the feedback gain.

For narrow targets, when I apply a perpendicular bump the resulting error is task-relevant. Therefore, the sensory-potent dimension that encodes the perpendicular bump should move into the motor output dimension that corrects for the bump. For example, neural activity in the leftward movement dimension will map onto a rightward restoring force (Figure 5.6D, black lines). This would indicate that the dynamics of the circuit (equivalently, the feedback transformations) are tuned to correct for this task-relevant perturbation.

For wide targets, when I apply a perpendicular bump the resulting error is task-null. Therefore, the sensory-potent dimension that encodes the perpendicular bumps should not be transformed into the output-potent space consistently across trials. For example, neural activity in the leftward movement dimension will not map onto a rightward restoring force (Figure 5.6D, grey line). The lack of transformation of sensory-potent to output-potent dimensions indicates that M1 dynamics cease to correct for the perturbation when it becomes task-null (Figure 5.6D, grey line).

How does the feedback controller map sensory inputs to motor outputs differently based on the width of the target? Changes in the location of the neural state during the preparatory period (between target appearance and go-cue) should encode the target type (Figure 5.6D, green axis); movements along this dimension will be accompanied by changes in the gain of the sensory-motor transformation. Given the short latency of transcortical reflexes (<100 ms), different sensory-motor mappings for wide and narrow targets (Figure 5.6D, comparison between black and grey lines) would provide strong evidence that those mappings are built by the intrinsic

dynamics of M1 circuitry.

With this experiment, we will have shown that 1) the dynamics of M1 activity transform sensory-potent dimensions into output-potent dimensions in a way that predicts the corrective forces generated by the monkey, and 2) that different locations along the preparatory dimensions of M1 house different dynamical landscapes; the landscape at each location is tuned to produce appropriate sensory-motor transformations that generate the movement and correct for task-relevant errors while ignoring task-null errors.

Extensions and Limitations of DFC:

Under DFC, inputs from planning modules designate the dynamical landscape used to generate a movement. To understand how these landscapes are chosen, we need to understand how basal ganglia and premotor inputs affect the neural state; i.e., the BG-M1 and Premotor-M1 input dimensions. The same analytical tools used to find output-potent dimensions to muscles from M1, or from PMd to M1 (Perich et al., 2018), can be used to compute output-potent spaces from basal ganglia and premotor areas and their corresponding input dimensions in M1. Given what we know about BG and PFC, I would predict that the variable encoded in the feedback gains along the BG-input dimensions to M1 should relate to costs of movement, while the variables encoded along premotor-input dimensions relate to the motor plan. Using DFC as a guide, we can map the functional consequences of inputs from other brain areas on M1 feedback control.

There are some major limitations to this theory. Many components presented here, though based on existing evidence, are still speculative. Further work to characterize area 3a is needed to confirm that it receives both predicted and actual somatosensory signals, and that it combines these signals as a state estimator. In addition, our incomplete understanding of the role of spinal circuitry in modulating descending inputs makes interpretation of signals recorded from motor cortex difficult.

This model has not yet been tested explicitly. However, DFC can retrospectively explain many results from OFC and NDS under a single framework, and presents specific, falsifiable, hypotheses. I propose this model as a unifying theory that can explain our current understanding of the motor system at multiple conceptual levels and guide future inquiry. Groups that study the neural control of movement from the perspectives of OFC and NDS are often not in close communication with one another. Dynamical Feedback Control bridges the gap between the high-level motor control theory presented by OFC and the empirically derived dynamical landscapes of NDS.

Chapter 6 – Discussion

During the course of my doctoral work, I characterized how the firing rates of single neurons in the Cuneate Nucleus (CN) relate to proprioceptive information from the arm during behavior; mine were the first ever such recordings from CN (Suresh et al., 2017). In Chapter 2, I detailed the improvement of surgical methods that produced these novel recordings. In chapter 3, I described the typical receptive fields of proprioceptive neurons in CN and their responses to

actively and passively generated arm movements. I demonstrated that, contrary to expectations raised by the tactile system, proprioceptive signals are mostly potentiated rather than attenuated during active movements relative to passive movements (Versteeg, Rosenow, et al., 2021). I also demonstrated that proprioceptive receptive fields in CN are spatially restricted, typically having their origins in only a single muscle. In chapter 4, I compared population level encoding properties in CN and area 2, a somatosensory cortical area. As part of this comparison, I described a simulation study suggesting that the standard tools that we use to quantify proprioceptive activity (e.g., PDs) are inadequate to reveal proprioceptive processing along the neuraxis (Versteeg, Chowdhury, et al., 2021). Taken together, these opening chapters suggest that proprioceptive activity in CN resembles a modulated version of the activity of a small number of peripheral receptors. In Chapter 5, I laid out a framework for the incorporation of proprioceptive feedback into the generation of motor output, combining optimal feedback control models with dynamical systems analysis into a combined Dynamical Feedback Control (DFC) model.

The chapters investigating CN, and their connection to the DFC presented in Chapter 5, raise an important question: what is CN "doing" in the proprioceptive pathway, given the similarity of the responses of CN proprioceptive neurons to responses in both the periphery and cortex? In this final chapter, I review how my findings affect major areas of the study of proprioception and of CN in particular. I first discuss how my data impact hypotheses about coordinate transformations in brainstem and cortex. Then, I present the major theories about sensory gain in CN and propose a new functional gain control model to account for my findings. I discuss

how the conflicting estimates of sensory convergence in CN may give insight into cortical remapping. I close by presenting a case for CN as an appealing site for neuroprosthetic implants for somatosensory restoration.

Proprioception and coordinate transformation

A major role of proprioception, its most salient in our day-to-day experience, is the conscious sensation of the position of our bodies in space. Proprioceptive perceptual acuity is often measured using a joint position matching task, in which individuals are asked to replicate a previously demonstrated joint angle without vision of the limb (Elangovan, Herrmann, & Konczak, 2014; Goble, 2010). These studies show that young healthy participants are able to reproduce target elbow angles with an error typically less than 5 degrees (Fuentes & Bastian, 2010).

Because 5 degrees error in elbow angle estimation translates into very large deviation of the fingertip position, one might predict that subject's estimates of fingertip position must be quite poor. On the contrary, subjects are able to report the location of their fingertip more accurately than the acuity of joint angles suggests that they should be able to. Fingertip position may be more perceptually available than raw joint angles (Fuentes & Bastian, 2010).

This finding, in combination with sinusoidal tuning of cortical proprioceptive neurons to the direction of hand movement has led some researchers to suggest that a goal of the proprioceptive pathway may be to transform muscle or joint based coordinates to an "extrinsic"

coordinate frame based around the hand. Indeed, one study suggested that this transformation could occur at as low a level as the spinal cord (Bosco, Rankin, & Poppele, 1996). Studies of CN have put forward a similar hypothesis, suggesting that CN may transform muscle signals that respond to articulations of multiple joints into a joint-based coordinate system (Leiras et al., 2010).

Conflicting with these hypotheses, we have found previously in the Miller lab that encoding models that predict the firing rates of neurons in area 2 have better predictions based on elbow and hand movement than do models that use only kinematics of the hand endpoint or of joint angles (Chowdhury et al., 2020). That area 2 neurons still encode kinematics of the full arm suggests that signals in area 2 have not yet been transformed into the hand-related coordinates of our perception. The transformation to hand coordinates reflected in our conscious experience may occur downstream of area 2, or in a different proprioceptive stream entirely.

Combining inputs from multiple muscles is a prerequisite for even simple spatial processing, much less a particular coordinate transformation. My sensory mappings of single CN neurons suggest there is relatively little convergence across muscles. A transformation from muscle to joint or endpoint-based coordinates does not seem to be a significant goal at the level of either area 2 or CN.

Gain modulation hypotheses:

Circuitry within CN is able to modulate the sensitivity of CN neurons to sensory inputs as a function of descending drive (Andersen, Eccles, Oshima, et al., 1964; Leiras et al., 2010; Loutit et al., 2021; Sánchez, Barro, Mariño, & Canedo, 2006). In this section, I review the major theories about what descending gain modulation may accomplish at the level of CN. My research provides evidence for a functional gain control model of descending input to CN, in which gains in CN are context-dependent and optimized for perceptual and motor goals.

Sensory Gating

From early studies of CN, descending drive from the motor cortex has been shown to exert pre-synaptic inhibition on synaptic terminals connecting afferent fibers to CN neurons (Andersen, Eccles, Oshima, et al., 1964; Palmeri et al., 1999). This robust inhibitory input led some researchers to hypothesize that sensory signals are attenuated during active movements in a process known as "sensory gating" (Crevecoeur & Kording, 2017; Juravle et al., 2017b; Ziat, Hayward, Chapman, Ernst, & Lenay, 2010). Among other roles, the sensory gating hypothesis suggests that presynaptic inhibition prevents self-generated proprioceptive and tactile signals from disrupting an ongoing movement (Ghez & Pisa, 1972).

In my experiments, I found no evidence that proprioceptive information is systematically gated during actively generated movements. In fact, I found that CN neurons with proprioceptive RFs tended to be more sensitive during active movements, not less. I also found that while cutaneous-receiving neurons in CN were more commonly attenuated than potentiated, most

commonly there was not a difference in their sensitivity across conditions. This suggests that for proprioceptive and tactile sensory signals, sensory gain modulation is more complex than blanket attenuation.

Sensory Cancellation

Recent advances in optogenetics have allowed researchers to build circuit models that seek to explain how descending inputs to CN from motor cortex affect the processing of sensory information. These circuit models have led to the hypothesis that CN computes "prediction errors" from the combination of descending cortical inputs and ascending peripheral afferent signals (Conner et al., 2021). Prediction errors signal deviation from expected sensory reafference. For CN to encode prediction error, it must perform an operation known as "sensory cancellation", in which predicted sensory signals are subtracted from the incoming sensory information, leaving behind only the error. The sensory cancellation hypothesis differs from the sensory gating hypothesis; while sensory gating changes the gain of both expected and unexpected sensory information, sensory cancellation selectively removes the expected portion of the signal and leaves only the sensory error.

The intriguing hypothesis that sensory cancellation happens in CN was proposed for the mouse tactile system, where it may be valid. However, it does not seem to apply to encoding of proprioception in the CN of the monkey. In the sensory-cancellation hypothesis, neurons in CN should be relatively insensitive to predictable sensory inputs. In my recordings, proprioceptive neurons were sensitive to both passively generated movements and highly trained active

reaching movements, for which sensory inputs should be predictable. My work in CN suggests, instead, a context-dependent gain modulation, in which gain is increased or decreased depending on requirements of the task.

This is not to say that error computation does not occur in the proprioceptive system; indeed, there is convincing evidence that the cerebellum is a "forward model" that transforms a copy of motor commands ("efference copy") into predictions of the anticipated sensory reafference due to the movement. The primary source of upper-limb proprioceptive inputs to the cerebellum is the external cuneate nucleus (ECN) (Cooke et al., 1971). Axons from ECN travel through the inferior cerebellar peduncle, as mossy fiber inputs to deep cerebellar nuclei. They also synapse onto the cortical granule cells, which form the parallel fiber inputs to Purkinje cells (Shadmehr, 2020). The cerebellum, if acting as a forward model, must predict the somatosensory signals from ECN (Shadmehr, 2020). Consequently, any gain modulation that occurs at the level of ECN must also be modeled by the cerebellum, lest sensory predictions be incorrect. Future investigations into the proprioceptive cerebellum should recognize that sensory gain in the medulla can change as a function of movement context.

Functional roles of somatosensory gain modulation:

My data suggest that something other than sensory cancellation or sensory gating occurs in CN. The fact that many, but not all proprioceptive neurons in CN are potentiated indicates that there is likely complex descending gain modulation that turns up the volume on some sensors, while turning the volume down on others. I hypothesize that the modular gain in CN is a mechanism

to improve proprioceptive acuity for motor control and perception by increasing the dynamic range of these signals when more precise feedback is necessary. In this section, I will review some possible situations in which gain changes in CN help accomplish perceptual or reflexive motor goals.

Perceptual sensory gain:

Recent studies have found that human tactile acuity depends on context. Standard tests require subjects to report the angle of a raised bar presented passively to their fingertip. In this passive presentation, acuity is typically on the order of ~ 20 degrees. In experiments where subjects are instead asked to actively align a narrow raised bar to a reference, subjects achieved an accuracy of ~ 3 degrees, better by more than a factor of five (Olczak, Sukumar, & Pruszynski, 2018).

Improved tactile acuity during active movement contradicts the tactile suppression literature, which finds that sensory gain goes down, not up, during active movements. This discrepancy may reflect gain modulatory circuitry that can selectively increase gain on receptors that are relevant to perception (Conner et al., 2021). Results from my recordings suggest that even in reaching tasks, some cutaneous neurons are attenuated during movement while others are potentiated, evidence for context-dependent gain modulation of tactile inputs in CN.

From a motor control perspective, high fidelity proprioceptive feedback may be more important during active movements than when the arm is not performing a movement. Tests of human proprioceptive acuity show that active joint angle matching is more precise than passive joint matching (Bhanpuri, Okamura, & Bastian, 2013). My findings in CN suggest that peripheral or

brainstem mechanisms contribute to this increased acuity during active movements by increasing the gain of proprioceptive signals that pass through CN. My research was unable, however, to disentangle gain effects inherited from the periphery from those applied in CN itself.

Reflex-related sensory gain:

A vital role for proprioception exists in motor control below the level of conscious perception. Subconscious proprioceptive signals supply critical feedback to motor circuits in the spinal cord, brainstem, and cortex (Scott, 2016), without which our ability to execute movements is crippled (Sainburg et al., 1995; Sainburg, Poizner, & Ghez, 1993). In this section, I review the importance of proprioceptive feedback for reflexes and pattern generating circuits in the spinal cord. I then extend these principles into the brain and discuss how findings of sensory gain at the level of CN might contribute to brainstem-mediated and transcortical reflex loops.

Sensory gain modulation conditions reflexive motor output (Azim & Seki, 2019; Confais, Kim, Tomatsu, Takei, & Seki, 2017b; Fink et al., 2014), in addition to altering perceptual salience. Gain modulation of this sort may allow for more complex reflex behavior at the level of brainstem and above. One recent study found evidence for a brainstem-level "position" controller that subconsciously generates postural responses that maintain the position of the endpoint (Albert et al., 2020). It is unclear how these reflex loops are built, but descending gain modulation to CN may contribute to their function.

In my investigations I found that stimulation in CN often evoked movements with levels of current comparable to those needed in M1 to evoke muscle activations. I could evoke movements with electrical stimulation even while the animal was under ketamine sedation, suggesting the movements were not simply voluntary responses to an electrically-evoked sensation. These data, in combination with my findings of modulated sensory gain, suggest that CN projections to motor areas may contribute to the flexible reflexes seen during movement.

Given my finding that proprioceptive gain changes across conditions, future studies of CN should attempt to isolate how such gain changes can affect motor reflex circuits, particularly those related to the position controller. An experiment that tests how disruptions of the descending gain modulatory circuitry affects the maintenance of arm posture would give valuable insight into how gain changes in CN might subserve these brainstem-level reflexes.

Medium and long latency reflexes change as subjects learn to move in different dynamical environments, such as a force curl field (Maeda et al., 2018). It is unclear by what mechanism these adaptations occur, but it is possible that sensory gain modulation may play a role. My experiment found that sensory gain was stable for single neurons in a well-learned task, even over the course of an hour-long experimental session. An experiment that tests sensory gain in CN during learning tasks known to alter long-latency reflexes such as reaching in a force field (Kurtzer et al., 2008) could quantify the role of CN sensory gain changes in the adaptation of reflex behaviors.

Functional Gain Control: Next steps

Tactile and proprioceptive gain may change flexibly depending on the needs of individual tasks

or changes in task context. There are many contexts in which increases in gain might impart an

advantage to perception or motor control, and others where an increased gain would be

detrimental. It will be important for future work to find principles that can predict whether gain

in CN goes up or down in a given task. To do this, future studies should test for sensory gain

during active sensing tasks, as well as reaching tasks when contact events are important for

subsequent grasping behaviors. My work predicts that sensory gain should increase during

these behaviors that rely on high-fidelity somatosensory information for perception and control.

My task activated tactile receptors only indirectly through the reaching movements. This raises

complications in interpretation, because the patterns of skin strain may also vary across

kinematic contexts. Subsequent experiments that activate skin receptors with a controlled

stimulus at different phases of reaching and rest will provide more direct evidence of how

cutaneous sensory gain modulates during normal reaching behaviors (He et al., 2019).

CN: A somatosensory switchboard?

An often-unappreciated question in studies of the adult brain is "how did this circuit even get

wired up in the first place?" Descending control of sensory gain requires axons projecting from

the cortex to find presynaptic terminals of appropriate neurons in the brainstem. Helping to

generate this amazing organization of connections, and permitting the system to remap even

during adulthood, may be another critical role for CN.

Remapping in CN

A classic result in the study of somatosensory cortex is that depriving a region of cortex of sensory inputs causes the representations of nearby regions to "invade" that deafferented area (Pons et al., 1991; Ramachandran, Rogers-Ramachandran, Stewart, & Pons, 1992). For example, deafferenting the hand by cutting dorsal roots that carry somatosensory information from the hand causes neurons in former hand area 3b to respond to the chin (Pons et al., 1991). This result has served as the basis for claims of "cortical remapping" (Jon H. Kaas et al., 2008; Merzenich et al., 1984), that plasticity at the level of cortex allows for flexible re-representation of body regions on the cortical surface. However, a recent study on monkeys demonstrated that inputs from the chin access the cortical hand representation not through cortical plasticity, but instead through changes in the brainstem.

This demonstration relied on targeted inactivation; if the chin inputs joined the hand pathway at the level of cortex, inactivating chin cortex should remove chin representation in the hand area; if the chin inputs joined the hand pathway at the level of the brainstem, inactivating CN should remove chin representation in the cortex. Inactivating CN with lidocaine removed chin representation in hand cortex, but inactivating chin cortex had no effect (Jain, Florence, Qi, & Kaas, 2000; Jain et al., 2008; Kambi et al., 2014). This result suggests that even in the adult monkey, brainstem nuclei can remap their representations across spatially distant body regions.

Cortical representations of the body can change for reasons other than injury. Indeed, use-dependent remapping has been hypothesized to contribute to improvements in motor ability through training (Nudo, Milliken, Jenkins, & Merzenich, 1996), which raises an interesting question: does brainstem remapping occur only following injury, or is use-dependent remapping mediated by the brainstem as well?

In a second study, monkeys were trained to detect changes in vibration frequencies applied to the fingertips. When the monkeys detected a change, they moved their hand away from the vibration for a reward. After learning, area 3a (a proprioceptive area) contralateral to the trained arm began to respond to tactile stimuli, while area 3a of the untrained arm developed no such representation. Control monkeys, in which the tactile stimulus was presented, but not used to obtain a reward, also had no 3a responses driven by tactile inputs (Recanzone, Merzenich, & Jenkins, 1992). It is unclear whether these tactile inputs enter area 3a from area 3b, or as a result of brainstem remapping as in the case of deafferentation. Future experiments should test CN's role in use-dependent remapping (Nudo et al., 1996).

Anatomically dense, functionally sparse convergence in CN

The ability of the brainstem to remap its inputs in response to injury seems to contradict the low-convergence receptive fields I found in CN. Proprioceptive CN neurons typically responded to inputs from only a single muscle, in accordance with previous literature that tested convergence by pulling individual muscles (Hummelsheim & Wiesendanger, 1985). However, another study in which researchers instead stimulated peripheral nerves found wide convergence across both

space and modality (C. L. Witham & Baker, 2011). The latter observation is consistent with the anatomy of inputs to single CN neurons. Most receive hundreds or thousands of synapses from a wide variety of peripheral receptors (Bengtsson et al., 2013a; Fyffe et al., 1986). How can we reconcile these latter observations with mine? The answer may require that we measure the strength of the inputs.

A recent study characterized the synaptic weights of inputs to CN neurons through patch-clamping (Bengtsson et al., 2013a), to measure the intracellular changes in voltage caused by synaptic events that may not cause the neuron to fire an action potential. Excitatory post-synaptic potentials (EPSPs) are discrete events that have a consistent amplitude related to the weight of the synapse that generated the EPSP. The distribution of the magnitude of EPSPs can therefore be used to estimate the distribution of synaptic strengths of neurons that project to the clamped neuron. They used this distribution to estimate the number of potent synaptic inputs to CN neurons (i.e., the number of synapses that could independently cause a post-synaptic action potential). These researchers found that in a typical CN neuron, only 4-8 synapses had potent synaptic weights, with the remaining hundreds or thousands being very weak. For what purpose do these weak synapses exist?

I propose that CN serves as a switchboard in the brainstem that transmits peripheral signals centrally with high fidelity and temporal precision but also maintains weak synapses that are not functionally relevant during normal behavior. These residual synapses can be reactivated in response to injury (and possibly through changing motor control requirements) to remap the

inputs to cortex in an adaptable manner. The fact that synaptic pruning occurs concurrently with invasion of cortico-cuneate fibers suggests that descending inputs from motor cortex may play a role in establishing the potency of synaptic inputs (Fisher & Clowry, 2009). Chronic recordings from CN during a learning task may shed light onto whether use-dependent remapping occurs at the level of the brainstem, and, if so, on what time scales previously latent synaptic inputs can become potent.

CN as a site for proprioceptive replacement

Loss of limb and spinal cord injury dramatically affect quality of life and the ability to perform activities of daily living (Adams & Hicks, 2005). In the past 15 years, researchers began implanting recording electrodes and using neural signals from the motor cortex to control robotic prostheses (Collinger et al., 2018, 2013; Hochberg et al., 2006). A major roadblock to the success of these "Brain Computer Interfaces" (BCIs) may be the lack of somatosensory feedback (Bensmaia & Miller, 2014a; Fagg et al., 2009). To address this lost function, some groups have begun to artificially provide somatosensory feedback by stimulating somatosensory cortices with the goal of evoking naturalistic percepts, or at least coherent signals that the subjects can learn to use as feedback (Flesher et al., 2016; Brian M London, Jordan, Jackson, & Miller, 2008; Tomlinson & Miller, 2016). While reliable and focal tactile percepts can be evoked by stimulating somatosensory cortex (Lee et al., 2018; Salas et al., 2018), proprioceptive percepts have been generally unnatural and difficult to describe. Thus, restoring proprioceptive sensation may be inherently more difficult than restoring tactile sensation, at

least when restricted to stimulation of the somatosensory cortex.

In our lab, we have attempted to probe the percepts caused by intracortical microstimulation (ICMS) in area 2 of monkeys. Unfortunately, monkeys can't tell us what they feel, so we need to get creative. We have trained monkeys to report the direction of passively applied bumps. We stimulated cortex during these bumps and interpreted the change between the normal report direction and the direction that the monkey reported on stimulation trials as a "perceptual bias" caused by the stimulation. This perceptual bias would indicate that we were evoking sensations that feel similar to those caused by passive movements of the arm.

Critically, we also tried to predict the perceptual bias of the stimulation by the neurons around the stimulating electrode. If we stimulated an electrode that recorded neural activity with a preferred direction (PD) to the right, we would predict a rightward bias in the perceptual report. If across electrodes, stimulation of cortex produces perceptual biases that are predictable, it is an indication that the stimulation is making the monkey feel something that they interpret as a movement of their arm. This stimulation-evoked percept could potentially serve as a naturalistic feedback signal for arm movements.

Unfortunately, we have encountered significant roadblocks in our attempts to provide artificial proprioceptive feedback via ICMS. While for one monkey, we were able to produce predictable biases, we were unable to replicate this result with several subsequent monkeys. In these later monkeys we were able to provoke biases, but we couldn't predict their direction. This suggests

that there may be a spatially diffuse proprioceptive representation in which "rightward" signaling neurons are distributed across arm area 2, and not locally clustered. In that circumstance, stimulation would need to activate spatially distant areas simultaneously. This representation would be difficult to replicate using electrical stimulation, even when delivered across many electrode sites (Tomlinson & Miller, 2016).

Even if stimulation of somatosensory cortex were effective at producing proprioceptive percepts, this stimulation cannot directly restore proprioceptive input to subcortical regions (in particular, the cerebellum) that are critical for motor control. While peripheral nerve interfaces have shown some promise in evoking artificial somatosensation (D'Anna et al., 2018; Tan et al., 2014) and improving amputees' control of prosthetic limbs (Schiefer et al., 2018), these peripheral interfaces would not be effective for patients with spinal cord injury whose peripheral nerves are disconnected from the brain.

CN, just central to the spinal cord, may be an ideal candidate site for proprioceptive replacement (Loutit & Potas, 2020). DCN is the site of major branching of the proprioceptive stream to a variety of motor nuclei; stimulation at the level of DCN could restore not only the cortical proprioceptive circuit, but also subcortical and cerebellar inputs that are essential for motor control.

While proprioceptive signals from individual muscles seem to be represented diffusely on the cortical sheet of area 2, we found a somatotopic arrangement of muscle receptor signals in CN

resembling the properties of single muscle spindle afferents. We know that muscle vibration provokes strong, natural-feeling, proprioceptive illusions, suggesting that stimulation of these "muscle-like" neurons in CN may also be able to produce proprioceptive percepts.

Further work needs to be done to evaluate the safety and efficacy of implanting CN in humans, including both psychophysical studies on its perceptual effects, as well as studies to assess whether implants in CN may present a health risk due to CN's proximity to homeostatic brainstem nuclei (Berger, 1977; Loutit & Potas, 2020).

Conclusion

There are relatively few studies of motor cortex that investigate how proprioceptive feedback helps to generate motor behavior. We know from patients who have lost the sense of proprioception that without it, the ability to make controlled movements is severely compromised. It is therefore my belief that motor control and proprioception can only be understood jointly, as a coupled system that acts hierarchically. Each level of the neuraxis performs a function subject to latency constraints and complexity requirements of the sensory-motor transformation, with dumb, fast reflexes occurring in the spinal cord and flexible but slow reflexes occurring in brainstem and transcortical loops. Almost all somatosensory information from the arm that travels into the brain for use in these motor and perceptual pathways travels through the CN and ECN.

In my doctoral work, I helped develop methods to implant and record chronically from the CN of monkeys, yielding the first ever recordings of its single neurons during behavior (Chapter 2). I characterized the encoding of proprioception in CN for the first time, finding signatures of gain modulation across kinematic contexts and demonstrating a low level of proprioceptive convergence onto single CN neurons (Chapter 3). I then compared the encoding of CN and area 2 and demonstrated that the standard tools to quantify proprioceptive encoding are insufficient to uncover processing along the neuraxis (Chapter 4). In a tangential perspective (Chapter 5), I presented an overall model of the motor system in which proprioceptive afference is critical to the function of dynamics of neural firing in motor cortex. In this final chapter, I discussed the impact of these results and set out future studies that could answer the next questions that this work raises. Future work should focus on specific aspects of proprioceptive function and attempt to explain features of proprioceptive coding with motor and perceptual end goals in mind.

I look forward to the future work that builds from my progress and hope to one day understand fully how the brain can use proprioceptive feedback to generate and control movements of the arm. I hope that this knowledge will lead to improvements in the ability of people with spinal cord injury to interact with the world in ways which improve their quality of life.

References

Adams, M. M., & Hicks, A. L. (2005). Spasticity after spinal cord injury. *Spinal Cord*, *43*, 577–586.
https://doi.org/10.1038/sj.sc.3101757

Aguilar, J., Rivadulla, C., Soto, C., & Canedo, A. (2003). New Corticocuneate Cellular Mechanisms Underlying the Modulation of Cutaneous Ascending Transmission in Anesthetized Cats. *Journal of Neurophysiology*, *89*(6), 3328–3339. https://doi.org/10.1152/jn.01085.2002

Albert, S. T., Hadjiosif, A. M., Jang, J., Zimnik, A. J., Soteropoulos, D. S., Baker, S. N., … Shadmehr, R. (2020). Postural control of arm and fingers through integration of movement commands. *ELife*, *9*. https://doi.org/10.7554/ELIFE.52507

Alessandro, C., Rellinger, B. A., Barroso, F. O., & Tresch, M. C. (2018). Adaptation after vastus lateralis denervation in rats demonstrates neural regulation of joint stresses and strains. *ELife*, *7*. https://doi.org/10.7554/eLife.38215

Andersen, P., Eccles, J. C., Oshima, T., & SCH, R. F. (1964). Mechanisms of synaptic transmission in the Cuneate Nucleus. *Journal of Neurophysiology*, *27*(6), 1096–1116. https://doi.org/10.1152/jn.1964.27.6.1096

Andersen, P., Eccles, J. C., & Schmidt, R. F. (1962). Presynaptic inhibitory actions: Presynaptic inhibition in the cuneate nucleus. *Nature*, *194*(4830), 741–743. https://doi.org/10.1038/194741a0

Andersen, P., Eccles, J. C., Schmidt, R. F., & Yokota, T. (1964a). Identification of relay cells and interneurons in the Cuneate Nucleus. *Journal of Neurophysiology*, *27*(6), 1080–1095. https://doi.org/10.1152/jn.1964.27.6.1080

Andersen, P., Eccles, J. C., Schmidt, R. F., & Yokota, T. (1964b). Slow potential waves produced in the Cuneate Nucleus by cutaneous volleys and by cortical stimulation. *Journal of Neurophysiology*, *27*, 78–91. https://doi.org/10.1152/jn.1964.27.1.78

Asanuma, H. (1975). Recent developments in the study of the columnar arrangement of neurons within the motor cortex. *Https://Doi.Org/10.1152/Physrev.1975.55.2.143*, *55*(2), 143–156. https://doi.org/10.1152/PHYSREV.1975.55.2.143

Azim, E., & Seki, K. (2019). Gain control in the sensorimotor system This review comes from a themed issue on Motor control systems. *Current Opinion in Physiology*, *8*, 177–187.

https://doi.org/10.1016/j.cophys.2019.03.005

Bakker, R., Tiesinga, P., & Kötter, R. (2015). The Scalable Brain Atlas: Instant Web-Based Access to Public Brain Atlases and Related Content. *Neuroinformatics*, *13*(3), 353–366. https://doi.org/10.1007/s12021-014-9258-x

Balaram, P., Young, N. A., & Kaas, J. H. (2014). Histological features of layers and sublayers in cortical visual areas V1 and V2 of chimpanzees, macaque monkeys, and humans. *Eye and Brain*, *6*(Suppl 1), 5–18. https://doi.org/10.2147/EB.S51814

Banks, R., & Stacey, M. (1988). Quantitative Studies on Mammalian Muscle Spindles and their Sensory Innervation. In *Mechanoreceptors* (pp. 263–269). Springer US. https://doi.org/10.1007/978-1-4899-0812-4_49

Bastian, A. J., Martin, T. A., Keating, J. G., & Thach, W. T. (1996). Cerebellar Ataxia: Abnormal Control of Interaction Torques Across Multiple Joints. *JOURNALOF NEUROPHYSIOLOGY*, *76*(1).

Bengtsson, F., Brasselet, R., Johansson, R. S., Arleo, A., & Jörntell, H. (2013a). Integration of Sensory Quanta in Cuneate Nucleus Neurons In Vivo. *PLoS ONE*, *8*(2), e56630. https://doi.org/10.1371/journal.pone.0056630

Bengtsson, F., Brasselet, R., Johansson, R. S., Arleo, A., & Jörntell, H. (2013b). Integration of Sensory Quanta in Cuneate Nucleus Neurons In Vivo. *PLoS ONE*, *8*(2). https://doi.org/10.1371/journal.pone.0056630

Benjamin, P. R., Staras, K., & Kemenes, G. (2010). What Roles Do Tonic Inhibition and Disinhibition Play in the Control of Motor Programs? *Frontiers in Behavioral Neuroscience*, *4*(JUN). https://doi.org/10.3389/FNBEH.2010.00030

Bennett, D. J., De Serres, S. J., & Stein, R. B. (1996). Regulation of soleus muscle spindle sensitivity in decerebrate and spinal cats during postural and locomotor activities. *Journal of Physiology*, *495*(3), 835–850. https://doi.org/10.1113/jphysiol.1996.sp021636

Bensmaia, S. J., Denchev, P. V., Dammann, J. F., Craig, J. C., & Hsiao, S. S. (2008). The representation of stimulus orientation in the early stages of somatosensory processing. *The Journal of Neuroscience*, *28*(3), 776–786. https://doi.org/10.1523/JNEUROSCI.4162-07.2008

Bensmaia, S. J., & Miller, L. E. (2014a). Restoring sensorimotor function through intracortical interfaces: progress and looming challenges. *Nature Reviews Neuroscience 2014 15:5*, *15*(5), 313–325. https://doi.org/10.1038/nrn3724

Bensmaia, S. J., & Miller, L. E. (2014b, May). Restoring sensorimotor function through intracortical interfaces: Progress and looming challenges. *Nature Reviews Neuroscience*. Nature Publishing Group. https://doi.org/10.1038/nrn3724

Berger, A. J. (1977). Dorsal respiratory group neurons in the medulla of cat: Spinal projections, responses to lung inflation and superior laryngeal nerve stimulation. *Brain Research*, *135*(2), 231–254. https://doi.org/10.1016/0006-8993(77)91028-9

Berkley, K. J., Budell, R. J., Blomqvist, A., & Bull, M. (1986, September 1). Output systems of the dorsal column nuclei in the cat. *Brain Research Reviews*. Elsevier. https://doi.org/10.1016/0165-0173(86)90012-3

Bermejo, P. E., Jiménez, C. E., Torres, C. V., & Avendaño, C. (2003). Quantitative stereological evaluation of the gracile and cuneate nuclei and their projection neurons in the rat. *Journal of Comparative Neurology*, *463*(4), 419–433. https://doi.org/10.1002/cne.10747

Bhanpuri, N. H., Okamura, A. M., & Bastian, A. J. (2013). Predictive Modeling by the Cerebellum Improves Proprioception. *Journal of Neuroscience*, *33*(36), 14301–14306. https://doi.org/10.1523/JNEUROSCI.0784-13.2013

Biedenbach, M. A. (1972). Cell density and regional distribution of cell types in the cuneate nucleus of the Rhesus monkey. *Brain Research*, *45*(1), 1–14. https://doi.org/10.1016/0006-8993(72)90212-0

Biedenbach, M. A., Jabbur, S. J., & Towe, A. L. (1971). *Afferent inhibition in the cuneate nucleus of the rhesus monkey*. *Brain Research* (Vol. 27). https://doi.org/10.1016/0006-8993(71)90381-7

Binda, P., & Morrone, M. C. (2018). Vision During Saccadic Eye Movements. *Annual Review of Vision Science*, *4*(1), 193–213. https://doi.org/10.1146/annurev-vision-091517-034317

Biryukova, E., & Sirotkina, I. (2020). Forward to Bernstein: Movement Complexity as a New Frontier. *Frontiers in Neuroscience*, *0*, 553. https://doi.org/10.3389/FNINS.2020.00553

Bloedel, J. R., & Courville, J. (1981). Cerebellar Afferent Systems. *Comprehensive Physiology*, 735–829. https://doi.org/10.1002/CPHY.CP010216

Blum, K. P., Lamotte D'Incamps, B., Zytnicki, D., & Ting, L. H. (2017). Force encoding in muscle spindles during stretch of passive muscle. *PLOS Computational Biology*, *13*(9), e1005767. https://doi.org/10.1371/journal.pcbi.1005767

Boivie, J., & Boman, K. (1981). Termination of a separate (proprioceptive?) cuneothalamic tract from external cuneate nucleus in monkey. *Brain Research*, *224*(2), 235–246. https://doi.org/10.1016/0006-8993(81)90856-8

Bosco, G., Rankin, A., & Poppele, R. (1996). Representation of passive hindlimb postures in cat spinocerebellar activity. *Journal of Neurophysiology*, *76*(2), 715–726. https://doi.org/10.1152/jn.1996.76.2.715

Boyd, I. A. (1962). The structure and innervation of the nuclear bag muscle fibre system and the nuclear chain muscle fibre system in mammalian muscle spindles. *Philosophical Transactions of the Royal Society of London. Series B, Biological Sciences*, *245*(720), 81–136. https://doi.org/10.1098/rstb.1962.0007

Bremmer, F., Kubischik, M., Hoffmann, K. P., & Krekelberg, B. (2009). Neural dynamics of saccadic suppression. *Journal of Neuroscience*, *29*(40), 12374–12383. https://doi.org/10.1523/JNEUROSCI.2908-09.2009

Brooks, J. X., Carriot, J., & Cullen, K. E. (2015). Learning to expect the unexpected: rapid updating in primate cerebellum during voluntary self-motion. *Nature Neuroscience*, *18*(9), 1310–1317. https://doi.org/10.1038/nn.4077

Buford, J., & Davidson, A. (2004). Movement-related and preparatory activity in the reticulospinal system of the monkey. *Experimental Brain Research*.

Burgess, P. R., & Clark, F. J. (1969). Characteristics of knee joint receptors in the cat. *The Journal of Physiology*, *203*(2), 317–335. https://doi.org/10.1113/jphysiol.1969.sp008866

Burke, D., Gandevia, S. C., & Macefield, G. (1988). Responses to passive movement of receptors in joint, skin and muscle of the human hand. *The Journal of Physiology*, *402*(1), 347–361. https://doi.org/10.1113/jphysiol.1988.sp017208

Canedo, A., Mariño, J., & Aguilar, J. (2000). Lemniscal recurrent and transcortical influences on cuneate neurons. *Neuroscience*, *97*(2), 317–334. https://doi.org/10.1016/S0306-4522(00)00063-4

Chan, S. S., & Moran, D. W. (2006). Computational model of a primate arm: From hand position to joint angles, joint torques and muscle forces. *Journal of Neural Engineering*, *3*(4), 327–337. https://doi.org/10.1088/1741-2560/3/4/010

CHANG, H. T., & RUCH, T. C. (1947). Organization of the dorsal columns of the spinal cord and their nuclei in the spider monkey. *Journal of Anatomy*, *81*(Pt 2), 140–149.

Chapman, C. E., Jiang, W., & Lamarre, Y. (1988). Modulation of lemniscal input during conditioned arm movements in the monkey. *Experimental Brain Research*, *72*(2), 316–334. https://doi.org/10.1007/BF00250254

Cheema, S., Whitsel, B. L., & Rustioni, A. (1983). The corticocuneate pathway in the cat: Relations among terminal distribution patterns, cytoarchitecture, and single neuron functional properties. *Somatosensory & Motor Research*, *1*(2), 169–205. https://doi.org/10.3109/07367228309144547

Chen, H., Hua, S. E., Smith, M. A., Lenz, F. A., & Shadmehr, R. (2006). Effects of Human Cerebellar Thalamus Disruption on Adaptive Control of Reaching. *Cerebral Cortex (New York, N.Y. : 1991)*, *16*(10), 1462. https://doi.org/10.1093/CERCOR/BHJ087

Chowdhury, R. H., Glaser, J. I., & Miller, L. E. (2020). Area 2 of primary somatosensory cortex encodes kinematics of the whole arm. *ELife*, *9*. https://doi.org/10.7554/eLife.48198

Chowdhury, R. H., Tresch, M. C., & Miller, L. E. (2017). Musculoskeletal geometry accounts for apparent extrinsic representation of paw position in dorsal spinocerebellar tract. *Journal of Neurophysiology*, *118*(1), 234–242. https://doi.org/10.1152/jn.00695.2016

Cohen, L. G., & Starr, A. (1987). Localization, timing and specificity of gating of somatosensory evoked potentials during active movement in man. *Brain*, *110*(2), 451–467. https://doi.org/10.1093/brain/110.2.451

Cole, M. (1996). Pride and a Daily Marathon. *Neurology*, *47*(3), 856.4-857. https://doi.org/10.1212/wnl.47.3.856-c

Collinger, J. L., Gaunt, R. A., & Schwartz, A. B. (2018, December 1). Progress towards restoring upper limb movement and sensation through intracortical brain-computer interfaces. *Current Opinion in Biomedical Engineering*. Elsevier. https://doi.org/10.1016/j.cobme.2018.11.005

Collinger, J. L., Wodlinger, B., Downey, J. E., Wang, W., Tyler-Kabara, E. C., Weber, D. J., … Schwartz, A. B. (2013). High-performance neuroprosthetic control by an individual with tetraplegia. *The Lancet*, *381*(9866), 557–564. https://doi.org/10.1016/S0140-6736(12)61816-9

Collins, D. F., Refshauge, K. M., Todd, G., & Gandevia, S. C. (2005). Cutaneous receptors contribute to kinesthesia at the index finger, elbow, and knee. *Journal of Neurophysiology*, *94*(3), 1699–1706. https://doi.org/10.1152/jn.00191.2005

Confais, J., Kim, G., Tomatsu, S., Takei, T., & Seki, K. (2017a). Nerve-specific input modulation to spinal neurons during a motor task in the monkey. *Journal of Neuroscience*, *37*(10), 2612–2626. https://doi.org/10.1523/JNEUROSCI.2561-16.2017

Confais, J., Kim, G., Tomatsu, S., Takei, T., & Seki, K. (2017b). Nerve-specific input modulation to spinal neurons during a motor task in the monkey. *Journal of Neuroscience*, *37*(10), 2612–2626. https://doi.org/10.1523/JNEUROSCI.2561-16.2017

Conner, J. M., Bohannon, A., Igarashi, M., Taniguchi, J., Baltar, N., & Azim, E. (2021). Modulation of tactile feedback for the execution of dexterous movement. *BioRxiv*, 2021.03.04.433649.

https://doi.org/10.1101/2021.03.04.433649

Cooke, J. D., Larson, B., Oscarsson, O., & Sjölund, B. (1971). Origin and termination of cuneocerebellar

tract. *Experimental Brain Research*, *13*(4), 339–358. https://doi.org/10.1007/BF00234336

Costanzo, R. M., & Gardner, E. P. (1981). Multiple-joint neurons in somatosensory cortex of awake

monkeys. *Brain Research*, *214*(2), 321–333. https://doi.org/10.1016/0006-8993(81)91197-5

Crevecoeur, F., & Kording, K. P. (2017). Saccadic suppression as a perceptual consequence of efficient

sensorimotor estimation. *ELife*, *6*. https://doi.org/10.7554/eLife.25073

Cross, K. P., Cook, D. J., & Scott, S. H. (2021). Convergence of proprioceptive and visual feedback on

neurons in primary motor cortex. *BioRxiv*, 2021.05.01.442274.

https://doi.org/10.1101/2021.05.01.442274

Cunningham, J. P., & Ghahramani, Z. (2014). Linear Dimensionality Reduction: Survey, Insights, and

Generalizations. https://doi.org/10.1002/cssc.201100629

Cunningham, J. P., & Yu, B. M. (2014). Dimensionality reduction for large-scale neural recordings,

17(11). https://doi.org/10.1038/nn.3776

D'Anna, E., Valle, G., Mazzoni, A., Strauss, I., Iberite, F., Patton, J., … Micera, S. (2018). A closed-loop

hand prosthesis with simultaneous intraneural tactile and position feedback. *BioRxiv*.

https://doi.org/10.1101/262741

Dale, A., & Cullen, K. E. (2019). The ventral posterior lateral thalamus preferentially encodes externally

applied versus active movement: Implications for self-motion perception. *Cerebral Cortex*, *29*(1),

1–14. https://doi.org/10.1093/cercor/bhx325

Delhaye, B. P., Long, K. H., & Bensmaia, S. J. (2018). Neural Basis of Touch and Proprioception in

Primate Cortex. *Comprehensive Physiology*, *8*(4), 1575–1602.

https://doi.org/10.1002/cphy.c170033

Delp, S. L., Anderson, F. C., Arnold, A. S., Loan, P., Habib, A., John, C. T., … Thelen, D. G. (2007).

OpenSim: Open-source software to create and analyze dynamic simulations of movement. *IEEE*

Transactions on Biomedical Engineering, *54*(11), 1940–1950.

https://doi.org/10.1109/TBME.2007.901024

Desmurget, M., Epstein, C. M., Turner, R. S., Prablanc, C., Alexander, G. E., & Grafton, S. T. (1999).

Role of the posterior parietal cortex in updating reaching movements to a visual target. *Nature*

Neuroscience, *2*(6), 563–567. https://doi.org/10.1038/9219

Dimitriou, M. (2014). Human Muscle Spindle Sensitivity Reflects the Balance of Activity between

Antagonistic Muscles. *Journal of Neuroscience*, *34*(41), 13644–13655.

https://doi.org/10.1523/JNEUROSCI.2611-14.2014

Dimitriou, Michael. (2014). Human muscle spindle sensitivity reflects the balance of activity between

antagonistic muscles. *The Journal of Neuroscience : The Official Journal of the Society for*

Neuroscience, *34*(41), 13644–13655. https://doi.org/10.1523/JNEUROSCI.2611-14.2014

Dimitriou, Michael, & Edin, B. B. (2008). Discharges in human muscle spindle afferents during a key-

pressing task. *Journal of Physiology*, *586*(22), 5455–5470.

https://doi.org/10.1113/jphysiol.2008.160036

Dimitriou, Michael, & Edin, B. B. (2010). Human muscle spindles act as forward sensory models.

Current Biology, *20*(19), 1763–1767. https://doi.org/10.1016/j.cub.2010.08.049

Dimitriou, Michael, Wolpert, D. M., & Franklin, D. W. (2013). The Temporal Evolution of Feedback

Gains Rapidly Update to Task Demands. https://doi.org/10.1523/JNEUROSCI.5669-12.2013

Dooley, J. C., Sokoloff, G., Blumberg, M. S., & Dooley, J. (2021). Developmental onset of a cerebellar-

dependent forward model of movement in motor thalamus 2 3.

https://doi.org/10.1101/2021.06.25.449956

Duque, J., & Ivry, R. B. (2009). Role of corticospinal suppression during motor preparation. *Cerebral*

Cortex, *19*(9), 2013–2024. https://doi.org/10.1093/cercor/bhn230

Dykes, R. W., Rasmusson, D. D., Sretavan, D., & Rehman, N. B. (1982). Submodality segregation and

receptive-field sequences in cuneate, gracile, and external cuneate nuclei of the cat. *Journal of*

Neurophysiology, *47*(3), 389–416. https://doi.org/10.1152/jn.1982.47.3.389

Earhart, G. M., & Bastian, A. J. (2001). Selection and coordination of human locomotor forms following cerebellar damage. *Journal of Neurophysiology*, *85*(2), 759–769. https://doi.org/10.1152/jn.2001.85.2.759

Edin, B. B. (1992). Quantitative analysis of static strain sensitivity in human mechanoreceptors from hairy skin. *Journal of Neurophysiology*, *67*(5), 1105–1113. https://doi.org/10.1152/jn.1992.67.5.1105

Edin, B. B., & Johansson, N. (1995). Skin strain patterns provide kinaesthetic information to the human central nervous system. *The Journal of Physiology*, *487*(1), 243–251. https://doi.org/10.1113/jphysiol.1995.sp020875

Efron, B., & Tibshirani, R. (1986). Bootstrap methods for standard errors, confidence intervals, and other measures of statistical accuracy. *Statistical Science*, *1*(1), 54–75. https://doi.org/10.1214/ss/1177013815

Eklund, G. (1972). *Position sense and state of contraction; the effects of vibration*. *Neurosurgery, and Psychiatry* (Vol. 35). BMJ Publishing Group. Retrieved from /pmc/articles/PMC494139/?report=abstract

Elangovan, N., Herrmann, A., & Konczak, J. (2014). Assessing Proprioceptive Function: Evaluating Joint Position Matching Methods Against Psychophysical Thresholds. *Physical Therapy*, *94*(4), 553–561. https://doi.org/10.2522/PTJ.20130103

Ellaway, P. H., Taylor, A., & Durbaba, R. (2015a, August 1). Muscle spindle and fusimotor activity in locomotion. *Journal of Anatomy*. Blackwell Publishing Ltd. https://doi.org/10.1111/joa.12299

Ellaway, P. H., Taylor, A., & Durbaba, R. (2015b, August 1). Muscle spindle and fusimotor activity in locomotion. *Journal of Anatomy*. Blackwell Publishing Ltd. https://doi.org/10.1111/joa.12299

Fagg, A. H., Hatsopoulos, N. G., London, B. M., Reimer, J., Solla, S. A., Wang, D., & Miller, L. E. (2009). Toward a biomimetic, bidirectional, brain machine interface. In *Proceedings of the 31st*

Annual International Conference of the IEEE Engineering in Medicine and Biology Society: Engineering the Future of Biomedicine, EMBC 2009 (pp. 3376–3380). IEEE Computer Society. https://doi.org/10.1109/IEMBS.2009.5332819

Fallon, J. B., & Macefield, V. G. (2007). Vibration sensitivity of human muscle spindles and Golgi tendon organs. *Muscle & Nerve*, *36*(1), 21–29. https://doi.org/10.1002/mus.20796

Fink, A. J. P., Croce, K. R., Huang, Z. J., Abbott, L. F., Jessell, T. M., & Azim, E. (2014). Presynaptic inhibition of spinal sensory feedback ensures smooth movement. *Nature*, *509*(7498), 43–48. https://doi.org/10.1038/nature13276

Fisher, T., & Clowry, G. J. (2009). Elimination of muscle afferent boutons from the cuneate nucleus of the rat medulla during development. *Neuroscience*, *161*(3), 787–793. https://doi.org/10.1016/j.neuroscience.2009.04.009

Flesher, S. N., Collinger, J. L., Foldes, S. T., Weiss, J. M., Downey, J. E., Tyler-Kabara, E. C., … Gaunt, R. A. (2016). Intracortical microstimulation of human somatosensory cortex. *Science Translational Medicine*, *8*(361), 361ra141-361ra141. https://doi.org/10.1126/scitranslmed.aaf8083

Florence, S. L., Wall, J. T., & Kaas, J. H. (1988). The somatotopic pattern of afferent projections from the digits to the spinal cord and cuneate nucleus in macaque monkeys. *Brain Research*, *452*(1–2), 388–392. https://doi.org/10.1016/0006-8993(88)90045-5

Florence, S. L., Wall, J. T., & Kaas, J. H. (1989). Somatotopic organization of inputs from the hand to the spinal gray and cuneate nucleus of monkeys with observations on the cuneate nucleus of humans. *The Journal of Comparative Neurology*, *286*(1), 48–70. https://doi.org/10.1002/cne.902860104

Friedman, D. P., & Jones, E. G. (1981). Thalamic input to areas 3a and 2 in monkeys. *Journal of Neurophysiology*, *45*(1), 59–85. Retrieved from http://www.ncbi.nlm.nih.gov/pubmed/7205345

Fuchs, A., & Luschei, E. (1970). Firing patterns of abducens neurons of alert monkeys in relationship to horizontal eye movement. *Journal of Neurophysiology*.

Fuentes, C. T., & Bastian, A. J. (2010). Where Is Your Arm? Variations in Proprioception Across Space and Tasks. *Journal of Neurophysiology*, *103*(1), 164–171. https://doi.org/10.1152/jn.00494.2009

Fyffe, R. E. W., Cheema, S. S., & Rustioni, A. (1986). Intracellular staining study of the feline cuneate nucleus. I. Terminal patterns of primary afferent fibers. *Journal of Neurophysiology*, *56*(5), 1268–1283. https://doi.org/10.1152/jn.1986.56.5.1268

Gandevia, S. C., Smith, J. L., Crawford, M., Proske, U., & Taylor, J. L. (2006). Motor commands contribute to human position sense. *Journal of Physiology*, *571*(3), 703–710. https://doi.org/10.1113/jphysiol.2005.103093

Gao, P., & Ganguli, S. (2015). On simplicity and complexity in the brave new world of large-scale neuroscience. *Current Opinion in Neurobiology*, *32*, 148–155. https://doi.org/10.1016/J.CONB.2015.04.003

Gao, Z., Davis, C., Thomas, A. M., Economo, M. N., Abrego, A. M., Svoboda, K., … Li, N. (2018). A cortico-cerebellar loop for motor planning. *Nature*, *563*(7729), 113–116. https://doi.org/10.1038/s41586-018-0633-x

Gardner, E. P., Babu, K. S., Ghosh, S., Sherwood, A., & Chen, J. (2007). Neurophysiology of Prehension. III. Representation of Object Features in Posterior Parietal Cortex of the Macaque Monkey. *Journal of Neurophysiology*, *98*(6), 3708–3730. https://doi.org/10.1152/jn.00609.2007

Gardner, E. P., & Costanzo, R. M. (1981). Properties of kinesthetic neurons in somatosensory cortex of awake monkeys. *Brain Research*, *214*(2), 301–319. https://doi.org/10.1016/0006-8993(81)91196-3

Georgopoulos, A P, Kalaska, J. F., Caminiti, R., & Massey, J. T. (1982). On the relations between the direction of two-dimensional arm movements and cell discharge in primate motor cortex. *The Journal of Neuroscience : The Official Journal of the Society for Neuroscience*, *2*(11), 1527–1537. Retrieved from http://www.ncbi.nlm.nih.gov/pubmed/7143039

Georgopoulos, Apostolos P., Schwartz, A. B., & Kettner, R. E. (1986). Neuronal population coding of movement direction. *Science*, *233*(4771), 1416–1419. https://doi.org/10.1126/SCIENCE.3749885

Ghez, C., & Pisa, M. (1972). Inhibition of afferent transmission in cuneate nucleus during voluntary movement in the cat. *Brain Research*, *40*(1), 145–155. Retrieved from http://www.ncbi.nlm.nih.gov/pubmed/4338259

Giesler, G. J., Nahin, R. L., & Madsen, A. M. (1984). Postsynaptic dorsal column pathway of the rat. I. Anatomical studies. *Journal of Neurophysiology*, *51*(2), 260–275. https://doi.org/10.1152/jn.1984.51.2.260

Goble, D. J. (2010). Proprioceptive Acuity Assessment Via Joint Position Matching: From Basic Science to General Practice. *Physical Therapy*, *90*(8), 1176–1184. https://doi.org/10.2522/PTJ.20090399

Goodwin, G. M., McCloskey, D. I., & Matthews, P. B. (1972a). Proprioceptive illusions induced by muscle vibration: contribution by muscle spindles to perception? *Science (New York, N.Y.)*, *175*(4028), 1382–1384. Retrieved from http://www.ncbi.nlm.nih.gov/pubmed/4258209

Goodwin, G. M., McCloskey, D. I., & Matthews, P. B. (1972b). Proprioceptive illusions induced by muscle vibration: contribution by muscle spindles to perception? *Science (New York, N.Y.)*, *175*(4028), 1382–1384. https://doi.org/10.1126/science.175.4028.1382

Gregory, J. E., Brockett, C. L., Morgan, D. L., Whitehead, N. P., & Proske, U. (2002). Effect of eccentric muscle contractions on Golgi tendon organ responses to passive and active tension in the cat. *The Journal of Physiology*, *538*(Pt 1), 209. https://doi.org/10.1113/JPHYSIOL.2001.012785

Hahamy, A., Macdonald, S. N., van den Heiligenberg, F., Kieliba, P., Emir, U., Malach, R., … Makin, T. R. (2017). Representation of Multiple Body Parts in the Missing-Hand Territory of Congenital One-Handers. *Current Biology*, *27*(9), 1350–1355. https://doi.org/10.1016/J.CUB.2017.03.053

Hamel-Pâquet, C., Sergio, L. E., & Kalaska, J. F. (2006). Parietal area 5 activity does not reflect the differential time-course of motor output kinetics during arm-reaching and isometric-force tasks. *Journal of Neurophysiology*, *95*(6), 3353–3370. https://doi.org/10.1152/jn.00789.2005

Harris, F., Jabbur, S. J., Morse, R. W., & Towe, A. L. (1965, December). Influence of the cerebral cortex on the cuneate nucleus of the monkey [27]. *Nature*. Nature Publishing Group.

https://doi.org/10.1038/2081215a0

Harvey, M A, Saal, H. P., Dammann 3rd, J. F., & Bensmaia, S. J. (2013). Multiplexing stimulus information through rate and temporal codes in primate somatosensory cortex. *PLoS Biol*, *11*(5), e1001558. https://doi.org/10.1371/journal.pbio.1001558

Harvey, Michael A., Saal, H. P., Dammann, J. F., & Bensmaia, S. J. (2013). Multiplexing Stimulus Information through Rate and Temporal Codes in Primate Somatosensory Cortex. *PLoS Biology*, *11*(5), e1001558. https://doi.org/10.1371/journal.pbio.1001558

Hasan, Z. (1983). A model of spindle afferent response to muscle stretch. *Journal of Neurophysiology*, *49*(4), 989–1006. https://doi.org/10.1152/jn.1983.49.4.989

Hayward, V., Terekhov, A. V., Wong, S.-C., Geborek, P., Bengtsson, F., & Jörntell, H. (2014). Spatio-temporal skin strain distributions evoke low variability spike responses in cuneate neurons. *Journal of The Royal Society Interface*, *11*(93), 20131015. https://doi.org/10.1098/rsif.2013.1015

He, Q., Suresh, A., Versteeg, C., Rosenow, J. M., & Bensmaia, S. J. (2019). Movement gating of cutaneous signals in the cuneate nucleus. Presented at Society for Neuroscience 2019.

Hebart, M. N., & Hesselmann, G. (2012). What Visual Information Is Processed in the Human Dorsal Stream? *Journal of Neuroscience*, *32*(24), 8107–8109. https://doi.org/10.1523/JNEUROSCI.1462-12.2012

Herzfeld, D. J., Kojima, Y., Soetedjo, R., & Shadmehr, R. (2018). Encoding of error and learning to correct that error by the Purkinje cells of the cerebellum. *Nature Neuroscience*, *21*(5), 736–743. https://doi.org/10.1038/s41593-018-0136-y

Hochberg, L. R., Serruya, M. D., Friehs, G. M., Mukand, J. A., Saleh, M., Caplan, A. H., … Donoghue, J. P. (2006). Neuronal ensemble control of prosthetic devices by a human with tetraplegia. *Nature*, *442*(7099), 164–171. https://doi.org/10.1038/nature04970

Hoffman, D., Dubner, R., & Hayes, R. (1981). Neuronal activity in medullary dorsal horn of awake monkeys trained in a thermal discrimination task. I. Responses to innocuous and noxious thermal.

Journal Of.

Holmes, N. P., & Spence, C. (2005). Visual bias of unseen hand position with a mirror: spatial and temporal factors. In *Experimental Brain Research* (Vol. 166, pp. 489–497). Exp Brain Res. https://doi.org/10.1007/s00221-005-2389-4

Holt, E. B. (1903). Eye-movement and central anaesthesia. *The Psychological Review: Monograph Supplements*, *4*(1), 1–45. Retrieved from https://psycnet.apa.org/record/1926-02629-001

Home, M. K., & Tracey, D. J. (1979). The afferents and projections of the ventroposterolateral thalamus in the monkey. *Experimental Brain Research 1979 36:1*, *36*(1), 129–141. https://doi.org/10.1007/BF00238473

Horch, K., Meek, S., Taylor, T. G., & Hutchinson, D. T. (2011). Object discrimination with an artificial hand using electrical stimulation of peripheral tactile and proprioceptive pathways with intrafascicular electrodes. *IEEE Transactions on Neural Systems and Rehabilitation Engineering*, *19*(5), 483–489. https://doi.org/10.1109/TNSRE.2011.2162635

Houk, J. C., Rymer, W. Z., & Crago, P. E. (1981). Dependence of dynamic response of spindle receptors on muscle length and velocity. *Journal of Neurophysiology*, *46*(1), 143–166. https://doi.org/10.1152/jn.1981.46.1.143

Houk, J., & Simon, W. (1967). Responses of Golgi tendon organs to forces applied to muscle tendon. *Journal of Neurophysiology*, *30*(6), 1466–1481. https://doi.org/10.1152/jn.1967.30.6.1466

Huffman, K. J., & Krubitzer, L. (2001a). Thalamo-cortical connections of areas 3a and M1 in marmoset monkeys. *The Journal of Comparative Neurology*, *435*(3), 291–310. https://doi.org/10.1002/cne.1031

Huffman, K. J., & Krubitzer, L. (2001b). Thalamo-cortical connections of areas 3a and M1 in marmoset monkeys. *Journal of Comparative Neurology*, *435*(3), 291–310. https://doi.org/10.1002/cne.1031

Hummelsheim, H., & Wiesendanger, M. (1985). Neuronal responses of medullary relay cells to controlled stretches of forearm muscles in the monkey. *Neuroscience*, *16*(4), 989–996.

https://doi.org/10.1016/0306-4522(85)90111-3

Hummelsheim, H., Wiesendanger, R., & Wiesendanger, M. (1985). The projection of low-threshold muscle afferents of the forelimb to the main and external cuneate nuclei of the monkey. *Neuroscience*.

Hummelsheim, H., Wiesendanger, R., Wiesendanger, M., & Bianchetti, M. (1985). The projection of low-threshold muscle afferents of the forelimb to the main and external cuneate nuclei of the monkey. *Neuroscience*, *16*(4), 979–987. https://doi.org/10.1016/0306-4522(85)90110-1

Inagaki, H. K., Fontolan, L., Romani, S., & Svoboda, K. (2019). Discrete attractor dynamics underlies persistent activity in the frontal cortex. *Nature*, *566*(7743), 212–217. https://doi.org/10.1038/S41586-019-0919-7

Inoue, M., & Kitazawa, S. (2018). Motor Error in Parietal Area 5 and Target Error in Area 7 Drive Distinctive Adaptation in Reaching. *Current Biology*, *28*(14), 2250-2262.e3. https://doi.org/10.1016/j.cub.2018.05.056

Izawa, J., Criscimagna-Hemminger, S. E., & Shadmehr, R. (2012). Cerebellar contributions to reach adaptation and learning sensory consequences of action. *Journal of Neuroscience*, *32*(12), 4230–4239. https://doi.org/10.1523/JNEUROSCI.6353-11.2012

Izumizaki, M., Tsuge, M., Akai, L., Proske, U., & Homma, I. (2010). The illusion of changed position and movement from vibrating one arm is altered by vision or movement of the other arm. *Journal of Physiology*, *588*(15), 2789–2800. https://doi.org/10.1113/jphysiol.2010.192336

Jabbur, S. J., & Banna, N. R. (1968). Presynaptic inhibition of cuneate transmission by widespread cutaneous inputs. *Brain Research*, *10*(2), 273–276. https://doi.org/10.1016/0006-8993(68)90135-2

Jain, N., Florence, S. L., Qi, H. X., & Kaas, J. H. (2000). Growth of new brainstem connections in adult monkeys with massive sensory loss. *Proceedings of the National Academy of Sciences of the United States of America*, *97*(10), 5546–5550. https://doi.org/10.1073/pnas.090572597

Jain, N., Qi, H. X., Collins, C. E., & Kaas, J. H. (2008). Large-scale reorganization in the somatosensory

cortex and thalamus after sensory loss in macaque monkeys. *Journal of Neuroscience*, *28*(43), 11042–11060. https://doi.org/10.1523/JNEUROSCI.2334-08.2008

Jami, L. (1992). Golgi tendon organs in mammalian skeletal muscle: Functional properties and central actions. *Physiological Reviews*, *72*(3), 623–666. https://doi.org/10.1152/physrev.1992.72.3.623

Jansen, J. K. S., & Rudjord, T. (1964). On the Silent Period and Golgi Tendon Organs of the Soleus Muscle of the Cat. *Acta Physiologica Scandinavica*, *62*(4), 364–379. https://doi.org/10.1111/J.1748-1716.1964.TB10435.X

Johnson, K. O., & Lamb, G. D. (1981). Neural mechanisms of spatial tactile discrimination: neural patterns evoked by braille-like dot patterns in the monkey. *The Journal of Physiology*, *310*, 117–144.

Jones, E. G., & Porter, R. (1980, May 1). What is area 3a? *Brain Research Reviews*. Elsevier. https://doi.org/10.1016/0165-0173(80)90002-8

Jones, K. E., Wessberg, J., & Vallbo, Å. B. (2001). Directional tuning of human forearm muscle afferents during voluntary wrist movements. *Journal of Physiology*, *536*(2), 635–647. https://doi.org/10.1111/j.1469-7793.2001.0635c.xd

Jörntell, H., Bengtsson, F., Geborek, P., Spanne, A., Terekhov, A. V., & Hayward, V. (2014). Segregation of Tactile Input Features in Neurons of the Cuneate Nucleus. *Neuron*, *83*(6), 1444–1452. https://doi.org/10.1016/j.neuron.2014.07.038

Juravle, G., Binsted, G., & Spence, C. (2017a). Tactile suppression in goal-directed movement. *Psychonomic Bulletin and Review*, *24*(4), 1060–1076. https://doi.org/10.3758/s13423-016-1203-6

Juravle, G., Binsted, G., & Spence, C. (2017b). Tactile suppression in goal-directed movement. *Psychonomic Bulletin and Review*, *24*(4), 1060–1076. https://doi.org/10.3758/s13423-016-1203-6

Kaas, J. H., Nelson, R. J., Sur, M., Dykes, R. W., & Merzenich, M. M. (1984). The somatotopic organization of the ventroposterior thalamus of the squirrel monkey,Saimiri sciureus. *The Journal of Comparative Neurology*, *226*(1), 111–140. https://doi.org/10.1002/cne.902260109

Kaas, Jon H., Qi, H. X., Burish, M. J., Gharbawie, O. A., Onifer, S. M., & Massey, J. M. (2008, February). Cortical and subcortical plasticity in the brains of humans, primates, and rats after damage to sensory afferents in the dorsal columns of the spinal cord. *Experimental Neurology*. https://doi.org/10.1016/j.expneurol.2007.06.014

Kaiser, D. (2012). In retrospect: The Structure of Scientific Revolutions. *Nature 2012 484:7393*, *484*(7393), 164–165. https://doi.org/10.1038/484164a

Kambi, N., Halder, P., Rajan, R., Arora, V., Chand, P., Arora, M., & Jain, N. (2014). Large-scale reorganization of the somatosensory cortex following spinal cord injuries is due to brainstem plasticity. *Nature Communications*, *5*(1), 1–10. https://doi.org/10.1038/ncomms4602

Kandel, E. R., Schwartz, J. H. (James H., & Jessell, T. M. (1991). Principles of neural science, 1135.

Karanjia, P. N., & Ferguson, J. H. (1983). Passive joint position sense after total hip replacement surgery. *Annals of Neurology*, *13*(6), 654–657. https://doi.org/10.1002/ana.410130612

Kaufman, M. T., Churchland, M. M., Ryu, S. I., & Shenoy, K. V. (2014). Cortical activity in the null space: permitting preparation without movement. *Nature Neuroscience*, *17*(3), 440–448. https://doi.org/10.1038/nn.3643

Kawato, M. (1999, December 1). Internal models for motor control and trajectory planning. *Current Opinion in Neurobiology*. Curr Opin Neurobiol. https://doi.org/10.1016/S0959-4388(99)00028-8

Kawato, M., Ohmae, S., Hoang, H., & Sanger, T. (2020, June 27). 50 Years Since the Marr, Ito, and Albus Models of the Cerebellum. *Neuroscience*. Elsevier Ltd. https://doi.org/10.1016/j.neuroscience.2020.06.019

Killebrew, J. H., Bensmaïa, S. J., Dammann, J. F., Denchev, P., Hsiao, S. S., Craig, J. C., & Johnson, K. O. (2007). A dense array stimulator to generate arbitrary spatio-temporal tactile stimuli. *Journal of Neuroscience Methods*, *161*(1), 62–74. https://doi.org/10.1016/j.jneumeth.2006.10.012

Korenberg, M. J., & Naka, K. I. (1988). White-noise analysis in visual neuroscience. *Visual Neuroscience*, *1*(3), 287–296. https://doi.org/10.1017/S0952523800001942

Krubitzer, L., Huffman, K. J., Disbrow, E., & Recanzone, G. (2004). Organization of area 3a in macaque monkeys: Contributions to the cortical phenotype. *The Journal of Comparative Neurology*, *471*(1), 97–111. https://doi.org/10.1002/cne.20025

Kubota, S., Sidikejiang, W., Kudo, M., Inoue, K., Umeda, T., Takada, M., & Seki, K. (2019). Optogenetic recruitment of spinal reflex pathways from large-diameter primary afferents in non-transgenic rats transduced with AAV9/Channelrhodopsin 2. *The Journal of Physiology*, *597*(19), 5025–5040. https://doi.org/10.1113/JP278292

Kurtzer, I. L., Pruszynski, J. A., & Scott, S. H. (2008). Long-Latency Reflexes of the Human Arm Reflect an Internal Model of Limb Dynamics. *Current Biology*, *18*(6), 449–453. https://doi.org/10.1016/J.CUB.2008.02.053

Lee, B., Kramer, D., Salas, M. A., Kellis, S., Brown, D., Dobreva, T., … Andersen, R. A. (2018). Engineering artificial somatosensation through cortical stimulation in humans. *Frontiers in Systems Neuroscience*, *12*. https://doi.org/10.3389/fnsys.2018.00024

Leiras, R., Velo, P., Martín-Cora, F., & Canedo, A. (2010). Processing Afferent Proprioceptive Information at the Main Cuneate Nucleus of Anesthetized Cats. *Journal of Neuroscience*, *30*(46).

Li, C. X., Yang, Q., & Waters, R. S. (2012). Functional and structural organization of the forelimb representation in cuneate nucleus in rat. *Brain Research*, *1468*, 11–28. https://doi.org/10.1016/j.brainres.2012.03.048

Li, N., Daie, K., Svoboda, K., & Druckmann, S. (2016). Robust neuronal dynamics in premotor cortex during motor planning. *Nature*, *532*(7600). https://doi.org/10.1038/nature17643

Lillicrap, T. P., & Scott, S. H. (2013). Preference Distributions of Primary Motor Cortex Neurons Reflect Control Solutions Optimized for Limb Biomechanics. *Neuron*, *77*(1), 168–179. https://doi.org/10.1016/J.NEURON.2012.10.041

London, B. M., & Miller, L. E. (2013). Responses of somatosensory area 2 neurons to actively and passively generated limb movements. *Journal of Neurophysiology*, *109*(6), 1505–1513.

https://doi.org/10.1152/jn.00372.2012

London, Brian M, Jordan, L. R., Jackson, C. R., & Miller, L. E. (2008). Electrical stimulation of the proprioceptive cortex (area 3a) used to instruct a behaving monkey. *IEEE Transactions on Neural Systems and Rehabilitation Engineering*, *16*(1), 32–36. https://doi.org/10.1109/TNSRE.2007.907544

London, Brian M, & Miller, L. E. (2013). Responses of somatosensory area 2 neurons to actively and passively generated limb movements. *Journal of Neurophysiology*, *109*(6), 1505–1513. https://doi.org/10.1152/jn.00372.2012

London, Brian M, Torres, R. R., Slutzky, M. W., & Miller, L. E. (2011). Designing stimulation patterns for an afferent BMI: representation of kinetics in somatosensory cortex. *Conference Proceedings : ... Annual International Conference of the IEEE Engineering in Medicine and Biology Society. IEEE Engineering in Medicine and Biology Society. Annual Conference*, *2011*, 7521–7524. https://doi.org/10.1109/IEMBS.2011.6091854

Loutit, A. J., & Potas, J. R. (2020). Restoring Somatosensation: Advantages and Current Limitations of Targeting the Brainstem Dorsal Column Nuclei Complex. *Frontiers in Neuroscience*, *14*, 156. https://doi.org/10.3389/fnins.2020.00156

Loutit, A. J., Vickery, R. M., & Potas, J. R. (2021). Functional organization and connectivity of the dorsal column nuclei complex reveals a sensorimotor integration and distribution hub. *Journal of Comparative Neurology*, *529*(1), 187–220. https://doi.org/10.1002/cne.24942

Lucier, G. E., Rüegg, D. C., & Wiesendanger, M. (1975). Responses of neurones in motor cortex and in area 3A to controlled stretches of forelimb muscles in cebus monkeys. *The Journal of Physiology*, *251*(3), 833–853. https://doi.org/10.1113/jphysiol.1975.sp011125

Ma, W. J., & Jazayeri, M. (2014). Neural Coding of Uncertainty and Probability. https://doi.org/10.1146/annurev-neuro-071013-014017

Macefield, V. G., & Knellwolf, T. P. (2018, August 1). Functional properties of human muscle spindles.

Journal of Neurophysiology. American Physiological Society. https://doi.org/10.1152/jn.00071.2018

Mackel, R., & Miyashita, E. (1993). Nucleus Z: A somatosensory relay to motor thalamus. *Journal of Neurophysiology*, *69*(5), 1607–1620. https://doi.org/10.1152/jn.1993.69.5.1607

Maeda, R. S., Cluff, T., Gribble, P. L., & Pruszynski, J. A. (2018). Feedforward and feedback control share an internal model of the arm's dynamics. *Journal of Neuroscience*, *38*(49), 10505–10514. https://doi.org/10.1523/JNEUROSCI.1709-18.2018

Maertens De Noordhout, A., Rapisarda, G., Bogacz, D., Gérard, P., De Pasqua, V., Pennisi, G., & Delwaide, P. J. (1999). Corticomotoneuronal synaptic connections in normal man. An electrophysiological study. *Brain*, *122*(7), 1327–1340. https://doi.org/10.1093/brain/122.7.1327

Mai, J., & Paxinos, G. (2011). *The human nervous system*.

Mathis, A., Mamidanna, P., Cury, K. M., Abe, T., Murthy, V. N., Mathis, M. W., & Bethge, M. (2018). DeepLabCut: markerless pose estimation of user-defined body parts with deep learning. *Nature Neuroscience*, *21*(9), 1281–1289. https://doi.org/10.1038/s41593-018-0209-y

Mathis, M. W., Mathis, A., & Uchida, N. (2017). Somatosensory Cortex Plays an Essential Role in Forelimb Motor Adaptation in Mice. *Neuron*, *93*(6), 1493-1503.e6. https://doi.org/10.1016/j.neuron.2017.02.049

McGlone, F., & Reilly, D. (2010). The cutaneous sensory system. *Neuroscience & Biobehavioral Reviews*, *34*(2), 148–159. https://doi.org/10.1016/J.NEUBIOREV.2009.08.004

Merzenich, M. M., Nelson, R. J., Stryker, M. P., Cynader, M. S., Schoppmann, A., & Zook, J. M. (1984). Somatosensory cortical map changes following digit amputation in adult monkeys. *Journal of Comparative Neurology*, *224*(4), 591–605. https://doi.org/10.1002/CNE.902240408

Meunier, S., & Pierrot-Deseilligny, E. (1989). Gating of the afferent volley of the monosynaptic stretch reflex during movement in man. *The Journal of Physiology*, *419*(1), 753–763. https://doi.org/10.1113/jphysiol.1989.sp017896

Miall, R. C., & Wolpert, D. M. (1996). Forward models for physiological motor control. *Neural Networks*, *9*(8), 1265–1279. https://doi.org/10.1016/S0893-6080(96)00035-4

Miall, R. Chris, Christensen, L. O. D., Cain, O., & Stanley, J. (2007). Disruption of State Estimation in the Human Lateral Cerebellum. *PLOS Biology*, *5*(11), e316. https://doi.org/10.1371/JOURNAL.PBIO.0050316

Mileusnic, M. P., & Loeb, G. E. (2006). Mathematical Models of Proprioceptors. II. Structure and Function of the Golgi Tendon Organ. *Journal of Neurophysiology*, *96*(4), 1789–1802. https://doi.org/10.1152/jn.00869.2005

Molinari, H. H., Schultze, K. E., & Strominger, N. L. (1996). Gracile, cuneate, and spinal trigeminal projections to inferior olive in rat and monkey. *Journal of Comparative Neurology*, *375*(3), 467–480. https://doi.org/10.1002/(SICI)1096-9861(19961118)375:3<467::AID-CNE9>3.0.CO;2-0

Mollazadeh, M., Aggarwal, V., Thakor, N. V., & Schieber, M. H. (2014). Principal components of hand kinematics and neurophysiological signals in motor cortex during reach to grasp movements. *Journal of Neurophysiology*, *112*(8), 1857–1870. https://doi.org/10.1152/jn.00481.2013

Morita, H., Petersen, N., & Nielsen, J. (1998). Gating of somatosensory evoked potentials during voluntary movement of the lower limb in man. *Experimental Brain Research*, *120*(2), 143–152. https://doi.org/10.1007/s002210050388

Mountcastle, V. B. (2011). Central Nervous Mechanisms in Mechanoreceptive Sensibility. In *Comprehensive Physiology* (pp. 789–878). Hoboken, NJ, USA: John Wiley & Sons, Inc. https://doi.org/10.1002/cphy.cp010318

Mountcastle, V. B., Talbot, W. H., Darian-Smith, I., & Kornhuber, H. H. (1967). Neural basis of the sense of flutter-vibration. *Science*, *155*(3762), 597–600.

Muniak, M. A., Ray, S., Hsiao, S. S., Dammann, J. F., & Bensmaia, S. J. (2008). The neural coding of stimulus of mechanoreceptive afferents with psychophysical behavior (vol 27, pg 11687, 2007). *JOURNAL OF NEUROSCIENCE*, *28*(7).

Musallam, S., Bak, M. J., Troyk, P. R., & Andersen, R. A. (2007). A floating metal microelectrode array for chronic implantation. *Journal of Neuroscience Methods*, *160*(1), 122–127. https://doi.org/10.1016/j.jneumeth.2006.09.005

Nashed, J. Y., Crevecoeur, F., & Scott, S. H. (2014). Rapid online selection between multiple motor plans. *Journal of Neuroscience*, *34*(5), 1769–1780. https://doi.org/10.1523/JNEUROSCI.3063-13.2014

Niu, J., Ding, L., Li, J., Kim, H., Liu, J., & Li, H. (2013). Modality-based organization of ascending somatosensory axons in the direct dorsal column pathway. *The Journal Of*.

Nowak, D. A., Timmann, D., & Hermsdörfer, J. (2007). Dexterity in cerebellar agenesis. *Neuropsychologia*, *45*(4), 696–703. https://doi.org/10.1016/j.neuropsychologia.2006.08.011

Nudo, R. J., Milliken, G. W., Jenkins, W. M., & Merzenich, M. M. (1996). Use-dependent alterations of movement representations in primary motor cortex of adult squirrel monkeys. *The Journal of Neuroscience : The Official Journal of the Society for Neuroscience*, *16*(2), 785–807. https://doi.org/10.1523/JNEUROSCI.16-02-00785.1996

O'Neal, J. T., & Westrum, L. E. (1973). The fine structural synaptic organization of the cat lateral cuneate nucleus. A study of sequential alterations in degeneration. *Brain Research*, *51*, 97–124. https://doi.org/10.1016/0006-8993(73)90367-3

Olczak, D., Sukumar, V., & Pruszynski, J. A. (2018). Edge orientation perception during active touch. *Journal of Neurophysiology*, *120*(5), 2423–2429. https://doi.org/10.1152/jn.00280.2018

Padberg, J., Cerkevich, C., Engle, J., Rajan, A. T., Recanzone, G., Kaas, J., & Krubitzer, L. (2009). Thalamocortical connections of parietal somatosensory cortical fields in macaque monkeys are highly divergent and convergent. *Cerebral Cortex*, *19*(9), 2038–2064. https://doi.org/10.1093/cercor/bhn229

Padberg, J., Cooke, D. F., Cerkevich, C. M., Kaas, J. H., & Krubitzer, L. (2018). Cortical connections of area 2 and posterior parietal area 5 in macaque monkeys. *Journal of Comparative Neurology*.

https://doi.org/10.1002/cne.24453

Padberg, J., Cooke, D. F., Cerkevich, C. M., Kaas, J. H., & Krubitzer, L. (2019). Cortical connections of area 2 and posterior parietal area 5 in macaque monkeys. *Journal of Comparative Neurology*, *527*(3), 718–737. https://doi.org/10.1002/cne.24453

Palmeri, A., Bellomo, M., Giuffrida, R., & Sapienza, S. (1999). Motor cortex modulation of exteroceptive information at bulbar and thalamic lemniscal relays in the cat. *Neuroscience*, *88*(1), 135–150. Retrieved from http://www.ncbi.nlm.nih.gov/pubmed/10051195

Pandarinath, C., O'Shea, D. J., Collins, J., Jozefowicz, R., Stavisky, S. D., Kao, J. C., … Sussillo, D. (2018). Inferring single-trial neural population dynamics using sequential auto-encoders. *Nature Methods 2018 15:10*, *15*(10), 805–815. https://doi.org/10.1038/s41592-018-0109-9

Pavlides, C., Miyashita, E., & Asanuma, H. (1993). Projection from the sensory to the motor cortex is important in learning motor skills in the monkey. *Journal of Neurophysiology*, *70*(2), 733–741. https://doi.org/10.1152/jn.1993.70.2.733

Perich, M. G., Gallego, J. A., & Miller, L. E. (2018). A Neural Population Mechanism for Rapid Learning. *Neuron*, *100*(4), 964-976.e7. https://doi.org/10.1016/j.neuron.2018.09.030

Phillips, C. G., Powell, T. P., & Wiesendanger, M. (1971). Projection from low-threshold muscle afferents of hand and forearm to area 3a of baboon's cortex. *The Journal of Physiology*, *217*(2), 419–446. Retrieved from http://www.ncbi.nlm.nih.gov/pubmed/5097607

Pons, T. P., Garraghty, P. E., Ommaya, A. K., Kaas, J. H., Taub, E., & Mishkin, M. (1991). Massive cortical reorganization after sensory deafferentation in adult macaques. *Science*, *252*(5014), 1857–1860. https://doi.org/10.1126/science.1843843

Pratt, C. A. (1995). Evidence of positive force feedback among hindlimb extensors in the intact standing cat. *Journal of Neurophysiology*, *73*(6), 2578–2583. https://doi.org/10.1152/jn.1995.73.6.2578

Prochazka, A., Hulliger, M., Zangger, P., & Appenteng, K. (1985a). "Fusimotor set": new evidence for α-independent control of γ-motoneurones during movement in the awake cat. *Brain Research*,

339(1), 136–140. https://doi.org/10.1016/0006-8993(85)90632-8

Prochazka, A., Hulliger, M., Zangger, P., & Appenteng, K. (1985b). "Fusimotor set": new evidence for

α-independent control of γ-motoneurones during movement in the awake cat. *Brain Research*,

339(1), 136–140. https://doi.org/10.1016/0006-8993(85)90632-8

Prochazka, Arthur, & Ellaway, P. (2012). Sensory systems in the control of movement. *Comprehensive*

Physiology. Compr Physiol. https://doi.org/10.1002/cphy.c100086

Proske, U., & Gandevia, S. C. (2012). The Proprioceptive Senses: Their Roles in Signaling Body Shape,

Body Position and Movement, and Muscle Force. *Physiological Reviews*, *92*(4), 1651–1697.

https://doi.org/10.1152/physrev.00048.2011

Prud'homme, M. J., Cohen, D. A., & Kalaska, J. F. (1994). Tactile activity in primate primary

somatosensory cortex during active arm movements: cytoarchitectonic distribution. *Journal of*

Neurophysiology, *71*(1), 173–181. Retrieved from http://www.ncbi.nlm.nih.gov/pubmed/8158227

Prud'homme, M. J., & Kalaska, J. F. (1994). Proprioceptive activity in primate primary somatosensory

cortex during active arm reaching movements. *Journal of Neurophysiology*, *72*(5), 2280–2301.

Retrieved from http://www.ncbi.nlm.nih.gov/pubmed/7884459

Pruszynski, J. A. (2014). Primary motor cortex and fast feedback responses to mechanical perturbations:

a primer on what we know now and some suggestions on what we should find out next. *Frontiers in*

Integrative Neuroscience, *8*, 1–7. https://doi.org/10.3389/FNINT.2014.00072

Pruszynski, J. A., Kurtzer, I., Nashed, J. Y., Omrani, M., Brouwer, B., & Scott, S. H. (2011a). Primary

motor cortex underlies multi-joint integration for fast feedback control. *Nature*, *478*(7369), 387–

390. https://doi.org/10.1038/nature10436

Pruszynski, J. A., Kurtzer, I., Nashed, J. Y., Omrani, M., Brouwer, B., & Scott, S. H. (2011b). Primary

motor cortex underlies multi-joint integration for fast feedback control. *Nature 2011 478:7369*,

478(7369), 387–390. https://doi.org/10.1038/nature10436

Qi, H. X., & Kaas, J. H. (2006). Organization of primary afferent projections to the gracile nucleus of the

dorsal column system of primates. *Journal of Comparative Neurology*, *499*(2), 183–217.

https://doi.org/10.1002/cne.21061

Ramachandran, V. S., Rogers-Ramachandran, D., Stewart, M., & Pons, T. P. (1992). Perceptual

correlates of massive cortical reorganization. *Science*, *258*(5085), 1159–1160.

https://doi.org/10.1126/SCIENCE.1439826

Ramnani, N. (2006). The primate cortico-cerebellar system: Anatomy and function. *Nature Reviews*

Neuroscience. https://doi.org/10.1038/nrn1953

Recanzone, G. H., Merzenich, M. M., & Jenkins, W. M. (1992). Frequency discrimination training

engaging a restricted skin surface results in an emergence of a cutaneous response zone in cortical

area 3a. *Journal of Neurophysiology*, *67*(5), 1057–1070. https://doi.org/10.1152/jn.1992.67.5.1057

Ribot-Ciscar, E., Hospod, V., Roll, J.-P., & Aimonetti, J.-M. (2009). Fusimotor drive may adjust muscle

spindle feedback to task requirements in humans. *Journal of Neurophysiology*, *101*(2), 633–640.

https://doi.org/10.1152/jn.91041.2008

Richardson, A.G., Weigand, P. K., Sritharan, S. Y., & Lucas, T. H. (2015). Somatosensory encoding

with cuneate nucleus microstimulation: Effects on downstream cortical activity (pp. 695–698).

https://doi.org/10.1109/NER.2015.7146718

Richardson, Andrew G., Weigand, P. K., Sritharan, S. Y., & Lucas, T. H. (2016). A chronic neural

interface to the macaque dorsal column nuclei. *Journal of Neurophysiology*, *115*(5). Retrieved from

http://jn.physiology.org/content/115/5/2255

Rincon-Gonzalez, L., Warren, J. P., Meller, D. M., & Helms Tillery, S. (2011). Haptic interaction of

touch and proprioception: Implications for neuroprosthetics. *IEEE Transactions on Neural Systems*

and Rehabilitation Engineering, *19*(5), 490–500. https://doi.org/10.1109/TNSRE.2011.2166808

Rosén, I. (1969). Afferent connexions to group I activated cells in the main cuneate nucleus of the cat.

The Journal of Physiology, *205*(1), 209–236. Retrieved from

http://www.ncbi.nlm.nih.gov/pubmed/5347718

Rosén, I., & Sjölund, B. (1973). Organization of group I activated cells in the main and external cuneate nuclei of the cat: identification of muscle receptors. *Experimental Brain Research*, *16*(3), 221–237. https://doi.org/10.1007/bf00233327

Rousche, P. J., & Normann, R. A. (1998). Chronic recording capability of the Utah Intracortical Electrode Array in cat sensory cortex. *Journal of Neuroscience Methods*, *82*(1), 1–15. https://doi.org/10.1016/S0165-0270(98)00031-4

Rushworth, M. F. S., Nixon, P. D., & Passingham, R. E. (1997). Parietal cortex and movement. I. Movement selection and reaching. *Experimental Brain Research*, *117*(2), 292–310. https://doi.org/10.1007/s002210050224

Russo, A. A., Bittner, S. R., Perkins, S. M., Seely, J. S., London, B. M., Lara, A. H., … Churchland, M. M. (2018). Motor Cortex Embeds Muscle-like Commands in an Untangled Population Response. *Neuron*, *97*(4), 953-966.e8. https://doi.org/10.1016/j.neuron.2018.01.004

Saal, H P, & Bensmaia, S. J. (2014). Touch is a team effort: interplay of submodalities in cutaneous sensibility. *Trends in Neurosciences*, *37*(12), 689–697. https://doi.org/10.1016/j.tins.2014.08.012

Saal, Hannes P., & Bensmaia, S. J. (2014). Touch is a team effort: interplay of submodalities in cutaneous sensibility. *Trends in Neurosciences*, *37*(12), 689–697. https://doi.org/10.1016/J.TINS.2014.08.012

Sainburg, R. L., Ghilardi, M. F., Poizner, H., & Ghez, C. (1995). Control of limb dynamics in normal subjects and patients without proprioception. *Journal of Neurophysiology*, *73*(2), 820–835. https://doi.org/10.1152/jn.1995.73.2.820

Sainburg, R. L., Poizner, H., & Ghez, C. (1993). Loss of proprioception produces deficits in interjoint coordination. *Journal of Neurophysiology*, *70*(5), 2136–2147. https://doi.org/10.1152/jn.1993.70.5.2136

Salas, M. A., Bashford, L., Kellis, S., Jafari, M., Jo, H., Kramer, D., … Andersen, R. A. (2018). Proprioceptive and cutaneous sensations in humans elicited by intracortical microstimulation.

ELife, *7*. https://doi.org/10.7554/eLife.32904

Saliba, G., & Sabra, A. I. (1992). The Optics of Ibn Al-Haytham: Books I-III, on Direct Vision. *Journal of the American Oriental Society*, *112*(3), 528. https://doi.org/10.2307/603118

Sánchez, E., Barro, S., Mariño, J., & Canedo, A. (2006). Cortical modulation of dorsal column nuclei: A computational study. *Journal of Computational Neuroscience*, *21*(1), 21–33. https://doi.org/10.1007/s10827-006-7058-5

Sandbrink, K. J., Mamidanna, P., Michaelis, C., Mathis, M. W., Bethge, M., & Mathis, A. (2020). Task-driven hierarchical deep neural network models of the proprioceptive pathway. *BioRxiv*. https://doi.org/10.1101/2020.05.06.081372

Santello, M., Flanders, M., & Soechting, J. F. (1998). Postural hand synergies for tool use. *Journal of Neuroscience*, *18*(23), 10105–10115. https://doi.org/10.1523/jneurosci.18-23-10105.1998

Sauerbrei, B. A., Guo, J.-Z., Cohen, J. D., Mischiati, M., Guo, W., Kabra, M., … Hantman, A. W. (2019). Cortical pattern generation during dexterous movement is input-driven. *Nature 2019 577:7790*, *577*(7790), 386–391. https://doi.org/10.1038/s41586-019-1869-9

Sauerbrei, B., Guo, J. Z., Mischiati, M., Guo, W., Kabra, M., Verma, N., … Hantman, A. (2018, February 15). Motor cortex is an input-driven dynamical system controlling dexterous movement. *BioRxiv*. bioRxiv. https://doi.org/10.1101/266320

Schaffelhofer, S., & Scherberger, H. (2016). Object vision to hand action in macaque parietal, premotor, and motor cortices. *ELife*, *5*(2016JULY). https://doi.org/10.7554/ELIFE.15278

Schiefer, M. A., Graczyk, E. L., Sidik, S. M., Tan, D. W., & Tyler, D. J. (2018). Artificial tactile and proprioceptive feedback improves performance and confidence on object identification tasks. *PLOS ONE*, *13*(12), e0207659. https://doi.org/10.1371/journal.pone.0207659

Schmidt, R. F., Schady, W. J. L., & Torebjörk, H. E. (1990). Gating of tactile input from the hand - I. Effects of finger movement. *Experimental Brain Research*, *79*(1), 97–102. https://doi.org/10.1007/BF00228877

Scott, S. H. (2004). Optimal feedback control and the neural basis of volitional motor control. *Nature Reviews Neuroscience*. Nature Publishing Group. https://doi.org/10.1038/nrn1427

Scott, S. H. (2016). A Functional Taxonomy of Bottom-Up Sensory Feedback Processing for Motor Actions. *Trends in Neurosciences*. https://doi.org/10.1016/j.tins.2016.06.001

Scott, S. H., Cluff, T., Lowrey, C. R., & Takei, T. (2015). Feedback control during voluntary motor actions. *Current Opinion in Neurobiology*, *33*, 85–94. https://doi.org/10.1016/j.conb.2015.03.006

Serrien, D. J., & Wiesendanger, M. (1999). Role of the cerebellum in tuning anticipatory and reactive grip force responses. *Journal of Cognitive Neuroscience*, *11*(6), 672–681. https://doi.org/10.1162/089892999563634

Shadmehr, R. (2020, December 1). Population coding in the cerebellum: A machine learning perspective. *Journal of Neurophysiology*. American Physiological Society Bethesda, MD. https://doi.org/10.1152/jn.00449.2020

Shadmehr, R., & Krakauer, J. W. (2008). A computational neuroanatomy for motor control. *Experimental Brain Research*. https://doi.org/10.1007/s00221-008-1280-5

Shenoy, K. V., Sahani, M., & Churchland, M. M. (2013). Cortical Control of Arm Movements: A Dynamical Systems Perspective. *Annual Review of Neuroscience*, *36*(1), 337–359. https://doi.org/10.1146/annurev-neuro-062111-150509

Sinkjær, T., Andersen, J. B., & Larsen, B. (1996). Soleus stretch reflex modulation during gait in humans. *Journal of Neurophysiology*, *76*(2), 1112–1120. https://doi.org/10.1152/jn.1996.76.2.1112

Smith, K. S., Bucci, D. J., Luikart, B. W., & Mahler, S. V. (2016, April 1). DREADDs: Use and application in behavioral neuroscience. *Behavioral Neuroscience*. American Psychological Association Inc. https://doi.org/10.1037/bne0000135

Smith, M. A., Ghazizadeh, A., & Shadmehr, R. (2006). Interacting Adaptive Processes with Different Timescales Underlie Short-Term Motor Learning. *PLoS Biology*, *4*(6), e179. https://doi.org/10.1371/journal.pbio.0040179

Stevenson, I. H., Cherian, A., London, B. M., Sachs, N. A., Lindberg, E., Reimer, J., … Kording, K. P. (2011). Statistical assessment of the stability of neural movement representations. *Journal of Neurophysiology*, *106*(2), 764–774. https://doi.org/10.1152/jn.00626.2010

Suresh, A. K., Greenspon, C. M., He, Q., Rosenow, J. M., Miller, L. E., & Bensmaia, S. J. (2021). Sensory computations in the cuneate nucleus of macaques. *BioRxiv*, 2021.07.28.454185. https://doi.org/10.1101/2021.07.28.454185

Suresh, A. K., Winberry, J. E., Versteeg, C., Chowdhury, R., Tomlinson, T., Rosenow, J. M., … Bensmaia, S. J. (2017). Methodological considerations for a chronic neural interface with the cuneate nucleus of macaques. *Journal of Neurophysiology*, *118*(6), 3271–3281. https://doi.org/10.1152/jn.00436.2017

Sussillo, D. (2014). Neural circuits as computational dynamical systems. *Current Opinion in Neurobiology*, *25*, 156–163. https://doi.org/10.1016/j.conb.2014.01.008

Sussillo, D., & Barak, O. (2013). Opening the black box: Low-dimensional dynamics in high-dimensional recurrent neural networks. *Neural Computation*, *25*(3), 626–649. https://doi.org/10.1162/NECO_a_00409

Sussillo, D., Churchland, M. M., Kaufman, M. T., & Shenoy, K. V. (2015). A neural network that finds a naturalistic solution for the production of muscle activity. *Nature Neuroscience*, *18*(7), 1025–1033. https://doi.org/10.1038/nn.4042

Sussillo, D., Jozefowicz, R., Abbott, L. F., & Pandarinath, C. (2016). LFADS - Latent Factor Analysis via Dynamical Systems. Retrieved from http://arxiv.org/abs/1608.06315

Tabot, G. A., Dammann, J. F., Berg, J. A., Tenore, F. V., Boback, J. L., Vogelstein, R. J., & Bensmaia, S. J. (2013). Restoring the sense of touch with a prosthetic hand through a brain interface. *Proceedings of the National Academy of Sciences of the United States of America*, *110*(45), 18279–18284. https://doi.org/10.1073/pnas.1221113110

Takei, T., Lomber, S. G., Cook, D. J., & Scott, S. H. (2021). Transient deactivation of dorsal premotor

cortex or parietal area 5 impairs feedback control of the limb in macaques. *Current Biology*, *31*(7), 1476-1487.e5. https://doi.org/10.1016/J.CUB.2021.01.049

Talbot, W. H., Darian-Smith, I., Kornhuber, H. H., & Mountcastle, V. B. (1968). The sense of flutter-vibration: comparison of the human capacity with response patterns of mechanoreceptive afferents from the monkey hand. *Journal of Neurophysiology*, *31*(2), 301–334.

Tan, D. W., Schiefer, M. A., Keith, M. W., Anderson, J. R., Tyler, J., & Tyler, D. J. (2014). A neural interface provides long-term stable natural touch perception. *Science Translational Medicine*, *6*(257). https://doi.org/10.1126/scitranslmed.3008669

Tashima, R., Koga, K., Sekine, M., Kanehisa, K., Kohro, Y., Tominaga, K., … Tsuda, M. (2018). Optogenetic activation of non-nociceptive aβ fibers induces neuropathic pain-like sensory and emotional behaviors after nerve injury in rats. *ENeuro*, *5*(1). https://doi.org/10.1523/ENEURO.0450-17.2018

Taylor, A., Ellaway, P. H., Durbaba, R., & Rawlinson, S. (2000). Distinctive patterns of static and dynamic gamma motor activity during locomotion in the decerebrate cat. *Journal of Physiology*, *529*(3), 825–836. https://doi.org/10.1111/j.1469-7793.2000.00825.x

Taylor, J. A., Krakauer, J. W., & Ivry, R. B. (2014). Explicit and implicit contributions to learning in a sensorimotor adaptation task. *The Journal of Neuroscience : The Official Journal of the Society for Neuroscience*, *34*(8), 3023–3032. https://doi.org/10.1523/JNEUROSCI.3619-13.2014

Thanawalla, A. R., Chen, A. I., & Azim, E. (2020, December 1). The Cerebellar Nuclei and Dexterous Limb Movements. *Neuroscience*. Elsevier Ltd. https://doi.org/10.1016/j.neuroscience.2020.06.046

Todorov, E., & Jordan, M. I. (2002). Optimal feedback control as a theory of motor coordination. *Nature Neuroscience*, *5*(11), 1226–1235. https://doi.org/10.1038/nn963

Tomlinson, T., & Miller, L. E. (2016). Toward a Proprioceptive Neural Interface That Mimics Natural CorticalActivity. *Advances in Experimental Medicine and Biology*, *957*, 367. https://doi.org/10.1007/978-3-319-47313-0_20

Tsay, A. J., Giummarra, M. J., Allen, T. J., & Proske, U. (2016). The sensory origins of human position sense. *The Journal of Physiology*, *594*(4), 1037–1049. https://doi.org/10.1113/JP271498

Umeda, T., Isa, T., & Nishimura, Y. (2019). The somatosensory cortex receives information about motor output. *Science Advances*, *5*(7), eaaw5388. https://doi.org/10.1126/sciadv.aaw5388

Vaidya, M., Dickey, A., Best, M. D., Coles, J., Balasubramanian, K., Suminski, A. J., & Hatsopoulos, N. G. (2014). Ultra-long term stability of single units using chronically implanted multielectrode arrays. In *2014 36th Annual International Conference of the IEEE Engineering in Medicine and Biology Society* (Vol. 2014, pp. 4872–4875). IEEE. https://doi.org/10.1109/EMBC.2014.6944715

Vallbo, Å. B. (1971). Muscle spindle response at the onset of isometric voluntary contractions in man. Time difference between fusimotor and skeletomotor effects. *The Journal of Physiology*, *218*(2), 405. https://doi.org/10.1113/JPHYSIOL.1971.SP009625

Versteeg, C., Chowdhury, R. H., & Miller, L. E. (2021, April 1). Cuneate nucleus: the somatosensory gateway to the brain. *Current Opinion in Physiology*. Elsevier. https://doi.org/10.1016/j.cophys.2021.02.004

Versteeg, C., Rosenow, J. M., Bensmaia, S. J., & Miller, L. E. (2021). Encoding of limb state by single neurons in the cuneate nucleus of awake monkeys. *Journal of Neurophysiology*. https://doi.org/10.1152/jn.00568.2020

Vincent, J. A., Gabriel, H. M., Deardorff, A. S., Nardelli, P., Fyffe, R. E. W., Burkholder, T., & Cope, T. C. (2017). Muscle proprioceptors in adult rat: mechanosensory signaling and synapse distribution in spinal cord. *J Neurophysiol*, *118*, 2687–2701. https://doi.org/10.1152/jn.00497.2017.-The

Wall, P. D. (1958). Excitability changes in afferent fibre terminations and their relation to slow potentials. *The Journal of Physiology*, *142*(1), i3-21. Retrieved from http://www.ncbi.nlm.nih.gov/pubmed/16992026

Wall, P. D., & Noordenbos, W. (1977). Sensory functions which remain in man after complete transection of dorsal columns. *Brain*, *100*(4), 641–653. https://doi.org/10.1093/brain/100.4.641

Walsh, L. D., Gandevia, S. C., & Taylor, J. L. (2010a). Illusory movements of a phantom hand grade with the duration and magnitude of motor commands. *Journal of Physiology*, *588*(8), 1269–1280. https://doi.org/10.1113/jphysiol.2009.183038

Walsh, L. D., Gandevia, S. C., & Taylor, J. L. (2010b). Illusory movements of a phantom hand grade with the duration and magnitude of motor commands. *Journal of Physiology*, *588*(8), 1269–1280. https://doi.org/10.1113/jphysiol.2009.183038

Wang, J., Narain, D., Hosseini, E. A., & Jazayeri, M. (2017). Flexible timing by temporal scaling of cortical responses. *Nature Neuroscience 2017 21:1*, *21*(1), 102–110. https://doi.org/10.1038/s41593-017-0028-6

Weber, D. J., London, B. M., Hokanson, J. A., Ayers, C. A., Gaunt, R. A., Torres, R. R., … Miller, L. E. (2011). Limb-state information encoded by peripheral and central somatosensory neurons: Implications for an afferent interface. *IEEE Transactions on Neural Systems and Rehabilitation Engineering*, *19*(5), 501–513. https://doi.org/10.1109/TNSRE.2011.2163145

Weiler, J., Gribble, P. L., & Pruszynski, J. A. (2019). Spinal stretch reflexes support efficient hand control. *Nature Neuroscience*, *22*(4), 529–533. https://doi.org/10.1038/s41593-019-0336-0

Wesselink, D. B., Mz Van Den Heiligenberg, F., Ejaz, N., Dempsey-Jones, H., Cardinali, L., Tarall-Jozwiak, A., … Makin, T. R. (2019). Obtaining and maintaining cortical hand representation as evidenced from acquired and congenital handlessness. https://doi.org/10.7554/eLife.37227.001

Westling, G., Johansson, R. S., & Vallbo, O. (1976). Method for mechanical stimulation of skin receptors. In Y. Zotterman (Ed.), *Functions of the Skin in Primates* (pp. 151-158.). Oxford: Pergamon Press.

Whelan, P. J. (1996). Control of locomotion in the decerebrate cat. *Progress in Neurobiology*, *49*(5), 481–515. https://doi.org/10.1016/0301-0082(96)00028-7

Williams, S. R., & Chapman, C. E. (2000). Time course and magnitude of movement-related gating of tactile detection in humans. II. Effects of stimulus intensity. *Journal of Neurophysiology*, *84*(2),

863–875. https://doi.org/10.1152/jn.2000.84.2.863

Williams, S. R., & Chapman, C. E. (2002). Time course and magnitude of movement-related gating of tactile detection in humans. III. Effect of motor tasks. *Journal of Neurophysiology*, *88*(4), 1968–1979. https://doi.org/10.1152/jn.2002.88.4.1968

Williams, S. R., Shenasa, J., & Chapman, C. E. (1998). Time Course and Magnitude of Movement-Related Gating of Tactile Detection in Humans. I. Importance of Stimulus Location. *Journal of Neurophysiology*, *79*(2), 947–963. https://doi.org/10.1152/jn.1998.79.2.947

Wimalasena, L. N., Miller, L. E., & Pandarinath, C. (2020). From unstable input to robust output. *Nature Biomedical Engineering 2020 4:7*, *4*(7), 665–667. https://doi.org/10.1038/s41551-020-0587-9

Witham, C. L., & Baker, S. N. (2011). Modulation and transmission of peripheral inputs in monkey cuneate and external cuneate nuclei. *Journal of Neurophysiology*, *106*(5), 2764–2775. https://doi.org/10.1152/jn.00449.2011

Witham, Claire L, & Baker, S. N. (2011). Modulation and transmission of peripheral inputs in monkey cuneate and external cuneate nuclei. *Journal of Neurophysiology*, *106*(5), 2764–2775. https://doi.org/10.1152/jn.00449.2011

Wolpert, D. M., Goodbody, S. J., & Husain, M. (1998). Maintaining internal representations: The role of the human superior parietal lobe. *Nature Neuroscience*, *1*(6), 529–533. https://doi.org/10.1038/2245

Wolpert, D. M., Miall, R. C., & Kawato, M. (1998). Internal models in the cerebellum. *Trends in Cognitive Sciences*, *2*(9), 338–347. https://doi.org/10.1016/S1364-6613(98)01221-2

Yau, J. M., Kim, S. S., Thakur, P. H., & Bensmaia, S. J. (2016, February 1). Feeling form: The neural basis of haptic shape perception. *Journal of Neurophysiology*. American Physiological Society. https://doi.org/10.1152/jn.00598.2015

Yu, B. M., Cunningham, J. P., Santhanam, G., Ryu, S. I., Shenoy, K. V, & Sahani, M. (2009). Gaussian-process factor analysis for low-dimensional single-trial analysis of neural population activity (Journal of Neurophysiology (2009) 102, (614-635) DOI: 10.1152/jn.90941.2008). *Journal of*

Neurophysiology. https://doi.org/10.1152/jn.z9k-9684-corr.2009

Yumiya, H., Kubota, K., & Asanuma, H. (1974). Activities of neurons in area 3a of the cerebral cortex during voluntary movements in the monkey. *Brain Research*, *78*(2), 169–177. https://doi.org/10.1016/0006-8993(74)90544-7

Zarzecki, P., & Asanuma, H. (1979). Proprioceptive Influences on Somatosensory and Motor Cortex. *Progress in Brain Research*, *50*(C), 113–119. https://doi.org/10.1016/S0079-6123(08)60812-2

Ziat, M., Hayward, V., Chapman, · C Elaine, Ernst, M. O., & Lenay, C. (2010). Tactile suppression of displacement. *Exp Brain Res*, *206*, 299–310. https://doi.org/10.1007/s00221-010-2407-z